UNIVERSITÀ DEGLI STUDI DI MILANO

DEPARTMENT OF PHARMACEUTICAL SCIENCES

PhD in PHARMACEUTICAL SCIENCES

CYCLE XXXVI

COORDINATOR Prof. Giulio Vistoli

Characterization and evaluation of clinically relevant readouts in a pre-clinical model of Idiopathic Pulmonary Fibrosis (IPF)

University Tutor: **Prof Angelo Sala**

Industrial Co-Tutor: **Dr.ssa Daniela Miglietta**
(Chiesi Farmaceutici S.p.A)

PhD Student: **Dr.ssa Annalisa Murgo**

Academic year 2022/2023

ABSTRACT

Idiopathic pulmonary fibrosis (IPF) is a chronic, progressive age-related interstitial lung disease (ILD) with a poor prognosis and very limited therapeutic options *(Raghu et al. 2015; Spagnolo et al. 2018)*. To date, Pirfenidone and Nintedanib are the only two therapies approved for IPF worldwide. However, these drugs can slow-down lung function decline without really stopping or reverting the fibrotic process, and in addition their use is associated with a series of side effects. These characteristics of IPF indicate the ongoing critical importance of drug discovery efforts and highlight as animal models have become an indispensable tool in translational research of human lung disease as IPF, pivotal to test potential new therapeutic drugs. Despite the wide variety of different in vivo model for IPF *(Tashiro et al. 2017)*, there is no consensus on preclinical tests best used to investigate IPF mainly due to some limitation that need to be considered when extrapolating findings from animal model to the human disease *(Carrington et al. 2018)*. In fact one of the most challenging aspects of drug discovery for IPF remains the identification of new therapies that can be translated effectively to the clinic, implying that very few compounds that have shown efficacy in animal models have been successful in human clinical trials and concluding that most of the preclinical models are poorly predictive and scarcely resembling the human disease. Currently the majority of new drugs investigated in preclinical models of IPF are dosed using a prophylactic dosing regimen, whereas patients are almost always treated after the fibrosis is well established but probably, one of the most relevant limitation remains some measurements that should not be easily done in both humans and mice.

In this scenario, the main goal of this PhD project was to generate a robust and reliable preclinical model of pulmonary fibrosis, introducing novel readouts, suitable to select and to identify new pharmacological treatments for IPF with an higher translational potential to make the model more impactful to identify new potential treatments for IPF. To achieve this aim, we have introduced in our bleomycin (BLM)-induced mouse model *(Stellari et al. 2017)*, novel readouts such as the Forced Vital Capacity (FVC) and the Diffusion Factor for Carbon Monoxide (DFCO) that are poorly used in preclinical practice but that are respectively the primary and secondary endpoints in clinical trials for IPF *(Spagnolo et al. 2013)* to monitor patients during the treatments. Additionally, also some emerging biomarkers currently under evaluation in the clinical setting were explored in the model. Finally, we have also worked to refine the histological analysis which still remains an important complementary evaluation to be coupled to the functional readouts.

Currently the common histological analysis utilized in preclinical models of lung fibrosis is represented by the Ashcroft scoring system, which revealed some disadvantages such as a time-consuming process, operator-dependent results, limited sensitivity and, most critical, inability to get a direct link to clinics. Therefore, we introduced an automated image analysis by using an artificial intelligence (AI) approach, which improved this analysis recognizing histological features with more accuracy and consistency, reducing significantly the time of the analysis and making the evaluation independent from the operator.

All these new readouts, explored firstly in a time course experiment at several time-points up to 49 days from the first bleomycin administration, showed the same profile over time observed with histology in terms of development of fibrotic disease. Next, the relevance of these novel readouts in the bleomycin model will be assessed by the pharmacological validation with Nintedanib, providing evidence of the robustness and the predictivity of these functional readouts with the final aim to enhance the translational and the predictivity values of the model.

In summary, this project demonstrated that in the mouse BLM-induced lung fibrosis model it has been possible to explore the same clinically relevant parameters used in IPF patients; in particular lung function tests such as FVC and DFCO, that for their high translational value together with the high sensitivity to assess the efficacy of the compounds has been chosen respectively as the primary and secondary endpoint to support the selection of novel treatments within our internal drug discovery IPF projects. Furthermore, the introduction of these different readouts, that all go to the same direction, has from one side increased the robustness of the model and from the other side has allowed to bring this preclinical model to a level of complexity that mirrors the one observed in human IPF.

Overall, this PhD work has enhanced the translational value of the data obtained with the mouse BLM model increasing the chance of selecting promising compounds to advance to clinical trials and has concretely led to significant benefits to drug discovery process in the IPF research, improving the quality and the reliability of the search of novel anti-fibrotic drugs.

TABLE OF CONTENTS

1. INTRODUCTION

1.1 Idiopathic Pulmonary Fibrosis

Idiopathic Pulmonary Fibrosis (IPF) is defined by the ATS/ERS/JRS/ALAT guidelines as a specific form of chronic, fibrosing interstitial pneumonia, of unknown cause, included in the heterogeneous group of Interstitial Lung Diseases (ILDs) *(Raghu et al. 2022*) **(Figure 1.1)**.

In particular, IPF is the most common and severe form of Idiopathic Interstitial Pneumonias (IIPs), characterized by progressive decline of lung function, respiratory failure and high mortality rate.

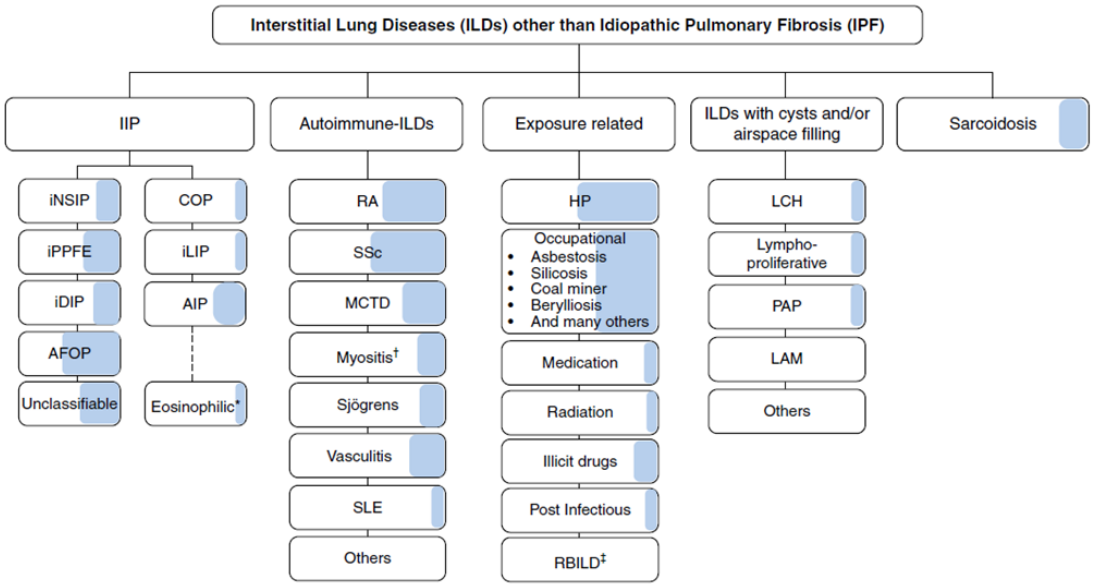

Figure 1.1 Classification of ILDs *(ATS International Consensus Statement, 2022)*

The reported incidence of IPF has been estimated to be in the range of 0.09 to 1.30 per 10,000 persons globally. Overall, the countries with the highest incidence of IPF are SouthKorea, Canada, and the United States *(Maher et al. 2021)* but with the population aging worldwide, the impact of IPF to patients and healthcare providers is expected to increase in the future. The disease, which occurs mainly in elderly males (typically in the sixth and seventh decades), is limited to the lungs, and associated with the histopathologic and/or radiologic pattern of Usual Interstitial Pneumonia (UIP) (*Raghu et al. 2022*). The histopathologic hallmark of UIP is a heterogeneous appearance in which areas, most commonly subpleural and paraseptal parenchyma, are severely affected by fibrosis leading to distortion of normal lung architecture and irreversible loss of lung function, but alternate with areas less compromised or normal parenchyma *(Glass et al. 2020).* These regions are

characterized by mild inflammation, usually consisting of a patchy interstitial infiltrate of lymphocytes, and fibrotic areas composed mainly of dense collagen and proliferating fibroblasts and myofibroblasts (so-called fibroblast foci).

In the past decade, significant progress has been made on our understanding of the mechanisms underlying this disease. It is proposed that repetitive micro-injuries to alveolar epithelial cells trigger abnormal epithelial-fibroblast communication, which eventually results in abnormal extracellular matrix (ECM) accumulation and pathological lung remodeling *(Heukels et al. 2019; Martinez et al. 2017; Richeldi et al. 2017)*.

As result, lung architecture is completely shuttered and the alveoli are replaced by large air spaces with thick fibrotic walls lined by bronchiolar epithelium and often filled with mucin and inflammatory cells, defined as honeycomb lung. These morphological alterations of lung tissue, in turn, lead to decreased lung compliance, disrupted gas exchange, and ultimately respiratory failure and death (*Myers 2014*).

Although IPF is, by definition, a disease of unknown causes, multiple factors have been shown to increase the risk of developing the disease. It is currently believed that IPF results from a complex interplay of genetic predisposition and environmental risk factors, which translates in profound changes to epithelial cells and fibroblasts (*Selman and Pardo, 2014*).

Genetic factors

The familial interstitial pneumonia (FIP) is an autosomal dominant genetic disease with variable penetrance in which rare genetic variants have been identified *(Kropski et al. 2015; Lorenzo-Salazar et al. 2019)*.

FIP rapresents <5% of all cases of IPF and it is clinically and histologically indistinguishable from sporadic IPF, although familial forms tend to present at an earlier age and may display some differences in radiological pattern *(Lee et al. 2005)*.

Large-scale genome-wide association studies have identified several specific genetic variants, both rare and common, associated with sporadic and familial forms of pulmonary fibrosis that confer risk for development of IPF *(Noth et al. 2013)* and that were grouped *(Kaur et al. 2017)* into three major categories based on their role in the pathogenesis of the disease:

- Genes related to alveolar stability: surfactant proteins are alveolar epithelial cells (AECs) type II specific products considered to be essential for normal lung function and homeostasis. Rare variants have been identified in the genes encoding surfactant protein C (SFTPC) and A (SFTPA2) *(Tanjore et al. 2012)*.

- Genes linked to telomere biology and associated with accelerated cell senescence: telomeres are specialized loop structures of repetitive nucleotide units at the ends of chromosomes that protect them from progressive shortening during the normal cell replication process. Recent studies have reported an association between numerous genes in the telomerase maintenance pathway and FIP, most importantly those related to catalytic activity, telomerase reverse transcriptase (TERT) and telomerase RNA component (TERC) *(Barros et al. 2019)*. TERT variants are the most frequently identified rare variants associated with IPF, occurring in approximately 15% of FIP and in 1–3% of sporadic cases *(Kaur et al. 2017)* and correlating with worse survival in IPF *(Stuart et al. 2014)*.
- Genes affecting host defense: genome-wide association studies indicated that the common variant polymorphism in the promoter region of mucin 5B oligomeric mucus/gel-forming (MUC5B), rs35705950, strongly associates with development of both familial and sporadic IPF (*Moore et al. 2019*). MUC5B, expressed by airway epithelial cells, contributes to airway mucus production and plays an important role in innate immunity of lungs. Overexpression of MUC5B is related to impaired mucociliary clearance (MCC) and the degree and duration of fibrosis (*Hancock et al. 2018*). The rs35705950 minor allele mutation can lead to overexpression of mucin 5B in small airway epithelial cells, and DNA methylation is closely related to genetic susceptibility of MUC5B *(Zhang Q et al. 2019)* and has been postulated to account for approximately 30% of the risk for developing IPF *(Evans et al. 2016)*. In addition, a study identified a positive feedback bistable ERN2-XBP1S pathway upregulated MUC5B mRNAs in IPF and further regulated mucus secretion, providing an unfolded protein response (UPR)-dependent mechanism with rs35705950 variant *(Chen G et al. 2019)*.

Environmental factors

Environmental exposure and genetic predisposition may have a synergistic effect in the development of IPF. In both sporadic and familial pulmonary fibrosis, environmental exposures to lung epithelium can increase the risk of IPF. Of them, smoking and metal dust are the strongest risk factors *(Pardo and Selman, 2020)*.

Cigarette smoke can cause a variety of cellular changes through epigenetic and can overexpress genes associate with epithelial-to-mesenchymal transition (EMT) and act negatively on important biological processes, like acceleration of telomere shortening and stress of the ER *(Song et al., 2019)*. Pollutants and ultrafine particles in cigarette smoke contain carbon black (CB) and cadmium (Cd) both increased significantly in IPF lung tissue, directly proportional to the amounts of citrullinated vimentin (Cit-Vim) that triggers

fibroblasts to infiltrate lung microspheres, promotes increased expression of collagen and α-smooth muscle actin (α-SMA), and induces lung fibrosis *(Li et al. 2023)*. Nicotine itself is able to induce the production of transforming growth factor-β (TGF-β), an important mediator of fibrosis in IPF. Moreover, the act of smoking involves repetitive mechanical stretch, which has been linked to micro-injury to the lung by increasing epithelial permeability, promoting the production of reactive oxidative species and impairing tissue regeneration *(Zaman and Lee, 2018)*.

Microorganisms (viruses, fungi and bacteria) play a potential role in the pathogenesis of IPF *(Lipinski et al. 2020)*. Compared with healthy individuals, IPF patients have an imbalance in the composition of the lung microbiota, which can serve as a persistent stimulus for repetitive alveolar injury *(Molyneauxet al. 2013)*. The inflammatory and fibrotic mediators as well as immune disorders in the lungs of IPF patients are related to bacterial load. Moreover, recent data suggest that IPF is characterized by an increased bacterial burden in bronchoalveolar lavage (BAL) that also predicts disease progression and death *(O'Dwyer et al. 2019)*. In addition, Epstein-Barr virus (EBV), cytomegalovirus (CMV) and human herpes virus are detected in alveolar epithelial cells of patients with IPF, suggesting a link between viral infection and increased risk of IPF. Treatment with the antibacterial co-trimoxazole (added to standard treatment), has been shown to reduce mortality in patients with fibrotic IIPs including IPF, an effect possibly related to a reduction of respiratory infections (*Shulgina et al. 2013*). Although the mechanisms by which viral infection is associated with IPF remains unclear, studies suggest that it may be related to activation of epithelial mesenchymal transition, promotion of TGF-β expression, and induction of epigenetic reprogramming *(Li et al. 2018; Sideset al. 2011)*. Interestingly, IPF patients expressing MUC5B risk alleles have a significantly lower bacterial burden compared with the patients who do not bear the risk allele *(Molyneaux et al. 2014).*

Some environmental and occupational exposures, particularly metal and wood dust, have also been linked with an increased risk for IPF (*Miyake et al. 2005*). Farming, stone cutting/polishing and exposure to livestock and to vegetable/animal dust have also been associated with IPF (*Baumgartner et al. 2000; Gustafson et al. 2007*). However, since epidemiologic studies of environmental risk factors are subject to a number of biases and limitations, these associations should be interpreted with caution.

Comorbidities

Emerging data support a role of gastroesophageal reflux (GER) with subsequent secondary and chronic micro-aspiration as the initial AECs insult driving aberrant tissue remodelling

in IPF (*Ruaro et al. 2022*). In pre-clinical studies, aspiration of gastric fluid was shown to activate fibrotic cascades in the pulmonary parenchyma (*Appel et al. 2007*). Moreover, in a prospective study, Raghu and colleagues found that 80% of patients with well-characterized IPF had GER as determined by esophageal pH monitoring, a predictor of acid reflux (*Raghu et al. 2006*). The precise relationship between GER and IPF has yet to be established, but several studies have hypothesized that GERD-associated microaspiration may lead to persistent inflammation impairing lung infrastructure, thereby possibly accelerating the progression of IPF. In addition, IPF may increase intrathoracic pressure, which can worsen GERD *(Methot et al. 2019)*. Currently, antiacid therapy (e.g., proton pump inhibitors and histamine-2-blocker receptor antagonists) for IPF patients with GERD symptoms has only a conditional recommendation according to IPF guidelines *(Raghu et al. 2015)*. Some studies show that it slows disease progression in terms of lung function decline, improves survival, decreases the number and frequency of acute exacerbations of the disease, and prolongs transplant free survival; however, there are post-hoc analyses which have demonstrated no benefit from antiacid therapy over a placebo in patients following treatment with Pirfenidone and Nintedanib *(Lee et al. 2011).* Laparoscopic fundoplication is another treatment option for patients with IPF and GERD because theoretically it may help to control reflux and avoid aspiration, with the same effects mentioned above on the progression of the disease *(Hoppo et al. 2015)*.

Obstructive sleep apnea (OSA), an upset characterized by periodic apneas and/or hypopneas caused by partial or complete collapse of the upper airway, is also reported to be common in IPF, with prevalence estimates from 59-88% (*Zaman and Lee 2018*). The hypothesis that OSA may be related to IPF is supported by the association between OSA and biomarkers that are associated with both lung injury and survival in IPF (*Lederer et al. 2009; Kim et al. 2017*). Despite these findings further research is needed to understand if OSA precedes IPF or viceversa, and to determine whether therapy for OSA can be of benefit in the management of IPF.

Several case-control studies have also suggested a link between IPF and diabetes mellitus (DM) (*Wang et al. 2020, Bai et a.l 2021*). The main theory regarding the mechanism by which DM may be a risk factor for IPF relates to hyperglycemia-mediated overproduction of advanced glycosylation end products leading to oxidative injury and subsequent overexpression of pro-fibrotic cytokines, fibroblast proliferation and ECM deposition (*Yang et al. 2011*). Metformin, the most commonly prescribed drug for DM, was shown to attenuate EMT mediated by TGF-β *in-vitro*. *In-vivo* studies of metformin provided

evidence of attenuation in the bleomycin-induced pulmonary fibrosis mouse model (*Sato et al. 2016*) and more recently, reversal of lung fibrosis (*Rangarajan et al. 2018*).

1.2 Pathogenesis of IPF

Research efforts in the last few years have reached important milestones in understanding the pathogenesis of IPF, making the concept "idiopathic" less compelling. The current paradigm suggests that IPF is an epithelial-fibroblastic disorder involving a multitude of cellular types and complex cell-matrix interactions, through various biochemical mediators and specific signalling pathways. The proposed abnormal wound healing model of IPF is schematized in **Figure 1.2**.

Alveolar epithelial injury

Repeated injury to the alveolar epithelium is believed to be the initiating trigger for the development and sustainment of the fibrotic process. Under normal circumstances, the damage of alveolar epithelial cells will lead to recruitment of inflammatory cells, fibrosis and matrix deposition in order to repair the damaged cells. This stage is temporary and then normal pulmonary homeostasis will be restored through activation of apoptotic pathways and phagocytosis of macrophages during the injury repair stage. However, in IPF lungs, mutations of lung epithelial restriction genes (SFTPC, SFTPA2 and ABCA3) and abnormal expression of genes such as MUC5B cause lung epithelial mucosal barrier dysfunction *(Hancock et al. 2018)*. Repeated stimulation of microorganisms, smoking, gastroesophageal reflux and other factors destroys the integrity of the lung epithelium. In addition, inflammation, excessive production of reactive oxygen species (ROS) and endoplasmic reticulum stress (ERS) in IPF lungs lead to repetitive damage to epithelial cells *(Ornatowski et al. 2020)*.

Lung Stem Cells Dysfunction and Exhaustion

The normal alveolar epithelial lining is composed by alveolar epithelial type I and II cells (AT1s and AT2s). The AT1s are the most represented cells in the alveolar-capillary interface, covering more than 96% of the total alveolar surface area. They are highly specialized and have a flat morphology, which provides a thin membrane for gaseous exchange. AT2s, serve as the predominant epithelial progenitor in alveoli, playing an important role in maintaining lung homeostasis *(Parimon et al. 2020)*. Specifically, they are involved in the secretion of surfactant proteins (SPs), retain proliferative capacity, and are

responsible for the regeneration of epithelium after injury, including trans-differentiation to type I cells *(Sandbo, 2013/ Chapter 8)*.

In IPF, genetic and environmental factors may cause damage to AT1s, while dysfunction of AT2s makes it difficult to repair the damaged AT1s. Abnormal function of alveolar epithelial cells is associated with activation of signal pathways such as Wnt/β-catenin and Sonic Hedgehog *(Reyfman et al. 2019)*. When injury occurs in epithelial cells, Wnt signaling pathway is activated and participates in "ancillary" AT2 stem cell progenitor cell activity *(Nabhan et al. 2018)*. Wnt-reactive alveolar epithelial progenitor cells (AEP) in AT2 are a stable lineage during alveolar homeostasis, but rapidly expand to regenerate most of the alveolar epithelium after acute lung injury, showing stronger "stemness". It has been believed that repetitive micro-injuries are a potential cause of AT2 depletion. However, the reduction of AT2 number in IPF lung supports the idea of stem cell exhaustion. In addition, aging, ERS and mitochondrial dysfunction play an important role in AT2 depletion and impaired self-renewal *(Borok et al. 2020; Parimon et al. 2020)*. Loss of Cdc42 in AT2s results in impaired differentiation, exposing alveolar cells to sustained elevated mechanical tension which activates a TGF-β signaling loop in AT2 cells in a spatially regulated manner, thereby promoting lung fibrosis progression from periphery to center *(Wu et al. 2020)*. The failure of AT2s to repopulate the epithelium and restore the normal condition leads to the activation of fibroblasts (*Knudsten et al. 2017*).

Role of fibroblast and origin of myofibroblast

Fibroblasts are elongated, spindle-shaped, not terminally differentiated mesenchymal cells, committed to re-establish a normal and well-structured ECM in wound healing repair process through the expression of matrix metalloproteinases (MMPs), which degrade ECM, and their inhibitors, tissue inhibitors of metalloproteinases (TIMPs). This cell type can respond to a broad series of stimuli, such as cytokines and growth factors. In IPF, pro-fibrotic mediators secreted by activated fibroblasts continue to act on fibroblasts to generate a positive feedback, which leads to production of ECM and myofibroblast differentiation *(Wipff et al. 2007)*. TGF-β is considered to be the primary factor that promotes fibroblast differentiation into myofibroblasts *(Huang et al. 2020)*. Myofibroblasts secrete more ECM than fibroblasts and are the main collagen-producing cells in the lung, characterized by expression of contractile protein α-SMA and fibroblast activation protein (FAP) *(Tsukui et al. 2020)*. FAP is a membrane-spanning protein essential for collagen remodeling. It is expressed at low state in most healthy cells but it can be used as a molecular marker to exploit for specifically target drugs to fibroblasts that cause fibrosis *(Hettiarachchi et al.*

2020). In the normal wound healing process, unwanted fibroblasts are eliminated by activating the apoptotic pathway that limits the ongoing matrix deposition and fibrosis. In IPF, myofibroblasts were found to resist FAS ligand-induced apoptosis and have stronger proliferation ability when grown on polymerized collagen *(Xia et al. 2008; Nho et al. 2011)*. Fas L, Tumor necrosis factor (TNF)-related apoptosis-inducing ligand (TRAIL) and Cav-1 protein expression in these cells decreased, while AKT activity increased (Hohmann et al., 2019). In addition, myofibroblast contraction is irreversible, which contribute to trigger the spatial structural reorganization of collagen fibrils, increasing their mechanical stress and stiffening the ECM *(Zhou et al. 2020)*. Periostin is highly expressed in IPF lungs. Further studies have found that in lung fibroblasts, periostin/integrin αVβ3 can play a vital role in the proliferation of lung fibroblasts *(Yoshihara et al. 2020).*

Role of Growth Factors

There is overwhelming evidence in support of a key role of TGF-β in the pathogenesis of IPF *(Huang et al. 2020)*. *TGF-β* promotes epithelial-mesenchymal transition, epithelial cell migration, fibroblast proliferation, activation, and differentiation into myofibroblasts. TGF-β can also increase the production of other fibrotic mediators and pro-angiogenic mediators *(Song et al. 2020)*. TGF-β is synthesized as a latent complex by binding to the latency related peptide (LAP), which covalently binds to the ECM protein *(Biernacka et al. 2011)*. Latent TGF-β can be activated by a range of factors, including αvβ6 integrin *(John et al. 2020)*. In IPF, expression of αvβ6 in alveolar epithelial cells is increased, which binds to LAP to induce TGF-β activation *(Jenkins et al. 2006)*. Once activated, TGF-β binds to its receptors and stimulates phosphorylation of transcription factor Smad3. Phospho-Smad3 interacts with Smad4 to form a complex which translocates into the nucleus to induce expression of target genes, including profibrotic genes such as α-SMA, CTGF and ECM major collagen 1A1 (COL1A1) *(Massague 2012)*.

CTGF, also known as cellular communication network factor 2 (CCN2), is an important mediator of organ fibrosis in human body *(Falke et al. 2020; Wang et al. 2019)* and it is secreted and activated under stimulation of TGF-β. CTGF mediates lung matrix deposition and fibroblast differentiation by activating downstream MAP kinase pathway *(Inui et al. 2021)*. In addition, CXCL12 can also induce the expression of CTGF in human lung fibroblasts by activating the MEKK1/JNK signaling pathway. Studies have found that gene promoter of CTGF contains numerous transcription factor binding sites such as NF-κB, signal transducer and activator of transcription (STAT), activator protein-1 (AP-1) and SMAD *(Lin et al. 2018)*, indicating these factors may affect IPF through CTGF.

PDGF is widely expressed in macrophages, platelets, endothelial cells and fibroblasts *(Hewlett et al. 2018)*. Highly expressed PDGF can be detected in BALF of IPF patients and bleomycin-induced IPF model mice *(Phan et al. 2021)*. The abnormal expression and signal transduction of PDGF ligands and receptors have been confirmed to be closely related to IPF. In IPF, TGF-β signaling promotes expression of PDGF-B through regulatory T cells (Tregs), thereby stimulating PDGF-B-mediated fibroblast proliferation and migration *(Kishi et al. 2018)*.

Insulin-like growth factor (IGF1) is a key molecule that regulates cellular senescence *(Duran-Ortiz et al. 2021)*. As mentioned above, senescence has been identified as an important reason for the weakened repair function of AT2s in IPF. Under pathological conditions, ATs release IGF1, which activates the surface of adjacent normal ATs. IGF receptor (IGFR-1), and further activate the PI3K/AKT signaling pathway, and participate in ATs senescence and IPF by releasing CTGF, TGF-β1 and MMP9 *(Sun et al. 2021)*.

ECM remodeling phase

During IPF, matrix organization is severely altered and excessive collagen deposition is one of the principal hallmarks of a fibrotic process, responsible of the stickiness and rigidity of the lung. The massive deposition of extracellular matrix in IPF is mainly involved in changes in two families of proteins: MMPs and tissue inhibitors of metalloproteinases (TIMPs). Studies have found that expression levels and localization of MMP and TIMP in IPF lungs undergo substantial changes and that the levels of MMP1, MMP2, MMP9 and the four TIMPs are up-regulated. Among them, MMP1 is more common in alveolar macrophages and epithelial cells, while TIMP is highly expressed by myofibroblasts in IPF fibroblastic foci *(Betensley et al. 2016)*. The extracellular matrix of IPF can also change transcriptional profile of lung fibroblasts and affect the translation of ECM proteins, such as COL1A1, COL1A2, COL3A1, COL5A2, COL4A2, MMP2, MMP3, MMP10 and TIMP2 *(Zolak and de Andrade, 2012)*. Together, these findings suggest that there is a positive feedback pathway between fibroblasts and abnormal ECM, in which the fibrotic extracellular matrix is both the cause and the result of fibroblast activation *(Guiot et al. 2017)*.

Inflammation and Immunity

The role of inflammation in the development of IPF remains controversial. In the early stage of alveolar injury, neutrophils are recruited into the injured sites, triggering an immune response by releasing pro-inflammatory cytokines and producing neutrophil

elastase (NE) to exacerbate fibrosis *(Le Saux and Chapman, 2018)*. Elevated IL-8 and G-CSF have been found in the bronchoalveolar lavage fluid (BALF) and sputum of IPF patients, suggestive of infiltration and activation of neutrophils. IL-8 promotes the development of fibrosis through elastase-mediated activation of TGF-β *(Heukels et al. 2019)*. IL-24 and IL-4 can synergistically induce M2 program of macrophages, thereby promoting the development of lung fibrosis *(Rao et al. 2021)*. IL17 secreted by Th17 cells can directly promote fibrosis. In acute exacerbation of pulmonary fibrosis, the levels of IL-17 and IL-23 are increased, and treatment with interleukin-23 antibody can significantly attenuate airway inflammation and fibrosis and reduce IL-17 level, suggesting IL-23 is essential for the development of acute exacerbation of pulmonary fibrosis *(Senoo et al. 2021)*. Monocyte and macrophages drive fibrosis through excessive repair responses to alveolar cell injury. Compared with normal lungs, the subpopulation of macrophages that highly express SPP1 and MERTK (SPP1hi) increased significantly in IPF lungs. The highly proliferated SPP1hi macrophages upregulate the expression of type 1 collagen and MMP2 and contribute to tissue repair and fibrosis *(Morse et al. 2019)*. CCL2 and colony stimulating factor (M-CSF/CSF1) derived from monocytes/macrophages may have a direct fibrotic effect *(Coward et al. 2010)*. Furthermore, recent studies have identified that immune cells in lung tissue predict the severity of IPF and participate in the progress of this disease, which can be used as a reference indicator *(Wang Z et al. 2020)*.

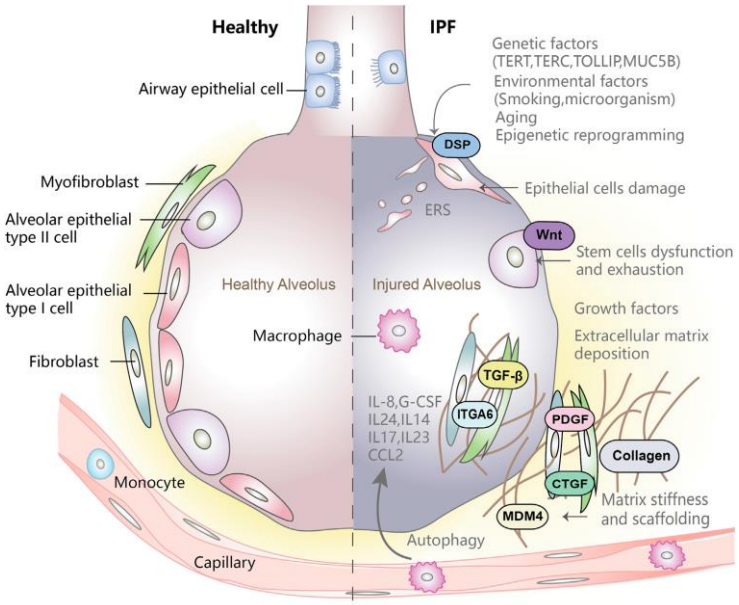

Figure 1.2 Pathogenesis of IPF *(Mei et al. 2022)*

1.3 Clinical history of IPF

The onset of IPF symptoms is usually progressive and insidious, and mainly consists of an unexplained chronic dyspnea, reported initially as exertional, and cough, that is often dry. Symptoms are reported to lung specialists after several months from their beginning, because often they are overlooked in the context of ageing in general and sometimes in the history of smoking or other associated comorbidities, such as emphysema, heart disease or a respiratory tract infection (*Lancaster et al. 2021*).

About physical examination, bibasal end-inspiratory crepitations, known as velcro-like crackles (rales), are the most common features during chest auscultation while the digital clubbing, present in 25% to 50% patients, is another clinical finding which can be observed in patients with IPF.

Pulmonary function tests typically demonstrate a restrictive pattern, characterized by reduction in forced vital capacity (FVC) and total lung capacity (TLC), reflecting the increased lung stiffness (and reduced lung compliance) caused by the accumulation of scar tissue and the subsequent architectural distortion of the lung parenchyma. Diffusing capacity of the lung for carbon monoxide (DLCO) is almost invariably reduced due to both a contraction of the pulmonary capillary volume and ventilation and perfusion mismatching. The decline in DLCO may represent the only functional abnormality in early or mild disease. In addition to its diagnostic role, pulmonary function tests are useful in quantifying disease severity and predicting outcome (*Alhamad et al. 2001*).

The rate of functional decline and disease progression in IPF is highly heterogeneous and unpredictable. Data from the placebo arms of large clinical trials show that the mean annual rate of decline in FVC ranges from 0.13 to 0.21 litres (*Ley et al. 2011*).

It is well recognized that symptoms precede diagnosis by a median of 1 to 2 years and radiographic evidence of disease may even precede symptoms, suggesting the existence of a relatively long period of subclinical disease. Progression of asymptomatic to symptomatic IPF and clinical phenotypes of IPF are represented in **Figure 1.3**. The classic clinical course of IPF is one of *slowly progressive* disease, with patients reporting a history of worsening dyspnea and/or dry cough lasting for months to years. A subgroup of patients, mainly male heavy smokers, experience a rapidly progressive disease course (referred to as *accelerated* IPF) characterized by a poor short-term prognosis. A study, conducted by Selman and coworkers, describes a series of features in patients with rapid decline comparing with slow progressors (*Selman et al. 2007*). Notably, accelerated IPF differs from the typical slowly progressive form in terms of outcome and gene expression profile, despite having similar age, lung function, chest imaging and histology findings at the time

of the diagnosis. In this work, rapid progressors show a median survival from the time of diagnosis of 25 months, while slow progressors had a median survival of 93 months.

Patients with IPF may also suffer sudden deterioration of their condition during a relatively stable disease course, defined as *acute exacerbation*. It remains uncertain whether acute exacerbations of IPF (AE-IPF) represent an acceleration of the underlying fibroproliferative lung process or the sequelae of clinically unrecognized triggers (e.g. infection) but clinical trials suggest that AE-IPF are infrequent events in patients with mild-to-moderate disease (*Kim et al. 2012*). There is no established consensus approach to the diagnosis of acute exacerbation of IPF, however it generally requires a combination of the following symptoms: worsening of dyspnea within days to weeks (generally < 30 d); evidence of abnormal gas exchange or a decrease in PaO2; new bilateral ground-glass opacities and/or consolidation superimposed on a UIP radiological pattern; and absence of infection, heart failure, pulmonary embolism, or other identifiable causes (*Collard et al. 2007*). Apparently, the risk of an exacerbation does not appear to be linked to the level of lung function impairment, age, or smoking history (*Kim et al. 2006*). The significance of AE-IPF rests on its poor prognosis, with mortality exceeding 60% during hospital stay and 90% within 6 months after discharge (*Collard et al. 2013*).

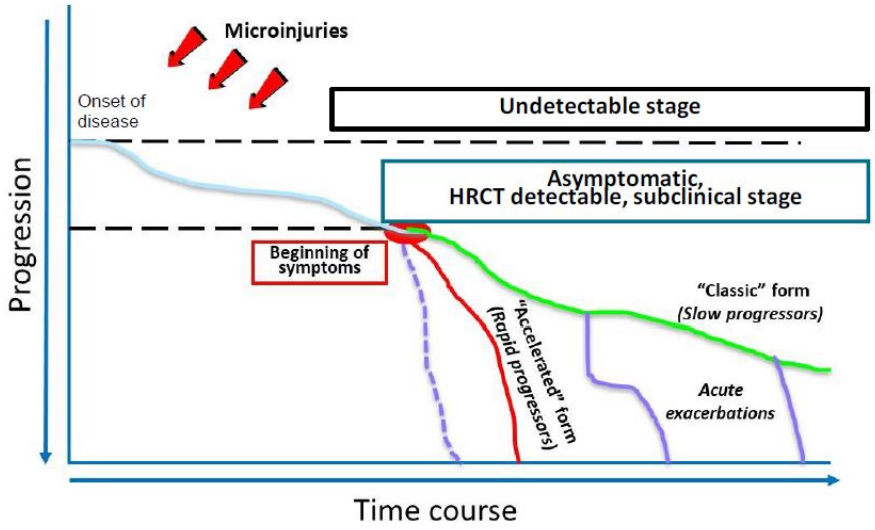

Figure 1.3 Heterogeneity of the natural history and clinical phenotypes of IPF patients (Image modified and adapted from *Selman et al. 2007*)

1.4 Diagnosis of IPF

Diagnosis and management of IPF patients were addressed in three guidance documents published by international experts representing major respiratory and radiological societies *(Raghu et al 2011; Raghu et al. 2018)*. According to these guidelines, a diagnosis of IPF require the following criteria:

- *Exclusion of other known causes of fibrosing ILD* [e.g. domestic and occupational environmental exposures, connective tissue disease (CTD), drug toxicity];
- *The presence of the High-Resolution Computer Tomography (HRCT) pattern of UIP;*
- *Specific combinations of HRCT patterns and histopathology patterns in patients subjected to surgical lung biopsy (SLB)*, when possible.

The clinical assessment requires a clear understanding of the differential diagnosis for IPF and a comprehensive and structured approach to confirm and exclude known causes and associations of other ILDs. A clear focus of a patient's clinical examination should be performed to establish the clinical probability of IPF, which is particularly increased when the patient is older than 60 years, male, and has a history of cigarette smoking (*Brownell et al. 2017*). If a specific diagnosis is not made or no potential cause for ILD is identified, further evaluation is influenced by the patterns of HRCT images of the chest to ascertain or exclude the diagnosis of IPF. The most recent 2022 guidelines for diagnosis of IPF suggested reconsidered the categories of HRCT patterns. Four HRCT categories were defined in the 2018 guidelines for diagnosis of IPF: UIP pattern, probable UIP pattern, indeterminate for UIP pattern, and alternative diagnosis. Despite the guideline committee decided to retain the

four categories with minor modifications ***(Table 1.1)***, a merger of the UIP and probable UIP patterns into a single category was considered, due to the evidences that patients with the probable UIP pattern and UIP pattern on HRCT have similar disease behavior and clinical courses *(Raghu et al. 2017; Fukihara et al. 2020; Kwon et al. 2020*), and that 80-85% of probable UIP pattern are histologically confirmed for UIP even if, the diagnostic approach is not different *(Lynch et al. 2018).*

Table 1.1 HRCT criteria for the UIP pattern (Table adapted from *Raghu et al. 2022)*

UIP	Probable UIP	Indeterminate for UIP	Alternative diagnosis
○ **Predominantly subpleural and basal distribution; distribution is often heterogeneous***	○ Predominantly subpleural and basal distribution; distribution is often heterogeneous	○ Subpleural and basal predominant	○ Upper-lung or mid-lung predominant fibrosis
○ **Reticular pattern with peripheral traction bronchiectasis or bronchiolectasis+**	○ Reticular pattern with peripheral traction bronchiectasis or bronchiolectasis	○ HRCT features and/or distribution of lung fibrosis that do not suggest any specific etiology	○ Peribronchovascular predominance with subpleural sparing
○ **Honeycombing**			○ Predominant consolidation, extensive pure ground glass opacity (without acute exacerbation), extensive mosaic attenuation with extensive sharply defined lobular air trapping on expiration, diffuse nodules or cysts

* Variants of distribution: occasionally diffuse, may be asymmetrical.
+ Reticular pattern is superimposed on ground glass opacity, and in these cases, it is usually fibrotic. Pure ground glass opacity, however, would be against the diagnosis of UIP or IPF and would suggest AE, hypersensitivity pneumonitis, or other conditions.

The typical HRCT features seen in UIP include reticular opacities with obligatory honeycombing, often associated with traction bronchiectasis/bronchiolectasis (**Figure 1.4**). Ground glass opacities may also be present, but they are not the predominant abnormalities and, if present, are usually admixed with reticular abnormality and honeycombing. All these features are characteristically peripheral/subpleural with basal predominance, although they are often patchy; some degree of upper lung involvement is also common, and in some cases the craniocaudal distribution of UIP may be relatively uniform (*Gruden et al. 2013*). Up to 25% of patients with IPF have an asymmetric distribution of fibrosis (*Tcherakian et al. 2011)*

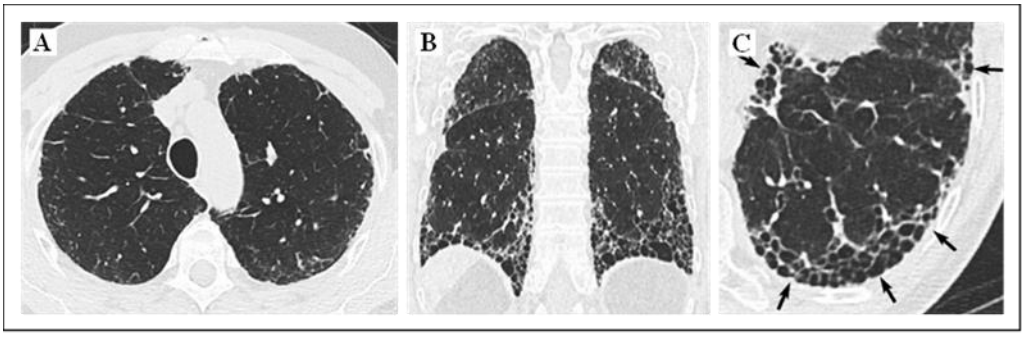

Figure 1.4 Typical UIP HRCT pattern (Image adapted *Raghu et. al 2018*). Axial and coronal HRCT images **(A-C)** for a patient with typical UIP showing the presence of subpleural and basal predominance of reticular abnormality with traction bronchiectasis and honeycombing, with a clear craniocaudal gradient on coronal images **(B). (C)** Magnified view of the left lower lobe illustrating typical characteristics of honeycombing, consisting of clustered cystic airspaces with well-defined walls and variable diameters (arrows).

The histopathological criteria that characterize UIP and probable UIP were reviewed and confirmed. A diagnosis of UIP made by biopsy is predicated on a combination of the following: 1) patchy dense fibrosis with architectural distortion (i.e., destructive scarring and/or honeycombing); 2) a predilection for subpleural and paraseptal lung parenchyma; 3) fibroblast foci; and 4) the absence of features that suggest an alternative diagnosis (2). When all of these features are present, a UIP pattern can be established with confidence. "Probable UIP" refers to biopsies in which some of these findings are present in the absence of features to suggest an alternative diagnosis.

The predictive positive value of radiological diagnosis of UIP pattern on HRCT has been reported to be between 90-100% in several studies *(Raghu et al. 2018)*. Therefore, in the appropriate clinical context, a typical UIP pattern by HRCT provides a secure diagnosis of IPF without the need to perform a SLB or other invasive tests *(Lynch et al. 2018*). Conversely, SLB should be considered when the CT pattern is "probable" or "indeterminate" with UIP, or when the clinical features suggest an alternative diagnosis. Despite histopathology is no longer the diagnostic gold standard in IPF, SLB remains in the 2018 guidelines an important method for the histological confirmation of the UIP pattern and consequently for the final diagnosis of IPF. Therefore, an appropriate combination of HRCT imaging patterns and histological patterns is essential to establish a final diagnosis (*Raghu et al. 2018)*. Video-assisted thoracoscopic surgery is the preferred approach to SLB for patients who can tolerate single lung ventilation, rather than open thoracotomy. In patients with severe physiologic impairment or substantial comorbidity, the risks associated with SLB may outweigh the benefits of establishing a secure diagnosis of IPF: therefore, the final decision regarding whether to pursue a biopsy must be tailored to the clinical situation of the individual patient. Ideally, the biopsy samples should be taken from multiple lobes, due to the high variability in the distribution and morphology of abnormalities and should measure at least 2-3 cm along the pleural margin and be 1-2 cm deep (*Cavazza et al. 2010*).

The histopathologic hallmark and chief diagnostic criterion of UIP is a low magnification appearance of patchy dense fibrosis that is causing remodeling of lung architecture, often resulting in honeycomb changes, and alternates with areas of less affected parenchyma (**Figure 1.5**). These histopathologic changes typically affect the subpleural and paraseptal parenchyma most severely. Inflammation is usually mild and consists of a patchy interstitial infiltrate of lymphocytes and plasma cells associated with hyperplasia of type II pneumocytes and bronchiolar epithelium.

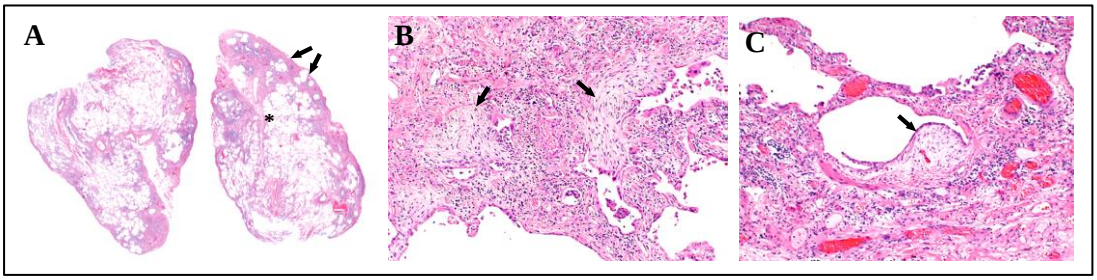

Figure 1.5 Typical histological UIP-IPF pattern (Image adapted from *Lynch et al. 2018*). **(A)** Scanning power microscopy showing classical UIP-IPF pattern characterized by dense fibrosis with a predilection for subpleural and paraseptal parenchyma with associated architectural distortion in the form of microscopic honeycomb change (arrows) and relatively unaffected lung parenchyma (*). **(B-C)** Higher-magnification photomicrograph shows readily identifiable fibroblast foci (arrows). The fibroblast foci are pale and oedematous and somewhat convex or rounded in appearance and adjacent to scarring.

The fibrotic areas are composed mainly of dense collagen, although scattered subepithelial foci of proliferating fibroblasts and myofibroblasts (fibroblast foci) are often present. Microscopic honeycombing is characterized by cystic fibrotic airspaces that are commonly lined by bronchiolar epithelium and filled with mucus and inflammatory cells. Smooth muscle metaplasia in the interstitium is commonly seen in areas of fibrosis and honeycombing.

A definitive pathologic diagnosis of the UIP pattern can be made when all these features are present, particularly when honeycombing is present. However, even in the absence of honeycombing, a definite diagnosis of a UIP pattern can still be made if all of the other typical features are present. Complete histopathological criteria for the diagnosis and exclusion of UIP pattern are reported in **Table 1.2**.

Table 1.2 Histopathological criteria for the UIP pattern (Table adapted from *Raghu et al. 2018*)

UIP	Probable UIP	Indeterminate for UIP	Alternative diagnosis
○ Dense fibrosis causing architecture remodelling with frequent honeycombing ○ Patchy lung parenchyma involvement by fibrosis ○ Predominant subpleural and/or paraseptal distribution of fibrosis ○ Fibroblast foci at the edge of dense scars	○ Some histologic features from column 1 are present but to an extent that precludes a definite diagnosis of UIP-IPF *And* ○ Absence of features to suggest an alternative diagnosis *Or* ○ Honeycombing only	○ Fibrosis with or without architectural distortion, with features favoring either a pattern other than UIP or features favoring UIP secondary to another cause ○ Some histologic features from column 1, but with other features suggesting an alternative diagnosis	○ Features of other histologic patterns of IIPs (e.g., absence of fibroblast foci or loose fibrosis) in all biopsies ○ Histologic findings indicative of other fibrotic disease (e.g., fibrotic hypersensitivity pneumonitis, Langerhans cell histiocytosis, sarcoidosis, or smoking-related interstitial fibrosis

1.5 Current treatment for IPF

Recent research on pathogenesis of IPF has promoted notable advances in pharmacotherapeutic treatment. There are currently two recommended antifibrotic drugs with pleiotropic mechanisms of action, Nintedanib and Pirfenidone, that both have been shown to delay the progression of pulmonary fibrosis and reduce mortality, but there is still no cure for IPF *(Cerri et al. 2019; Somogyi et al. 2019)*.

Pirfenidone (Esbriet®), an orally administered pyridine, is a small molecule with a pleiotropic effect developed by Roche and approved for clinical use in the treatment of mild-to-moderate IPF by the two major drug agencies, the European Medicines Agency (EMA) and the American Food and Drug Administration (FDA) in 2011 and 2014 respectively. The mechanism of Pirfenidone is currently unclear. It can inhibit TGF-β-mediated fibroblast proliferation and differentiation of fibroblasts into myofibroblasts by attenuating signal transduction induced by TGF- β1/Smad3 *(Molina-Molina et al. 2018)*. In addition, Pirfenidone can also inhibit differentiation of myofibroblasts by regulating PDFG, a fibroblast mitogen receptor, even if the specific mechanism is still unclear *(Ruwanpura et al. 2020)*. Studies have found that Pirfenidone can resist the loss of E-cadherin, the main intermediary protein of A549 cell epithelial cell transformation induced by TGF-β, and pulmonary fibrosis in a rat model of silicosis, indicating that PFD can also inhibit epithelial cell transformation *(Zhang Y et al. 2019)*. The oxidative stress process in lung diseases leads to irreversible oxidative modification of protein and DNA and mitochondrial dysfunction. Pirfenidone treatment can improve mitochondrial respiration, possibly by detoxifying mitochondrial peroxidase, such as glutathione peroxidase, thus revealing ability to maintain normal mitochondrial function *(Plataki et al. 2019)*. Therefore, its anti-fibrosis effect may function through reducing the formation of reactive oxygen species and oxidative stress. The conditional recommendation in international guidelines for the use of Pirfenidone in patients with IPF is essentially based on the outcomes of three phase III clinical trials: CAPACITY-004, CAPACITY-006 and ASCEND (*Noble et al. 2011; King et al. 2014*). Specifically, the two concurrent CAPACITY trials involved patients with mild-to-moderate IPF, and the primary endpoint was change in percentage predicted FVC from baseline to week 72. Although the study CAPACITY-004 met this primary endpoint showing an average decline in FVC of 8.0% in the high-dose Pirfenidone arm (2,403 mg/day) compared to 12.4% in the placebo arm at 72 weeks of treatment (p=0.001), in the study CAPACITY-006 the difference between groups in predicted FVC change at week 72 was not significant (–9.0% *versus* –9.6% in the treatment and placebo arms respectively, p=0.501) **Figure 1.6 A** (*Noble et al. 2011*). Due to discrepancies between the two

CAPACITY trials in meeting their primary endpoints, the US FDA requested a subsequent double-blind, randomized, placebo-controlled phase III trial to confirm the efficacy and safety of Pirfenidone in IPF. In the ASCEND study, the inclusion criteria were modified to enroll patients at higher risk of disease progression and the primary endpoint was the change from baseline to week 52 in the percentage of predicted FVC. The mean decline from baseline in FVC was 235 mL in the Pirfenidone group and 428 mL in the placebo group (absolute difference 193 mL, relative difference 45.1%; p<0.001) **Figure 1.6 B** (*King et al. 2014*). Furthermore, a pooled analysis of the two CAPACITY and the ASCEND studies (a total of 1247 patients) revealed a positive outcome in terms of mortality. At 1 year, Pirfenidone at 2,403 mg/day reduced the proportion of patients with a ≥10% decline in percentage predicted FVC or death by 43.8% and increased the proportion of patients with no decline by 59.3% compared with placebo (*Noble et al. 2016*). Overall, Pirfenidone was generally well tolerated in practice, with the most common side effects being gastrointestinal discomfort and skin-related complications which, however, rarely led to treatment discontinuation.

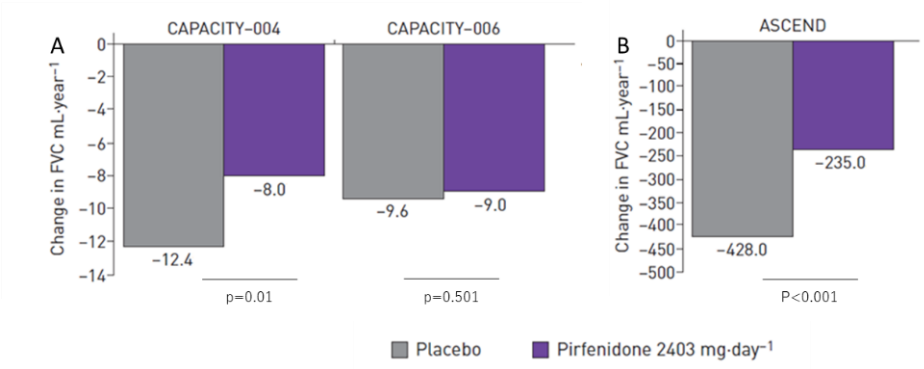

Figure 1.6 Mean change from baseline in percentage predicted FVC in the **(A)** phase III CAPACITY-004, CAPACITY-006, and **(B)** ASCEND studies (from *Richeldi et al. 2018*).

Nintedanib (Ofev®), an indolinone derivative, is an orally active small molecule developed by Boehringer Ingelheim and approved for the treatment of IPF by the EMA and FDA, in 2015 and 2014 respectively. Nintedanib, also known as BIBF 1120, is a potent intracellular tyrosine kinases inhibitor which acts on multiple downstream signalling pathways involved in fibrogenesis. Specifically, Nintedanib competitively binds to the adenosine triphosphate binding pocket of these targets inhibiting the activation of the platelet-derived growth factor receptors (PDGFR), vascular endothelial growth factor receptors (VEGFR) and fibroblast

growth factor receptors (FGFR) signalling cascades which are critically involved in the proliferation, migration and differentiation of lung fibroblasts/myofibroblasts, the hallmark cells in IPF (*Hilberg et al. 2008*). Originally developed as a potent angiogenesis inhibitor for cancer treatment, Nintedanib also proved to exert anti-fibrotic activities both *in-vitro* in human lung fibroblasts and *in-vivo* in bleomycin-induced pulmonary fibrosis in rodents. In human lung fibroblasts, Nintedanib has been shown to inhibit fibroblast proliferation, growth factor-stimulated fibroblast motility and contraction, and TGF-β-induced fibroblast to myofibroblast transformation (*Hostettler et al. 2014*). In animal models of pulmonary fibrosis, Nintedanib has demonstrated anti-fibrotic effects including reductions in lung collagen content and morphometric fibrosis scores and reduced expression of TGF-β and procollagen I. Anti-inflammatory effects of Nintedanib have been also demonstrated by reductions in lymphocytes and neutrophils counts in BALF, reduced inflammatory cytokines and reduced histological inflammation (*Wollin et al. 2014; Wollin et al. 2015*).

At a clinical level, the conditional recommendation for the use of Nintedanib in international guidelines is based on the outcomes from three clinical studies: TOMORROW, INPULSIS-1 and INPULSIS-2 (*Richeldi et al. 2011; Richeldi et al. 2014*). The phase II TOMORROW trial showed that Nintedanib, 150 mg twice daily, effectively reduced the annual rate of decline in FVC by 68.4%, as compared to placebo group (60 mL *versus* 190 mL, respectively; $p<0.06$ with the closed testing procedure for multiplicity; $p<0.01$ with hierarchical testing) (**Figure 1.7A**) (*Richeldi et al. 2011)*. Subsequently, the phase III program INPULSIS, consisting of two 52-week parallel, identical placebo-controlled, multicentral trials was developed to further evaluate the efficacy and safety of Nintedanib in 1066 patients with IPF. Outcomes from both studies confirmed Nintedanib efficacy in reducing significantly the annual rate of decline in FVC, the primary endpoint, as compared with placebo group (INPULSIS-1: difference 125.3 mL (−114.7 mL and −239.9 mL, respectively; $p<0.001$); INPULSIS-2: difference 93.7 mL (−113.6 mL and −207.3 mL, respectively; $p<0.001$)) (**Figure 1.7B**) (*Richeldi et al. 2014)*. A pooled and meta-analyses of the TOMORROW and the two INPULSIS studies further supported the beneficial effect of Nintedanib versus placebo over 52 weeks both in terms of disease progression, time to first acute exacerbation, maintenance of health-related quality life and time to all-cause and on-treatment mortality (*Richeldi et al. 2016*). As observed for Pirfenidone, post-hoc analysis suggested that Nintedanib is equally efficacious in patients with mild or severe disease irrespective of baseline characteristics (*Costabel et al. 2016)* and appears to be equally effective in patients with a "possible UIP" pattern compared to those with "definite UIP" radiologically (*Raghu et al. 2017*). The most common adverse

events related to the use of Nintedanib mainly affect the gastro-intestinal tract. Particularly, diarrhea is the most frequent adverse event, followed by nausea and vomiting; weight and appetite loss are also quite frequent (*Richeldi et al. 2016*).

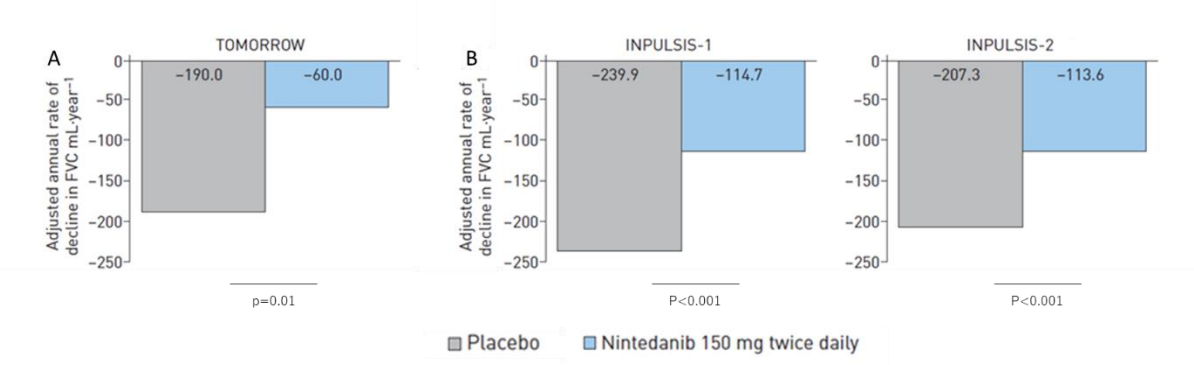

Figure 1.7 Annual trate of change from baseline over time in FVC in the **(A)** phase II TOMORROW and **(B)** from phase III INPULSIS-1 and INPULSIS-2 studies (*Richeldi et al. 2018*).

Since the two drugs have very similar beneficial effects in treating IPF (*Rochwerg et al. 2016*), there is no general answer about which drug prescribe to a patient with IPF. Actually, there have been no head-to-head comparisons, and there are no biomarkers that may help to identify responders to either drug. Therefore, in the absence of clear evidence, treatment decision will depend on what is more appropriate for each single patient (e.g. patient preference, comorbidities and concurrent medications). For instance, photosensitivity and cutaneous rash limit the use of Pirfenidone in patients that possess dermatologic pathology or that cannot avoid sun exposure. Conversely, Nintedanib will be prescribed with caution in patient who receives concomitant anticoagulant therapy due to the anti-angiogenic properties of the drug. Moreover, no data are available to guide clinicians regarding the timing of initiation of therapy, how a response should be defined, and when the therapy should be discontinued (*Raghu and Selman, 2015*).

1.6 Future pharmacological approaches in IPF

IPF treatment remains one of the major challenges for the respiratory physicians and for the community of clinical and translational investigators. Despite Pirfenidone and Nintedanib, has been approved for the treatment of IPF, many gaps are still to be filled. First, neither of the two drug stops the disease, but they only slow the pace of disease progression; moreover, both therapies have tolerability issues, and because side effects are relatively common, they lead to treatment discontinuation in a non-negligible proportion of patients. Second, neither drug improves quality of life or symptoms, such as dyspnea and cough without mirroring clearly a significant survival effect. Finally, at present, there is no treatment that can cure IPF. The only possibility to improve the survival of patients with IPF is the lung transplantation, but, due to age and comorbidities, this represents a realistic therapeutic option only for a small portion of selected patients. For this reason, the remaining unmet medical needs continue to stimulate the research toward the identification of new concepts or interventions aimed at treating IPF. These strategies may include the use of combination therapies, novel drugs and biomarkers guiding therapy.

1.6.1 Combination Therapies

As mentioned above, pulmonary fibrosis is a complex pathological progression in which pathogenic factors activate complex fibrotic pathways in various cells *(Schafer et al.2020)*. Therefore, combined treatment of multiple drugs with different targets and mechanisms involved in IPF is of great significance, but adverse effects and tolerance also need attention.

So far, three studies have mainly explored the feasibility of combined treatment with Nintedanib and Pirfenidone in individuals with IPF. In 2015, the first randomized phase II trial in Japanese patients with IPF demonstrated that Nintedanib had an acceptable safety profile when added to ongoing Pirfenidone therapy *(Ogura et al. 2015)*. Later in 2017, in the INJOURNEY trial, Vancheri and colleagues investigated the safety of combining Pirfenidone and Nintedanib in treating IPF. In this trial, IPF patients were randomized to receive Nintedanib with add-on Pirfenidone or Nintedanib alone in an open-label study for 12 weeks. The total number of adverse effects were similar in the two groups and in keeping with the adverse event profiles of each drug; however, gastrointestinal adverse events occurred with greater frequency in the combination group. Despite this, adherence rates were similar in both groups, thus suggesting that Nintedanib plus Pirfenidone therapy had a feasible safety and tolerability profile in IPF. Moreover, although the study was not appropriately powered to assess efficacy, there were promising exploratory effects on lung

function decline in the combination therapy compared to Nintedanib alone (12-week FVC decline of −13.3 mL versus −40.9 mL, respectively) *(Vancheri et al. 2018)*. In another study, the safety of Nintedanib added to pre-existing Pirfenidone treatment in 89 IPF patients showed no new safety signals to the known safety profile of either therapy alone *(Flaherty et al. 2018)*. Another recent open-label trial also indicated that co-administration of these drugs had no relevant effect on their pharmacokinetic drug-drug interaction *(Richeldi et al. 2019)*. However, other combination therapies in IPF have been less promising, such as in the phase II PANORAMA study, that investigated the tolerability and safety of pirfenidone with add-on N-acetylcysteine, based on its antioxidative effects, yielding negative results *(Behr et al. 2016)*, and the INSTAGE study, which failed to meet its primary endpoint when comparing Nintedanib with Sildenafil, a phosphodiesterase-5 inhibitor, versus Nintedanib alone *(Kolb et al. 2018)*. Combination treatment with inhaled N-acetylcysteine and pirfenidone for 48 weeks even appeared to lead to a worse prognosis of IPF *(Sakamoto et al. 2021)*

Overall, although the results of these trials provide evidence that the combination of Pirfenidone and Nintedanib are promising with regards to tolerance and safety, whether combination therapy adds benefit over single-agent therapy is still unknown. The next step in this regard should be to perform larger controlled studies to investigate the efficacy of these combination therapies. This may require the use of different endpoints, or the enrolment of subgroups of patients with IPF, for example patients with rapidly progressing disease, or disease that is refractory to monotherapy

1.6.2 Novel therapeutics targets

Due to the adverse effects of current drugs for IPF and their inability to reverse or even stop the pathology, IPF research is increasingly focused on developing new molecular targets and treatment options **(Figure 1.8)**. Currently, there are 39 assets in phase I, 31 in phase II and three drugs in phase III.

Phosphodiesterase 4B (PDE-4) inhibitors

Phosphodiesterase 4, also known as PDE4, is a group of proteins that have important roles in human cells. PDE4 has traditionally been implicated in the regulation of inflammation and the modulation of immunocompetent cells, and the three selective PDE4 inhibitors currently available support a beneficial role for PDE4 inhibitors in inflammatory and/or autoimmune diseases *(Sakkas et al. 2017; Li et al. 2018)*. Evidence points to the involvement of a range of immune cells and inflammatory responses in IPF, particularly

studies in animals or with human cells have shown that drugs that block the activity of PDE4 reduce inflammation and scarring. *(Matsuhira T et al. 2020; Phillips JE et al. 2020)*. BI 1015550 is a new oral drug, developed by Boehringer Ingelheim, that blocks the activity of PDE4B. BI 1015550 successfully completed a Phase II trial in 147 IPF patiens (NCT04419506), including those using anti-fibrotic treatments (n=49) and those without them (n=48). The drug was able to prevent the decrease in lung function (measured by FVC) after 12 weeks, both in participants using antifibrotic treatment and those not using antifibrotic treatment in contrast to with placebo. Moreover also effects on some biomarkers such as KL-6, MMP-7, SP-D and E-selectin were observed following treatment with BI 1015550 irrespective of use of antifibrotics Currently two Phase III studies are ongoing in 642 IPF patients (NCT05321069) and 694 PF-ILD patients (NCT05321082) In both studies the primary endpoint will be FVC at 52 weeks. Studies are estimated to be completed in March 2025.

Prostacyclin receptor agonist

Proliferation of human lung fibroblasts in the pulmonary interstitial tissue is a hallmark of this disease and is driven by prolonged ERK signalling in the nucleus in response to growth factors such as platelet-derived growth factor (PDGF). Agents that increase cAMP have been suggested as alternative therapies, as this second messenger can inhibit ERK *(Roberts et al. 2021)*. Treprostinil, a full agonist of the prostacyclin receptor currently approved for the treatment of pulmonary arterial hypertension and PH-ILD to improve exercise ability leads to intracellular cAMP increased concentrations and causes complete inhibition of PDGF-induced proliferation. Treprostinil also possesses a significant effect on PPARs. PPARβ and PPARγ both demonstrated antiproliferative effects on human lung fibroblasts upon in vitro treprostinil treatment. Preclinical and animal model research supports that treprostinil may exert its therapeutic effect via multiple pathways, including inhibiting fibroblast-to-myofibroblast differentiation, fibroblast proliferation *(Ayabe et al. 2013; Corboz et al. 2019)*, fibroblast migration *(Clapp et al. 2020)*, fibronectin deposition *(Lambers et al. 2018)*, and mast cell-mediator release *(Safholm et al. 2015)*. The *in vitro* and *in vivo* evidence of treprostinil's antiproliferative potential is intriguing for its therapeutic potential as an inhaled treatment for lung fibrosis in that there is yet to be an inhaled therapy with proven antifibrotic efficacy. Treprostinil is unique among the prostacyclin mimetics approved for PAH in that it shows distinct activity at additional prostaglandin receptors that may contribute to its therapeutic benefit. Patients with IPF may benefit from an inhaled therapy owing to targeted deposition of drug at the disease site,

rapid onset of action, and fewer systemic side effects than with oral administration. In addition, with fibrosis causing lung architectural distortion and associated vascular ablation, it is uncertain where in the lung any systemically delivered agent is actually delivered to target areas of interest to affect fibrosis. Based on these biologic and physiologic basis a Phase III clinical trial (NCT04708782) is currently underway to assess the efficacy of inhaled treprostinil in patients with pulmonary fibrosis.

Lysophosphatidic acid (LPA) pathway inhibitors

LPA, which acts through at least six G protein-coupled receptors, called LPARs, is the origin of the signalling cascade of various fibrogenic pathways. LPA1R has been implicated in the development of IPF given its role in mediation of fibroblast recruitment, vascular leak, and endothelial barrier dysfunction in animal models. In the bleomycin mouse model of pulmonary fibrosis, for example, LPA1R-deficient mice showed reduced levels of fibroblast recruitment and decreased vascular permeability, indicating a protective role for decreased LPA signaling (*Tager et al. 2008*).

BMS986020 is an oral, selective small-molecule antagonist of LPA1R, developed by Bristol-Myers Squibb. In a phase II, multiple-dose, placebo-controlled trial (NCT01766817), that assessed the efficacy and safety of BMS-986020 in patients with IPF (who were not on Pirfenidone or Nintedanib), treatment with BMS986020 600 mg twice a day exhibited significantly slower rates of decline in FVC from baseline to 26 weeks versus placebo. Although dose regimens of BMS-986020 were well tolerated in most patients, they were associated with presumed hepatobiliary toxicity as manifested by dose-related elevations in hepatic transaminases and blood alkaline phosphatase in some patients, and treatment-related serious adverse events of cholecystitis, which led to early termination of the study (*Palmer et al. 2018*). Preclinical research indicated that these hepatobiliary effects observed with BMS-986020 were likely off-target effects specific to this molecule and not mediated via antagonism of LPA, based on comparing BMS-986020 with a structurally distinct LPA1R (*Rosen et al. 2017*). These results suggest that structural variations in LPA1R antagonists may result in different safety profiles in patients with IPF. A Phase 2 Study (NCT04308681) of a novel promising LPA1R antagonist with oral bioavailability and antifibrotic activity (BMS-986278) in 270 participants with pulmonary fibrosis was completed. The positive findings supported the launch of a Phase 3 study (NCT06003426). Recruitment of patients has started and data will be completed in October 2023.

1.6.3 Attrition rate of anti-fibrotic drugs

Despite the great effort of the scientific community to discover novel anti-fibrotic approaches and the improved knowledge of the pathogenic process, there is still a significant attrition rate in the development of new drugs as shown by the failure of drugs in phase II and III clinical trials.

CTGF inhibitors

As mentioned above, *CTGF* is an important pro-fibrotic growth factor associated with extracellular matrix secretion and abnormal tissue repair *(Yanagihara et al. 2020)*. CTGF is normally expressed in low levels in healthy individuals, however, when expressed in excess it leads to upregulation of TGF-β, deposition of ECM and inhibition of ECM degradation through the inhibition of MMPs (*Wang et al. 2011*). In preclinical studies, rodents knocked out for Smad3 genes expressed lower production of CTGF and were found to be resistant to TGF-β-induced lung fibrosis (*Bonniaud et al. 2004*). Moreover, elevated CTGF levels has been measured in serum and BALF of IPF patients (*Kono et al. 2011*).

In consideration of its important role in fibrosis development, CTGF has been suggested as a potential molecular target in IPF. Pamrevlumab (FG-3019), a fully humanised monoclonal antibody directed against CTGF, was developed by FibroGen. In the PRAISE study (NCT01890265), a phase II, randomised, double-blind, placebo-controlled trial, Pamrevlumab, administered at two doses (15 mg/kg and 30 mg/kg) by intravenous infusion every 3 weeks, demonstrated a good safety and tolerability profile and yielded promising outcomes with regard to changes from baseline in FVC percentage predicted at week 48, disease progression and extent of pulmonary fibrosis by quantitative HRCT imaging (*Gorina et al. 2017; Richeldi et al. 2020*). Two parallel phase III trials, ZEPHYRUS and ZEPHYRUS-2 (NCT03955146 and NCT04419558) were announced to further evaluate the efficacy and safety of Pamrevlumab (30 mg/kg intravenous administered every 3 weeks), in subjects with IPF who are not being treated with approved IPF therapies and in subjects with IPF who were previously treated with an approved therapy but who discontinued that therapy, respectively. Recently (July 2023), Fibrogen announced the stop of these clinical trials because Pamrevlumab failed to significantly improved FVC in treated IPF patients. Pamrevlumab was generally safe, with most treatment-related side effects being mild or moderate. Serious side effects occurred in about the same proportion of patients in the Pamrevlumab and placebo groups (28.2% vs. 34.3%). Further details were not provided in the press release.

Pentraxin (PTX)-2

PTX-2 also known as serum amyloid P, is a circulating innate immune regulatory protein that binds to Fc-gamma receptors on monocytes and inhibits their differentiation into pro-fibrotic fibrocytes and TGF-β producing macrophages, thus promoting epithelial healing and resolution of fibrosis (*Pilling et al. 2007*). Low serum PTX-2 levels have been observed in patients with IPF (*Dillingh et al. 2013*), and in animals with bleomycin-induced fibrosis administration of recombinant PTX-2 has been shown to reduce collagen content and α-SMA levels (*Murray et al. 2010*).

Zinpentraxin alpha (PRM-151) was an intravenously administered recombinant form of human PTX-2 protein (*Getsy et al. 2011*), which was developed by Roche. A phase I trial (NCT01254409) assessing safety, tolerability and pharmacokinetics of PRM-151 in patients with IPF has shown a trend towards improvement on FVC percentage predicted and 6-min walk distance (6MWD) during the treatment period (*van den Blink et al. 2016*). A further phase II study (NCT02550873) demonstrated significant effects in reducing pulmonary function decline and stability in 6MWD over 24 weeks compared to placebo with an acceptable safety profile (*Raghu et al. 2018*). A phase III trial (NCT04552899) for Zinpentraxin alpha in IPF was announced, using change from baseline to week 52 in FVC as a primary endpoint and 6MWD as a key secondary endpoint. However, in February 2023 Roche discontinued the asset after the pivotal Starscape trial was stopped for futility.

Autotaxin (ATX) inhibitors

ATX is an enzyme that plays a central role in epithelial cell apoptosis and endothelial cell damage through the release of bioactive LPA (*Aoki et al. 2008*). Specifically, ATX converts lysophosphatidylcholine into LPA, and represents the main source of extracellular LPA.. Furthermore, levels of LPA and ATX have been found to be elevated in BALF and exhaled breath condensate in patients with IPF, thus suggesting a role of the ATX-LPA pathway in fibrogenesis (*Tager et al. 2012; Oikonomou et al. 2012; Montesi et al. 2014*).

GLPG1690 was an oral selective ATX inhibitor, developed by Galapagos, targeting the LPA signaling. GLPG1690 has been shown to be effective as anti-fibrotic in several animal models. In mice with bleomycin-induced pulmonary fibrosis, GLPG1690 reduced collagen content and lung fibrosis (*Tager et al. 2008*) and was superior to Pirfenidone on both of these measures (*Ongenaert et al. 2016*). Moreover, in GLPG1690-treated mice, there was an inverse relationship between LPA and GLPG1690 plasma levels (*van der Aaar et al. 2016*). The safety, tolerability, pharmacokinetic and pharmacodynamic profile of GLPG1690 was analyzed over a 12-week period, in the phase IIa FLORA trial

(NCT02738801). GLPG1690 was well tolerated by IPF patients with a similar safety profile, as placebo and preliminary efficacy analyses demonstrated encouraging results towards halting FVC decline (*Maher et al. 2018*). The two parallel phase III multicenter studies (ISABELA 1 and 2) started in November 2018 to further evaluate the efficacy of GLPG1690 for the treatment of IPF (NCT03733444 and NCT03711162) (*Maher et al. 2019*). Unfortunately, in February 2021, the ISABELA phase III trials were discontinued, following a regular review of unblinded data, that concluded that GLPG1690 benefit-risk profile no longer supported continuing these studies.

1.6.4 Biomarkers

The IPF disease course and response to anti-fibrotic therapy demonstrates marked heterogeneity, making diagnosis and individual prognosis very difficult. Thus, a prerequisite for future personalized therapy for IPF could be the development of biomarkers that can guide diagnostic, prognostic and therapeutic approaches in managing the disease. Currently, several potential biomarkers categorized according to the different pathways involved in the pathogenesis of IPF in three groups, namely biomarkers associated with AEC dysfunction, biomarkers associated with ECM remodeling and fibroproliferation, as well as biomarkers related to immune dysfunction, are under study and some of the most promising candidates are summarized in **Table 1.3**.

Diagnostic biomarkers

Despite advances in imaging technology and disease classification systems, accurate diagnosis of IPF can remain elusive. Therefore, the identification of specific and non-invasive biomarkers that can guide the early diagnosis and differential diagnosis of IPF is of great interest. A number of peripheral blood biomarkers, including markers of AEC damage, immune dysfunction as well as ECM remodeling such as MMPs, have been studied with the aim to discriminate IPF patients from healthy individuals. However, their ability to distinguish IPF from other forms of ILDs is still conflicting (*Jee et al. 2019*). The PROFILE (Prospective Study of Fibrosis in Lung Endpoints) study, the first study performing a sequential evaluation of >100 serum protein biomarkers, demonstrated the importance of these markers in IPF, showing significantly elevated levels of MMP-1, MMP-7 and SP-D in IPF patients compared to healthy controls (*Saini et al. 2012*). Notably, in the pioneer work by Rosas et al., levels of MMP-1 and MMP-7 were found to be elevated in plasma, in BAL fluid (BALF), and in tissue of IPF patients as compared to healthy controls, and their combination appeared to be able to distinguish IPF patients

from those with either chronic respiratory disorders (*Rosas et. al 2008*) or other ILDs (*Morais et al. 2015*). The biomarkers of AEC damage and dysfunction, SP-D and Krebs von den Lungen (KL-6)/Mucin 1 (MUC1), have also been widely used in clinical practice in Japan as part of the diagnostic work-up for ILDs for more than 10-years, although evidence from clinical trials validating their clinical efficacy in IPF remains limited (*Ishikawa et al. 2012; Homma et al. 2018*). Further studies in broader prospective cohorts will be needed to establish the reliability of these markers in routine clinical settings and thus, currently none of these are recommended by guidelines for diagnostic purposes in IPF (*Raghu et al. 2022*).

Prognostic biomarkers

Progression in IPF is challenging to predict due to the heterogeneity of the population. FVC decline has been shown to be a predictor of mortality in IPF (*Brown et al. 2022*) and is the most robust parameter adopted in clinical trials. However, baseline FVC is not an early predictor of the disease. Therefore, prognostic biomarkers that reflect disease state, in term of severity or progression are urgently needed to guide patient management. Several biomarkers are currently under exploration, with promising significant association with prognosis of IPF. Threshold serum levels of KL-6, or sequential changes in KL-6 levels, have been shown to predict lung function decline or outcome in patients with IPF. Elevated baseline KL-6 levels have been also associated with increased risk of AE-IPF. High serum levels of SP-A and SP-D have been associated with decreases in DLCO and FVC as well as with early mortality. Among the biomarkers associated with immunity dysfunction, C-C motif chemokine ligand 18 (CCL-18) demonstrated to correlate with lung function and mortality in both IPF patients. Finally, among those associated with ECM remodeling, MMP7 is considered one of the most promising biomarkers in IPF *(Inoue et al. 2020)*. Pooled data from ISABELA 1 and 2 studies indicate that MMP-7 is a prognostic biomarker of IPF disease progression, and that circulating levels correlate with disease severity assessed by FVC and DLCO *(Maher et al. 2023)*. Remodelling of extracellular matrix is pivotal to the development and progression of IPF and results in distinct alterations in collagen turnover. A recent study *(Organ et al. 2019)* demonstrated that synthesis markers for type-3 (PRO-C3) and-6 (PRO-C6) collagen are elevated in subjects with IPF compared with healthy controls and distinguish individuals with progressive disease, suggesting that these biomarkers may reflect underlying pathophysiology driving disease activity in IPF.

Collagen type-3, a fibrillar collagen, forms a major component of the lung interstitial extracellular matrix and is synthesized by activated fibroblasts *(Frantz et al. 2010)*.

Collagen type-3 is increased in IPF, with high levels of type-3 pro-collagen peptide reported in serum and lavage fluid. In the case of collagen type-3, the synthesis neoepitope, PRO-C3, appears to be a better biomarker of progressive disease than the paired degradation biomarker, C3M. Interestingly, in subjects with more stable disease, the ratio of PRO-C3 to C3M is significantly lower; supporting the idea that synthesis, and increased turnover in general, may be reflective of active remodelling and disease progression. Moreover, PRO-C3 was also found to be modulated in patients dosed daily with Nintedanib, in Phase III clinical trial INBUILD, suggesting its role as therapeutic biomarker.

Collagen type-6 filaments are an integral component found at the interface between the basement membrane and interstitial matrix of the lung, and act as an important network for attachment of basement membranes, collagen fibers and cells. Previous research suggests that collagen type-6 fragments have signalling properties during wound healing and fibrogenesis and may drive poorer outcomes in fibrotic diseases *(Karsdal et al. 2017)*. Compared with other collagens, type-6 collagen has been shown to be a potent inducer of the differentiation and activation of fibroblasts to highly synthetic myofibroblasts; a key pathway leading to the production of collagen and ECM proteins *(Naugle et al. 2006)*. In addition, increased levels of serum collagen type-6 markers have been demonstrated to act as an early predictor of fibrosis in the liver *(Veidal et al. 2011)*. This evidence, coupled with data from the current study, suggest that collagen type-6 may in itself be a driver of the fibrotic process, which in turn serves as a useful marker of IPF progression.

Additional, promising predictors of progression and survival in patients with IPF are the cancer antigen (CA)19-9 and CA-125, as recently reported in the multicenter PROFILE longitudinal cohort study (*Maher et al. 2017*).

Therapeutic biomarkers

Despite some diagnostic and prognostic biomarkers are showing some promise, there is still a lack of biomarkers that can help to identify those individuals that most likely benefit from treatment (stratification biomarkers) and biomarkers that can measure the individual's treatment response (pharmacodynamic biomarkers). KL-6 levels decreased in stable IPF patients on Pirfenidone (*Kuwano et al. 2002; Okuda et al. 2013*) and Nintedanib (INBUILD Phase III clinical trial). Similarly, reduced levels of SP-D have been reported after Pirfenidone treatment in IPF in a small Japanese study (*Okuda et al. 2013; Ikeda et al. 2017*) and after Nintedanib treatment (INBUILD Phase III clinical trial). However, even if interesting, these data are quite limited, and confirmation and validation in prospective and

larger cohorts is required. Finally, the INMARK trial also investigated the effect of Nintedanib on the two markers of epithelial damage, CA19-9 and CA-125, suggesting a potential role of this latter as a biomarker of response to Nintedanib in patients with IPF (*Jenkins et al. 2020*). Taken together, reliable predictive therapeutic biomarkers are still missing and the information available so far is very limited.

Despite the last decade saw great interest, motivation, and progress in biomarkers research, driven by significant advances in the understanding of IPF pathogenesis, none of the previously described biomarkers has been validated for clinical use so far. The main reasons concern the fact that most of these biomarkers have been studied in an observational and retrospective manner, and the samples were generally limited; the lack of a longitudinal analysis in the majority of biomarkers investigated; the absence of a robust validation of the assays in independent validation cohorts; furthermore, the comparability of different studies is hindered due to the use of different collection protocols and biological materials for biomarker analysis. Other challenges that preclude pooling of results and accurate comparison of studies include the lack of a gold standard for measuring disease activity, standardized assays for biomarker testing, discrepancy in thresholds defining positive and negative results, and the highly heterogeneous nature of IPF itself.

The development of clinically validated biomarkers for IPF represents, therefore, the central challenge to translational research in the field over the next decade. In this context, an encouraging work is represented by the project PROLIFIC (PROgnostic Lung FIbrosis Consortium), that in collaboration with the Pulmonary Fibrosis Foundation and several pharmaceutical companies, is developing Multiplex well-qualified assays of a selected group of 12 relevant biomarkers in IPF, to be used within the clinical setting; such platforms should contribute to an improved screening, prognosis, and care of IPF patients.

Overall, future investigations, including longitudinal and high throughput biomarker analyses into prospective clinical trials with huge patient numbers, ideally in combination with clinical endpoints and with genotyping of these patients, will allow the identification of early predictors of disease progression and different subgroups of patients with heterogeneous disease courses, different prognosis and response to treatment. These studies should be the prerequisite for a more “personalized” medicine in patients affected by IPF.

Table 1.3 Candidate biomarkers for IPF and the strength of evidence supporting their clinical role. (Table adapted from *Inchingolo et al. 2018*)

Biomarkers	Mechanism of action	Significance in IPF
Alveolar epithelial cell damage and dysfunction		
KL-6/MUC1	High molecular-weight glycoprotein strongly expressed on bronchiolar and type II AECs, promoting migration, proliferation and survival of lung fibroblasts	Correlation with disease severity (imaging and lung function tests); increased levels suggest worse prognosis; higher levels in AE-IPF
SP-A and SP-D	Surfactant proteins produced by type II AECs and Clara cells, involved in the lung host innate immunity	Strong predictors of early mortality
CA-125 and CA19-9	Tumor markers, mucous associated carbohydrate antigens increasing in metaplastic epithelium in fibrotic lesions	Predictor of progression and increased mortality
Aberrant fibrogenesis and ECM remodelling		
MMP-1, MMP-3, MMP-7	Zinc-dependent proteases involved in the breakdown of ECM components	Correlation with disease severity; predictors of worse outcome
Neoepitopes	Circulating protein fragments generated as result of the ECM remodeling and released from the tissue into the circulation	Association with mortality; potential predictors of occurrence and outcome
Periostin	ECM protein promoting ECM deposition and mesenchymal cells proliferation	Correlation with physiological progression
Osteopontin	Glycoprotein involved in cell adhesion and migration	Support for differentiation with non-IPF ILD
Circulating fibrocytes	Bone-marrow-derived progenitor cells that circulate in the bloodstream and migrate to sites of tissue injury, differentiate into fibroblasts and are capable of producing ECM components	Correlation with lung function tests; increased level associated with worse survival
Lysyl oxidase-like 2 (LOXL2) protein	Enzyme secreted by activated fibroblasts that facilitates the cross-linking of type 1 collagen Molecules and plays a key role in ECM remodeling and fibrogenesis	Association with risk of progression and higher mortality
Immune dysregulation and inflammation		
CCL-18	Chemokine produced by alveolar macrophages involved in the stimulation of collagen production by lung fibroblasts	Predictor of progression and increased mortality
Intercellular adhesion molecule 1 (ICAM-1)	Adhesion molecule expressed on leukocytes and vascular endothelial cells; marker of oxidative stress in the lungs	Predictor of mortality
C-X-C motif chemokine 13 (CXCL-13)	Chemokine playing a role in autoimmune processes, mediating B-cell homing to inflammatory foci	Predictor of progression and mortality

Table 1.3 (continued)

Biomarkers	Mechanism of action	Significance in IPF
Immune dysregulation and inflammation		
Chitinase-3-like protein 1 (YKL-40)	Chitinase-like protein produced by alveolar macrophages and type II AECs involved in innate immunity and ECM remodeling	Predictor of worse outcome
Damaged endothelium		
VEGF	Growth factor regulating angiogenesis enhancing vascular permeability	Association with disease severity, and predictor of progression

1.7 Preclinical models of pulmonary fibrosis

IPF as a whole is intrinsically challenging to model due to its age-related, idiopathic nature and the highly complex underlying pathobiology. However, most of our understanding of this disease is based on experimental models that have improved over time, increasing in complexity and accuracy as rapidly as the availability of new and emerging technologies. To date, several models of pulmonary fibrosis are available to be used in preclinical studies, both *in-vitro*/*ex-vivo* and *in-vivo* (**Figure 1.8**).

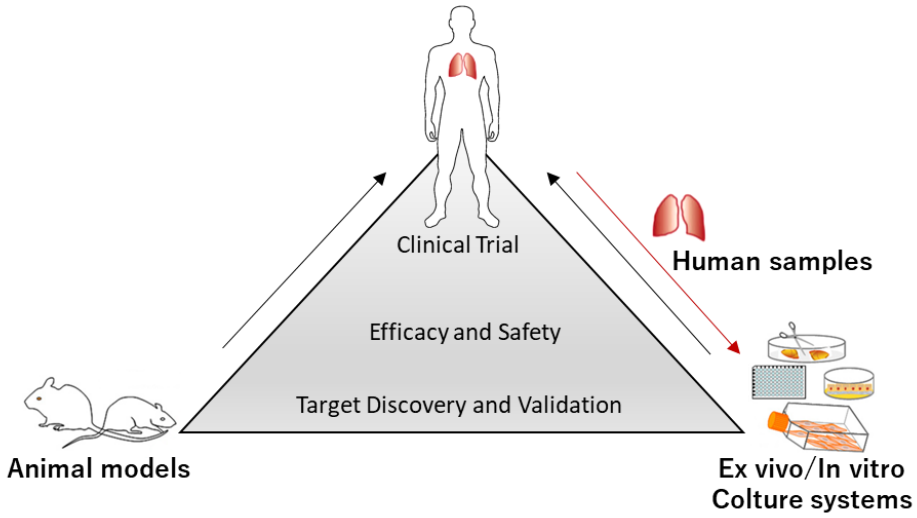

Figure 1.8 Overview of modeling for pulmonary fibrosis and integration with human disease (Image adapted and modified from *Yanagihara et al. 2020*). An integrated approach to drug development pipeline using both relevant animal models and appropriate *in-vitro/ex-vivo* approaches, should provide robust validation of pharmacological mechanisms of action and help to move promising targets to clinical trials.

1.7.1 *In-vitro* models of pulmonary fibrosis

Different lung cell types, including epithelial, endothelial, mesenchymal, and immune cells, contribute to IPF pathology. Immortalized human lung cells lines (e.g., non-small cell adenocarcinoma: A549; lung fibroblasts: IMR-90s; submucosal adenocarcinoma cell: Calu-3) have been used to model specific aspects of pulmonary fibrotic disease (*Sundarakrishnan et al. 2018*). Cell lines are feasible and easy to maintain as they are able to divide infinitely; however, immortalization induces permanent phenotypic changes in these cells and hence, results obtained using cell lines may not accurately replicate human lung physiology.

Most *in-vitro* models for pulmonary fibrosis have been based on two-dimensional (2D) cultures of cells. The simplicity of 2D culture has aided in understanding individual cellular phenomena and has led to the identification of several fibrotic mediators. However, it

remains an unsatisfactory approach due to a series of disadvantages. For instance, the primary limitation of 2D monolayer culture is their inability to mimic the three-dimensional (3D) nature of lung tissue, and so the fact that it investigates the response of cells that are completely isolated from their biological context. Moreover, the tissue culture plastic or glass are extremely stiff (106 kPa) substrates, completely different from that of the normal lung parenchyma (1–15 kPa) (*Engler et al. 2006*), and because matrix stiffness has been shown to affect cellular phenotype, standard tissue culture substrates do not permit studies evaluating cellular mechanics.

Scar-in-a-jar *in-vitro* assay has become increasingly popular in many research laboratories for screening compounds. This assay is similar to a 2D culture as it involves seeding a monolayer of fibroblasts into a tissue culture treated plastic substrate. However, the uniqueness of this model is that it involves the addition of Ficoll which is a non-interacting, natural hydrophilic polysaccharide capable of causing macromolecular crowding promoting collagen synthesis at a faster rate, thus reducing incubation time. Therefore, this assay allows *in situ* assessment of the area of collagen type I deposition per cell and it is also possible to detect collagen cross-linking. Furthermore, it is considered high-throughput assay for compound screening as the effect of compounds on TGF-β-induced collagen synthesis, α-SMA expression, proliferation, and cell toxicity can be measured simultaneously within a single well (*Chen and Raghunath, 2009*). Although this model is considered a good system to identify therapeutic targets compared to the standard 2D monolayer *in-vitro* culture, the Scar-in-a-jar assay also has several disadvantages. For example, the assay only involves one cell type, cells are grown on a stiff substrate, the cells require exogenous TGF-β to promote collagen synthesis, and the model is unable to recapitulate fibroblast foci.

Based on these limitations, over the past few years, the development of more complex *in-vitro* models of lung fibrosis capable to mimic microenvironments observed in normal tissues have now become of great interest. Complex matrices of biological origin have therefore begun to be used to cultivate cells in an environment similar to the humans lung and the models gradually increased dimensionality, moving from 2D to 2.5D, until 3D. 3D *in-vitro* models, where cells are embedded in a complex environment with different polarity, exposing them to ECM interactions and soluble growth factor/cytokine gradients, mimic native lung tissue microenvironment with greater accuracy compared to 2D and 2.5D models. 3D systems can replicate cell-cell and cell-matrix interactions, matrix stiffness, and structure. Moreover, these models permit migration, chemotaxis, cellular traction and integrin adhesions, in all three planes. Due to these benefits, different 3D

models have been developed such as the hydrogel systems, lung spheroids and organoids, lung-on-a-chip and precision-cut lung slides (PCLS).

Hydrogels are water-swollen cross-linked natural or synthetic polymers that are employed as scaffold for *in-vitro* models, especially fibroblast cultures, to mimic the native structure of the ECM (*Smithmyer et al. 2014*). Collagen type I-based hydrogels *in-vitro* models are very helpful in the study of fibroblast behavior when exposed to chemical and physical stimuli induced by the ECM.

Lung spheroids refers to adult lung cells or lung stem cell populations cultured in the form of aggregates utilizing low-adhesion plates, hanging drop cultures, suspension cultures or micropatterned plates (*Fang and Eglen, 2017*). Lung organoids are self-assembling structures of lung stem cells that follow sequential lung developmental paradigms, with discrete pseudo-glandular, canalicular and saccular stages (*Chen et al. 2017*). Both lung spheroids and organoids are superior to 2D cultures since they can replicate the typical cell-cell and cell-matrix interactions, similar to *in-vivo* conditions *(Surolia et al. 2017)*. Spheroids may enable high throughput drug testing. However, spheroids have a too simple of an architecture to mimic real organs, while organoids mimic some, but not all the structure and function of real organs and lack vasculature and air-liquid interface.

Organ-on-a-chip systems are complex, 3D bioengineered devices which replicate organ/tissue level responses in miniature chips created using lithography techniques. Specifically, lung-on-a-chip are systems that replicate not only the lung structure with all the cell and matrix interactions but they also allow investigation under a much more dynamic environment, with biomechanical signals in the form of shear stress due to perfusion and strain, similar to human breathing and blood flow (*Yanagihara et al. 2020*).

Among the 3D approaches, the PCLS model has emerged as the most useful and promising *ex-vivo* tools for studying human lung fibrosis, and to support preclinical studies (*Alsafadi et al. 2017*). This model involves fresh human lung tissue from lung resections or explants or animal tissues, which are filled with low melting point agarose (to prevent organ collapse) and subsequently cut with precision into 250-1000 μm thick slices and cultured in vitro. In this way, the PCLS used as 3D lung tissue cultures retain native lung tissue architecture, ECM protein composition, and stiffness with viable multiple lung resident cells. Therefore, the generated lung tissue cultures can offer a large range of applications for biomechanical, physiological, toxicological and pharmacological studies. The most important advantage of using PCLS is that they can be used to assess the effects of drugs directly in situ on the lung structural cells. However, one of the most significant limiting factors using PCLS is the lack of fresh tissue availability. Additionally, PCLS are limited in

that they can be used only in short-term studies of one week or less (*Uhl et al. 201*5), are difficult to standardize and they do not reproduce the lung functions. Nevertheless, this model represents the best combination of biological complexity, high-throughput capacity for pre-clinical testing of novel anti-fibrotic drugs and give mechanistic insights in modulating lung cell phenotypes. Despite the development of innovative *in-vitro* models with the addition of an increasing level of biological complexity, these models do not yet possess the same physiological environment of the *in-vivo* models and all the intricate cellular and matrix connections and stimulus that are present in living tissues.

1.7.2 In-vivo models of pulmonary fibrosis

Attempts to elucidate disease pathogenesis, identify potential biomarkers and unravel novel therapeutic targets have relied on *in-vivo* models. Over the past few decades, several animal models of pulmonary fibrosis have become available to study the pathobiology of IPF (*Tashiro et al. 2017*), but no one seems to be able to fully recapitulates the histopathologic pattern of UIP or exhibit features of progressive and irreversible disease like human IPF (*Moore et al. 2013*). In addition, although several compounds have shown efficacy in reducing the progression of pulmonary fibrosis using animal models, only few of these compounds have confirmed their beneficial effects for IPF in clinical trials. This, however, should do not underestimate the fact that animal models are essential prerequisites for revealing molecular mechanisms involved in the pathogenesis of lung fibrotic processes and the subsequent development and validation of prognostic tests and therapeutic interventions.

Pulmonary fibrosis like features can be induced in different species by a variety of agents, and these different agents can be administered via many different routes and using distinctive dosing regimens. Although cases of spontaneous lung fibrosis are known in some common mammalians (like dogs, horses, cats and donkeys), rodents remain the most used preclinical models for lung fibrosis, since in these species fibrotic lesions have a rapid onset and their duration enable drug testing. Moreover, rodents, being small animals, are easy to house and handle and the management costs are reduced compared to larger species (*Gelfand, 2002)*. Regarding the study of IPF, as recently recommended by the "Official ATS Workshop Report about the Use of Animal Models for the Preclinical Assessment of Potential Therapies for Pulmonary Fibrosis", mice are the first-line animals for preclinical testing, especially due to the ease of handling, availability of reagents, their well characterized immune systems, and the possibility of utilizing transgenic models (*Jenkins et al. 2017*). However, murine models do not fully recapitulate classical IPF histopathology,

likely explained by anatomic differences between murine and human lungs, temporal homogeneity of animal models and potentially distinctive pathobiological mechanisms involved in human disease. Since rats may have histopathology that is more reminiscent of IPF, in the same report, the rat is recommended as the second species, that can be used subsequently if the confirmation of the efficacy of a compound is required or in case of an impossibility to use the mouse (*Jenkins et al. 2017*). Moreover, considering that a single model does not resemble all the characteristic of the disease, the possibility to expand the model with two or more animal models of different species could be a good choice to improve the efficacy of preclinical studies (*Tashiro et al. 2017*).

Different approaches to model experimental models of pulmonary fibrosis exist, and most of them are characterized by the use of an agent, which is able to induce the first injury triggering the fibrotic process in the lung. Among the various experimental agents, bleomycin is the most widely used and best characterized agent to induce pulmonary fibrosis, due to its fast action leading to the early appearance of histopathological alterations that closely mimic the acute phase of the disease (*Jenkins et al. 2017*).

Several other fibrotic agents have also been used with varying degrees of success.

Fluorescein isothiocyanate (FITC) has been shown to cause fibrosis like changes over a similar time scale to bleomycin. FITC is a fluorescent molecule with the advantage that molecular deposition in the lung can be easily visualized. The disadvantages of this model are that certain histopathological features, such as fibroblast foci, are not observed, and there is a large amount of variation in the fibrotic response generated by different batches of FITC (*Degryse and Lawson, 2011*).

Administration of silica or asbestos to the lungs has also been shown to illicit persistent fibrosis (*Koli et al. 2016; Cheresh et al. 2015*). However, as with FITC, there are histopathological features that are missing with respect to the histopathological features seen in patients with IPF.

Systemic delivery of paraquat also produces fibrosis in the lungs of animals (*Guo et al. 2015; Shao et al. 2015*). However, paraquat is a broad-spectrum herbicide that has been shown to cause necrosis in organs other than the lungs (such as kidney and liver) which can cause significant mortality.

In addition to these models, certain non-chemical *in-vivo* approaches can induce pulmonary fibrosis. For example, an exposure of the thorax of animals to radiation has been shown to result in persistent fibrosis-like changes in the lungs (*Paun et al. 2015*). However, as the fibrosis takes a long time to develop and the cost of the irradiating equipment can be high, this model is very expensive and difficult to run.

Intratracheal delivery of transgenes using viral vectors has shown some success, with delivery of genes for factors such as TGF-β1 eliciting fibrotic responses in the lungs of animals (*Kolb et al. 2001*). Although delivery of these transgenes leads to a progressive and persistent fibrosis, the downside of such models can be that the animals may have an immune response to the viral vector, and the expression of the transgenes is much higher than physiologically possible.

Another animal model of pulmonary fibrosis that has been developed is the humanized mouse model of IPF, where cells from human patients of IPF are injected into severe combined immune deficient (SCID) mice. Infusion of human fibroblasts has been shown to lead to increases in fibrosis seen histologically and up-regulation of pro-fibrotic genes such as TGF-β1 and surfactant proteins at 63 days post-infusion (*Murray et al. 2013*). However, the main issue with this model is the length of time to generate fibrosis and the availability of cells from human patients with IPF.

Recently are growing in importance also the age-related models, considering that IPF is a disease affecting the elderly population. Indeed, it has been demonstrated that older mice are more inclined to developed lung fibrosis when exposed to pro-fibrotic stimuli (*Tashiro et al. 2017*). Moreover, a model with a specific deletion of one telomeric gene, demonstrated that telomere dysfunction (one of the principal characteristics of aging) in AECs type II is sufficient to cause lung fibrosis (*Naikawadi et al. 2016*). However, the ATS guidelines do not consider necessary the prioritization of the use of aged mice for preclinical testing.

1.7.2.1 The bleomycin (BLM)-induced pulmonary fibrosis model

As mentioned in the previous paragraph, the BLM-induced pulmonary fibrosis model is the most used animal model to study pulmonary fibrosis and it is the most employed in preclinical studies during the drug development process for IPF. Indeed, the BLM model has proven invaluable in understanding many of the cellular and molecular pathways in fibrogenesis that are central to the current understanding of IPF pathogenesis. Furthermore, this model was used for the preclinical characterization of Nintedanib (*Wollin et al. 2015*).

BLM is a glycosylated linear non-ribosomal peptide antibiotic produced by the bacterium "Streptomyces verticillus" (*Umezawa et al. 1966*), with an important role in chemotherapy for the treatment of some forms of cancer such as germinative tumors and Hodgkin's lymphoma. However, its use can be life-threatening in up to 10% of the patients receiving the drug, since the treatment is associated with the occurrence of interstitial pulmonary fibrosis (also called fibrosing alveolitis) (*Balikian et al. 1982; Calaway et al. 2018*).

Indeed, BLM induces pulmonary fibrosis by production of DNA-cleaving superoxide and hydroxide free radicals, which cause single and double stranded DNA breaks (*Claussen and Long, 1999*). This damage preferentially occurs in the lungs because of low levels of bleomycin hydrolase, a BLM-inactivating enzyme. Given the capabilities of the molecule to produce lung fibrosis in human, BLM was used to modelling IPF in a wide variety of experimental animals and has allowed the replication of some key hallmarks of the disease, such as damage to AECs, fibroblast and myofibroblast activation and collagen deposition (*Scotton and Chambers, 2010; Liu et al. 2017; Carrington et al. 2018*).

So far, BLM has been used in a variety of different species, including mice, rats, hamsters, rabbits, guinea pigs, dogs, and non-human primates, via a number of different administration routes. For instance, it has been delivered directly into the lung by intratracheal, oropharyngeal and inhaled administration, systemically by intravenous and intraperitoneal treatment or subcutaneously by mini-osmotic pumps. However, among these approaches, intratracheal instillation of BLM is the most frequently used route of administration because it better reproduces the human phenotype that is limited to the lungs, causing direct damage to AECs and leading to fibrotic changes mainly in the lung parenchyma (*Moore et al. 2013*). The recently published ATS workshop report on pulmonary fibrosis animal models confirmed that there is a consensus view of the murine intratracheal BLM model as "the best-characterized animal model available for preclinical testing" (*Jenkins et al. 2017*).

The BLM model leads to an initial inflammatory phase, characterized by up-regulation of acute inflammatory cytokines together with an influx of neutrophils (*Kim et al. 2010*). This primary inflammatory phase lasts for approximately 7-10 days before subsiding into a fibrotic phase (from day 14) which more appropriately mimics some of the manifestation of IPF in human patients (**Figure 1.9**) (*Izbicki et al. 2020*). Terminal investigations are typically carried out three-four weeks after the initial BLM administration, approximately on day 21-28. Indeed, the fibrotic phase in the BLM model is self-limited and, in the end, differently from the disease in humans, reversible over a variable period of time.

It is important to note that in the BLM model there is overlap between the inflammatory and fibrotic phases, with the initial strong inflammatory response taking up to 10 days post-injury to completely clear. Typically, the 7-day time point is used as a separation between the inflammatory and fibrotic phases (*Moeller et al. 2008*). However, since there is no clear distinction between the two phases, using this time point to differentiate between prophylactic and therapeutic studies is arbitrary and represents a limitation that needs to be considered, especially when using the BLM model to assess the efficacy of anti-fibrotic

compounds. These considerations notwithstanding, it is now apparent that drug testing should be performed during the fibrotic phase, at least 7 days after BLM administration (*Moore et al. 2013*).

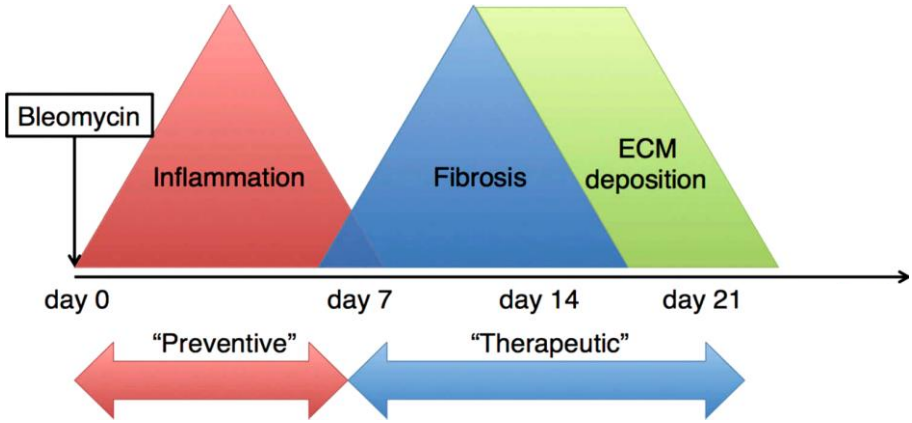

Figure 1.9 Schematic image of BLM-induced pulmonary fibrosis model (Image adapted from *Yanagihara et al. 2020*). The switch from inflammatory to fibrosis phase is around the seventh day post-BLM with fibrotic lesions appearance starting from day 14 and followed by fibrogenic changes with ECM deposition until day 21. These changes resolve after a variable time period. Interventions during the first seven days are considered as 'preventive' while interventions in the later stages are considered as 'therapeutic.' Anti-fibrotic treatments should be tested during 'therapeutic' timing

Another important aspect to consider related to the "therapeutic window" for compound dosing, is that the development of pulmonary fibrosis induced by a single intratracheal administration of BLM in mice is often unpredictable. In fact, there is a high degree of variability between individual animals in the extent of fibrosis, and this represents a limitation in pharmacological studies given the restricted time window available for testing new anti-fibrotic drugs. Considering that fibrosis does not resolve in most patients with pulmonary fibrosis and the hypothesis that repeated events of lung injury are responsible of the disease development, one possibility to overcome this issue in mice could be to perform repeated administration of BLM instead of a single intratracheal administration. Indeed, the repeated intratracheal administration of BLM has been shown to produce a more robust and long-lasting response that could, at least in part, reproduce IPF progression. For example, Stellari and colleagues directly addressed this point showing that double intratracheal instillation of BLM produces a more severe and diffuse fibrosis when compared to the single BLM instillation in mice (*Stellari et al. 2017*). Another approch could be to consider the administration of BLM via oropharyngeal aspiration. Indeed, it has been reported that the oropharyngeal route leads to pulmonary fibrosis persisting for up to 6 months (*Scotton*

et al. 2013), and the fibrotic response that develops after this method appears similar to the intratracheal instillation. Results from Ruscitti et al., demonstrated that lung fibrosis severity and duration after double oropharyngeal or intratracheal administration are comparable, with the oropharyngeal administration resulting in a more uniform distribution of fibrotic lesions throughout the lung lobes (*Ruscitti et al. 2020*).

Other aspects related to the sex, strain and age of the mice should be considered when using the BLM model. It has been demonstrated that male mice are more susceptible to BLM-induced pulmonary injury than female mice, which is similar to human IPF, though the precise mechanism is not fully understood (*Redente et al. 2011*). Therefore, the National Institutes of Health currently recommends the use of both male and female animals in all research studies. The response to BLM is also strain-dependent: some strains, such as C57Bl/6 mice are more susceptible than BALB/c mice, presumably due to different expression patterns of cytokines and proteases (*Phan et al. 1992*). Furthermore, although IPF is a disease of advanced age most of the studies use young mice, generally aged 8-12 weeks, which are equivalent to teenager phase in a human life span. Some studies using BLM in aged mice (over 18 months) demonstrated more fibrosis and impaired resolution after injury, which may more closely reflect the human disease, however, due to the practical difficulties in the generation of aged mice combined with much higher cost, the ATS guidelines do not consider necessary the prioritization of the standard use of aged mice for preclinical testing (*Jenkins et al. 2017*).

Finally, the most accurate analysis for lung fibrosis in preclinical models involves several endpoints, which should be as much as possible clinically relevant and validated. Current outcome measurements in the BLM and other experimental lung fibrosis models mainly involve the histological scores of fibrosis in stained tissue sections (commonly modified Ashcroft scoring), morphometric quantification, and biochemical analysis such as lung collagen or hydroxyproline (a major component of collagen) content. Although these endpoints give valuable information about the levels of fibrosis in the lungs of animals, they may not provide the whole picture for preclinical assessments of anti-fibrotic drugs. The ATS panel of experts suggests the possibility of integrating clinically relevant assessments such as functional readouts, imaging techniques, measurement of arterial blood oxygen saturation with pulse oximetry, and most recently, the measurements of blood and molecular biomarkers which may predict disease progression and responses to new treatments (*Jenkins et al. 2017*). Furthermore, these techniques, as well as being more clinically relevant, provide researchers with the opportunity to longitudinally examine the progression of pulmonary fibrosis in a single animal, rather than having to sacrifice

numerous animals to examine fibrosis, and may ultimately give a better indication of translational potential from the *in-vivo* models to the clinic of a specific treatment. Finally, other additional evaluations could include BALF analysis for the assessment of inflammatory cells counts as well as body weight, lung index (lung wet weight in mg compared to body weight in g) and survival rate (*Moeller et al. 2008*).

Regardless the limitations that animal models may have, the idea to replace it with innovative and refined *in-vitro* models is promising and encouraging, but there is still a long way to go. Despite the growing ethical need to reduce the number of animals used in research, without animal models, complicated diseases such as IPF, could remain without a pharmacological solution for a long time. It is therefore critical to develop the best animal model in terms of translatability and management, and characterize it as thoroughly as possible in order to understand what kind of "questions" can be asked to the model that may help to solve problems related to the disease that cannot be asked to human patients.

2. AIM OF THE WORK

Idiopathic Pulmonary Fibrosis (IPF) is a chronic, progressive, and fibrotic lung disease with a poor prognosis and very limited therapeutic options. To date, only two drugs are available on the market for the treatment of IPF: Nintedanib and Pirfenidone. Both therapies show pleiotropic mechanisms of action and have proven efficacy in slowing the rate of functional decline and disease progression in mild-to-moderate IPF patients. However, none of these two drugs is able to definitively reverse or cure the disease and both are affected by tolerability issues. Therefore, the incomplete understanding of the disease and lack of safe and effective treatment makes IPF a disease with a high medical need requiring novel approaches to treatment.

Drug discovery for IPF had to face a lot of challenges probably due to a very complex disease, difficult to fully understand and mimic with animal models. Beside the intrinsic differences between human and rodent disease, an inappropriate use of the animal model in terms of dosing regimen and evaluated readouts has limited the identification of new therapies effective in the clinical practice, resulting in a high attrition rate for anti-fibrotic drugs and leading the conclusion that most of the pre-clinical models are poorly predictive and scarcely resembling the human disease.

In this scenario, the aim of the PhD project was to improve the bleomycin model, one of the most used among preclinical models for IPF, making this model more robust and improving its translational value, so as to provide a better indication of a compound's potential efficacy in support of Drug Discovery projects.

To achieve this goal, during this PhD project, the following steps were covered:

- Refining the most widely used preclinical readout, namely the Ashcroft score, by the introduction of an automated analysis of lung fibrosis based on the Artificial Intelligence (AI) that was able to distinguish and to quantify different levels of fibrotic tissue;
- Introducing clinically relevant endpoints, not commonly evaluated at the preclinical level but used as primary and secondary endpoints in clinical practice, such as the Diffusion Factor for Carbon Monoxide (DFCO) and the Forced Vital Capacity (FVC);
- Evaluating biomarkers already under investigation in the clinic for the diagnosis, the prognosis and to tailor personalized treatments for patients.

The robustness and the consistency of these novel readouts were explored in two experimental sets: first, in a time course experiment to follow the progression of the readouts over time after the BLM injury, and second, they were pharmacologically

validated in a therapeutic protocol with Nintedanib, one of the two currently approved drugs.

Finally, in both experimental sets, the gene profile expression of the model was also explored in order to evaluate not only which set of genes was involved but also the impact of an anti-fibrotic treatment, matching the results with the biomarkers explored and possibly opening the chance to discover novel relevant biomarkers.

Overall this project aimed at developing an improved BLM model compared to that currently described in the literature, and thanks to the introduction of clinically relevant endpoints help filling the gap between preclinical models and clinical needs, therefore improving the translatability and the reliability of Drug Discovery compound screening for the identification of novel anti-fibrotic drugs.

3. MATERIALS AND METHODS

3.1 *In-vivo* mouse model of pulmonary fibrosis

3.1.1 Animals

Male C57BL/6J mice, 5-6 weeks old, were supplied by Envigo RMS Italy, San Pietro al Natisone (Udine, Italy). Prior to use, animals were housed 5 per cage and acclimatized for at least 3-4 weeks to the local vivarium conditions (room temperature: 20-24 ºC; relative humidity: 40-70%; 12-h light-dark cycle), having free access to standard certified rodent chow and controlled tap water. Animals were checked for abnormalities or signs of health problems after arrival in the animal facility and were acclimatized for a period of at least 1 week before starting any experimental procedure.

During the experimental phase, mice were given daily high calories dietary supplement (DietGel Recovery purchased by Clear H20, ME, USA) and sterile sunflower seeds (Sunflower kernels w/o hulls, purchased by ssniff Spezialdiäten GmbH, Soest, DE) in addition to the standard rodent chow, since in our experience with the BLM model this food supplementation helps in reducing body weight loss and percentage of mortality. Moreover, mice health conditions (pain rating by visual analogue scale) was checked every day while the body weight was measured every two days throughout the duration of all the studies. All the experimental procedures and conditions involving experimental animals were reviewed and approved by the local ethics committees and authorized by the Italian Ministry of Health and were performed in full compliance with the international European ethics standards in conformity to directive 2010/63/EU, Italian D.L. 43 26/2014, and the revised “Guide for the Care and Use of Laboratory Animals” (Committee for the Update of the Guide for the Care and Use of Laboratory Animals and National Research Council, 2010).

3.1.2 Oropharyngeal (OA) administration

Mice were lightly anesthetized with 4% isoflurane in oxygen delivered in a box and then placed on an animal support stand facing upward by using a clean wire positioned under the animal’s front incisors. The tongue was retracted with forceps to visualize the epiglottis. 50 µl/mouse of saline (control group) or BLM solution were instilled using a small laryngoscope and with a micropipette the liquid was placed onto the distal part of the oropharynx while the nose was gently closed. Mice were monitored in cages until they had fully recovered. BLM sulphate, 1.5 International Units (IU), powder for solution for

injection/infusion (BAXTER Oncology GmbH, Germany), was dissolved in saline solution to obtain the correct dose of 0.03 IU/mouse (0.02 mg/mouse). This procedure was performed at days 0 and 4.

3.1.3 Oral administration of drugs

Nintedanib (Carbosynt, Compton, UK) was dissolved in 1% of tween 80 (Sigma-Aldrich, St. Louis, MO, USA) in milliQ water and administered at 50 mg/kg twice daily (b.i.d.) as esylate salt by oral gavage, according to the experimental plan.

3.2 Experimental design

3.2.1 Time course study - novel readouts assessment

After the acclimatization period, animals were weighed and randomized in the different experimental groups. Mice were instilled OA with saline (control group, n=4 for each time point) or BLM solution (n=15 for each time point), at day 0 and day 4. The dose used for the BLM was 0.03 IU/mouse for each instillation. During the experimental study, the health condition of the animals was checked every day while the body weight was measured every two days. At different time-points (7, 14, 21, 28, 35, 42 and 49 days from the first administration of BLM or saline solution), mice were anesthetized by intraperitoneal injection of ketamine (Anesketin®, Dechra Inc., Handelsweg, NL) and xylazine (Xilagesic®, Calier Inc., Barcelona, ES) solution (100 mg/Kg and 10 mg/Kg, respectively). Once anesthesia was achieved, mice were tracheostomized and measured for their Diffusion Lung Capacity for Carbon Monoxide (DFCO) exchange. Then, to prevent spontaneous breathing, mice received 1 mg/Kg Pancuronium Bromide (Sigma-Aldrich) intraperitoneally before assessing lung function (particularly FVC). After these in-life tests, blood and BALF were collected for the biomarkers analysis, while lung tissues were harvested for histological analysis consisting of Ashcroft score evaluation and automated quantification of lung fibrosis by AI (**Figure 3.1**).

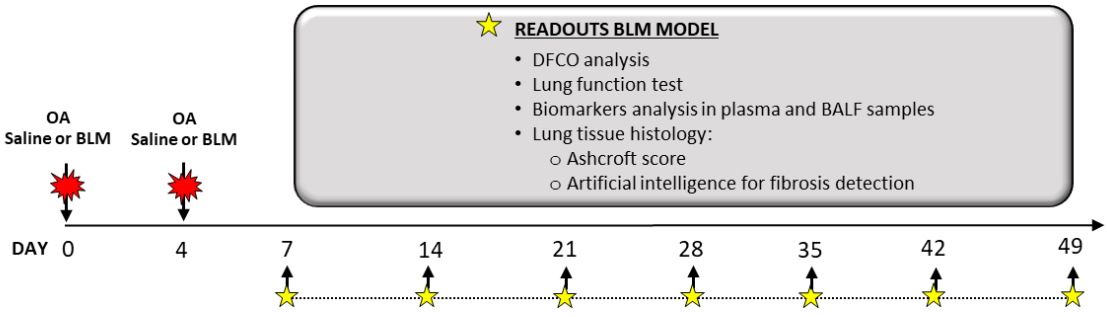

Figure 3.1 Experimental protocol of the time course BLM OA study for the novel readouts assesment

3.2.2 Time course study – gene expression evaluation

After the acclimatization period, animals were weighed and randomized in the different experimental groups. Mice were instilled OA with saline (control group, n=5 for each time point) or BLM solution (n=10 for each time point), at day 0 and day 4. The dose used for the BLM was previously described in *Paragraph 2.2.1*. During the experimental study, the health condition of the animals was checked every day while the body weight was measured every two days. At different time points (7, 14, 21, 28 days from the first administration of BLM or saline solution) **(Figure 3.2)**, mice were sacrificed with an overdose of ketamine (Anesketin®, Dechra Inc., Handelsweg, NL) and xylazine (Xilagesic®, Calier Inc., Barcelona, ES) solution (100 mg/Kg and 10 mg/Kg, respectively) given intraperitoneally. Then lung samples were collected for the gene expression evaluation as described in the *Paragraph 3.4.3*. In this study some naïve mice (n=4) were included as control.

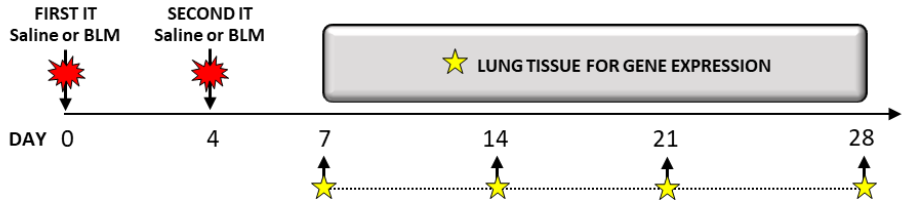

Figure 3.2 Experimental protocol of the time course BLM OA study for the gene expression evaluation

3.2.3 Therapeutic protocol study – Pharmacological validation of novel readouts

After the acclimatization period, mice were instilled OA with saline or BLM solution, at day 0 and day 4. The dose used for the BLM was 0.03 IU/mouse for each instillation. The therapeutic protocol started seven days after the first administration of BLM, when fibrosis was well established, and then continued for two weeks until T21, when extensive fibrotic lesions were still evident. At T7, mice treated with BLM were weighed, randomized, and divided in two groups: one of them received daily Nintedanib and the other received daily vehicle during the two weeks of treatment.

Specifically, the experimental groups were as follows:

-Saline (control group), n=5: mice were instilled OA with saline solution and received vehicle (1% of tween 80 in milliQ water) administered orally b.i.d. for two weeks.

-BLM group, n=15: mice were instilled OA with BLM and received vehicle (1% of tween 80 in milliQ water) administered orally b.i.d. for two weeks.

-Nintedanib group, n=15: mice were instilled OA with BLM and received Nintedanib (50 mg/kg, esylate) administered orally b.i.d. for two weeks.

During the experimental study, the health condition of the animals was checked every day while the body weight was measured every two days. After being anesthetized and injected with Pancuronium Bromide as described in the *Paragraph 3.2.1*, FVC and DFCO were assessed. Blood was then collected from the heart for the biomarkers analysis, and after being bled from the abdominal aorta, BALF and lung samples were collected for biomarkers and histological analysis respectively. A graphical explanation of the experimental protocol and the groups classification is reported in **Figure 3.3**.

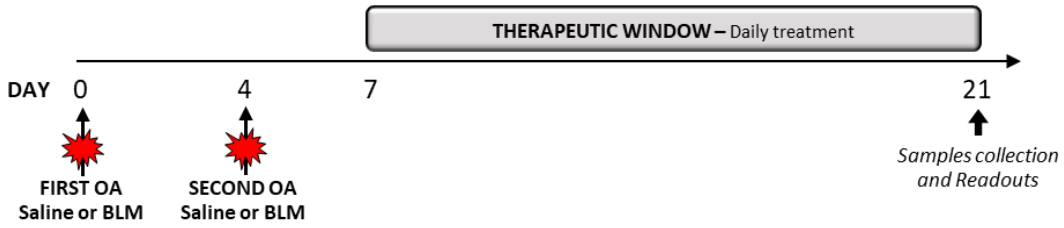

Group Name	Challenge* (*OA administration at days 0 and 4)	Treatment* (*Oral administration from day 7 to 21)	N. Animals
Saline	Saline solution	Vehicle b.i..d.	5
BLM	BLM 0.03 IU/mouse	Vehicle b.i.d.	15
Nintedanib	BLM 0.03 IU/mouse	Nintedanib 50 mg/kg b.i.d.	15

Figure 3.3 Therapeutic BLM OA Study for pharmacological validation of novel readouts. Experimental protocol and groups classification.

3.2.4 Therapeutic protocol study – *gene expression evaluation*

Following the same experimental described in the *Paragraph 2.2.3*, the experimental groups were as follows:

-Saline (control group), n=4: mice were instilled OA with saline solution and received vehicle (1% of tween 80 in milliQ water) administered orally b.i.d. for two weeks.

-BLM group, n=13: mice were instilled OA with BLM and received vehicle (1% of tween 80 in milliQ water) administered orally b.i.d. for two weeks.

-Nintedanib group, n=13: mice were instilled OA with BLM and received Nintedanib (50 mg/kg, esylate) administered orally b.i.d. for two weeks.

In this study some naïve mice (n=4) were also included as controls. (**Figure 3.4**)
During the experimental study, the health condition of the animals was checked every day while the body weight was measured every two days. At T21, mice were sacrificed with an overdose of anesthesia as described in the *Paragraph 3.2.2.* and lung samples were collected for gene expression evaluation as described in the *Paragraph 3.4.3*.

Group Name	Challenge* (*OA administration at days 0 and 4)	Treatment* (*Oral administration from day 7 to 21)	N. Animals
Saline	Saline solution	Vehicle b.i..d.	4
BLM	BLM 0.03 IU/mouse	Vehicle b.i.d.	13
Nintedanib	BLM 0.03 IU/mouse	Nintedanib 50 mg/kg b.i.d.	13
Naive	----------	----------	4

Figure 3.4 Therapeutic BLM OA Study for gene expression evaluation. Experimental protocol and groups classification

3.3 Readouts evaluation

3.3.1 Diffusion Factor for Carbon Monoxide

According to the procedure described by *Limjunyawong et al. 2015*, a single module Micro GC Fusion (Micro GC Fusion-Inficon), configured with a 10m Molsieve 5A column, was used to perform the analysis of gas and was set up to measure peaks for nitrogen, oxygen, neon, and carbon monoxide. The chromatographic column, a molecular sieve column with helium as carrier gas, has a volume of 0.8 ml and its temperature was operated isothermally at 130° C for 40 seconds. Before each experimental session, 2 ml of sample were taken directly from a gas mixture bag containing approximately 0.3% Ne, 0.3% CO, and balance air, to calibrate the instrument. Despite the chromatograph column has a volume of 0.8ml, we used 2 ml to ensure adequate clearing of the connecting tubing with the sample. At the selected time-points, after the BLM administration, mice were anesthetized with ketamine and xylazine as previously described and tracheostomized with a stub needle cannula (18 G). After collecting 0.8ml of gas from the gas mixture bag, the syringe was connected to

the tracheal cannula and quickly inflate the lung. After waiting for 9 sec, 0.8ml of exhaled air will be quickly withdrawn, diluted with air up to get the volume of 2ml and injected into the gas chromatograph for analysis. The sampling was done two times in order to calculate an average of the two DFCO measurements. DFCO was calculated as $1–(CO_9/CO_c)/(Ne_9/Ne_c)$, where c and 9 subscripts refer to concentrations of the calibration gases injected and the gases removed after a 9 sec breath hold time, respectively. Differences among the different groups were analyzed and compared as described in "Statistical analysis".

3.3.2 Lung function tests

At selected experimental time-points, respiratory system mechanics and Pressure-Volume (PV) relationships were measured using the FlexiVent System (SCIREQ Inc., Montreal Qc, Canada) (*Vanoirbeek et al. 2010*). Briefly, mice were anesthetized by intraperitoneal injection of ketamine and xylazine solution as previously described. Once surgical anesthesia was achieved, as assessed by loss of withdrawal reflex and absence of response to external stimuli, the mouse was tracheotomized using a 18-gauge metal cannula, connected via an endotracheal cannula to the FlexiVent and ventilated at a respiratory rate of 150 breaths/min and tidal volume of 10 ml/kg against a positive end-expiratory pressure of 3 cmH2O to achieve a mean lung volume close to that during spontaneous breathing. To prevent spontaneous breathing mice also received pancuronium bromide 1 mg/kg intraperitoneally. FlexiVent software version 8.1 was used to perform the perturbations.

Different maneuvers were carried out in a script customized protocol, lasting about 4 min. Particularly, the negative pressure-driven forced expiration (NPFE) maneuver, the most relevant for this model, was performed by inflating the mouse lungs to a pressure of 30 cm H_2O over 1 s, holding this pressure for 2 s before connecting the animal's airways to the negative pressure reservoir (−50 cm H_2O) for 2 s. The NFPE maneuver mimics spirometry in humans generating some outcomes resembling those obtained in IPF patients, such as the forced expiratory volume in 0.1 s ($FEV_{0.1}$) and FVC. All maneuvers and perturbations were performed until three acceptable measurements (coefficient of determination ≥ 0.95) were achieved. For each parameter, an average of the three measurements was calculated and depicted per mouse.

3.4 Biological samples collection and processing

3.4.1 Plasma sampling

Immediately after animals' sacrifice, blood samples were collected from the right heart ventricle and placed in a tube containing heparin as anticoagulant. Plasma was then separated by centrifuging the tubes at 2000 x g and 4°C for 10 minutes (Thermo Scientific Heraeus centrifuge). Plasma samples were aliquoted and stored at -80°C for quantitative determination of the biomarkers.

3.4.2 BALF sampling

Following blood collection, and after the bleeding from the abdominal aorta, lungs were gently washed three times using a cannula inserted into the trachea with 0.6 ml of clear BAL solution [10X HBSS (Hanks' Balanced Salt Solution), 10 mM EDTA (Ethylenediaminetetraacetic acid; Fluka analytical, Sigma-Aldrich, MO, USA), 10 mM HEPES ((4-(2-hydroxyethyl)-1-piperazineethanesulfonic acid; Gibco, ThermoFisher Scientific, MA, USA) and distilled water]. The obtained BALF was centrifuged at 1000 x g and 4°C for 10 minutes and the cell-free supernatant was aliquoted and stored at -80°C for quantitative determination of the biomarkers.

3.4.3 Lungs collection

For histological analysis the whole lung, after BALF procedure and cardiac perfusion, was excised, inflated with a tracheal cannula using a customized closed system that fixed lungs with 10% formalin solution (Formaldehyde solution 4%, buffered, pH 6.9; Sigma-Aldrich, MO, USA) at a constant pressure (25 cmH2) for at least 2 hours with at room temperature. Sample processing was performed by the laboratory unit of Jane Schofield from the Histology Department at Covance, Eye, UK. After fixation, lungs were dehydrated in graded ethanol series, clarified in xylene and paraffin embedded. Each longitudinally oriented lung was cut to obtain one representative slice of 5 µm thick, which were subsequently stained with Masson's Trichrome histological staining. Masson's Trichrome is a histological staining protocol that employs three different reagents for staining collagen and ECM, muscle fibers, and erythrocytes. This staining protocol is usually applied for distinguishing collagen fibers in blue/green, and for this reason it is one of the staining protocols recommended for the histologic assessment of morphology in lung fibrosis related studies. For gene expression analysis the whole lungs were excised without performing any procedure previously described to avoid the degradation of RNA. After a

quick wash in a clean NaCl solution, the whole lungs were dried off on a gauze pad, weighed and then preserved in 10ml of RNAlater solution before processing as described in the *Paragraph 3.6.1*.

3.5 Protein analysis

3.5.1 Biomarkers analysis

The total amount of Surfactant Protein-D (#MSFPD0; R&D systems, MN, USA) was quantified in plasma samples with commercial Enzyme-linked immune-sorbent assay (ELISA) kits specific for mouse proteins according to the manufacturer's protocol. Matrix Metalloproteinase-7 (#NBP3-06895; Novus Biologicals CO, USA), Collagen Type I (#Sea571Mu; Cloud-Clone, TX, USA), Collagen Type III (#Sea175Mu; Cloud-Clone, TX, USA), Osteopontin (#MOST00; R&D System, MN, USA), CXCL13 (#MCX130; R&D System, MN, USA), IL-6 (#M6000B-1; R&D System, MN, USA), rPRO-C3 (undisclosed method assessed by Nordic Bioscience, Herlev, Denmark) were quantified in BALF. All these biomarkers were evaluated by ELISA kits specific for mouse proteins according to the manufacturer's protocols. Briefly, the wells of a microplate had been pre-coated with the antibody specific for the protein to be measured. Standards and samples, at appropriate dilutions, were pipetted into the wells and any protein present was bound by the immobilized antibody. After removing any unbound substances with a series of washing cycles, a biotin-conjugated antibody, again specific for the protein to be measured, was added to each well. After washing, avidin conjugated Horseradish Peroxidase (HRP) was added to the wells, and following a series of washes to remove any unbound avidin-enzyme reagent, a substrate solution was added to the wells and a specific colour was developed in proportion to the amount of protein bound. The colour development was stopped with a stop solution provided by the supplier and its intensity was measured at a specific wavelength (nm), using a microplate spectrophotometer (xMark, Biorad, California, USA). Specific protein concentrations were extrapolated from a standard curve plotted by relating the intensity of the colour (O.D.) to the concentration of standards. Results were expressed as pg of protein per mL of sample.

3.6 Gene expression analysis

3.6.1 Sample Processing for RNA extraction

After being excised, lungs were weighed and preserved in a RNAlater solution (#R0901; Sigma Aldrich MO, USA) to stabilize and protect RNA with immediate RNase

inactivation. RNAlater-preserved tissues were frozen at -80°C until the extraction procedure when they are added with 1ml for each 100 mg of tissue of a QIAzol® Lysis Reagent (phenol-based reagent supplied by QIAGEN, Netherlands). Then samples were then homogenized with gentleMACS™ Dissociator (Miltenyi Biotec, Germany).
After this step, the obtained lung homogenates were aliquoted and one aliquot was added with Chloroform (#516726; Sigma Aldrich MO, USA; 200µl for each ml of homogenate) and centrifuged at 12000 g for 10 minutes at 4°C. 350µl of upper aqueous phase were transferred to a new tube to proceed with the following step.

3.6.2 RNA Extraction and Analysis

The RNA was extracted from the QIAZOL lung homogenate using the QIAcube robotic workstation with the miRNeasy Mini Kit (QIAGEN, Netherlands). DNase I treatment was performed in column following manufacturer's instructions. RNA purity and concentration were determined by spectrophotometry (Nanodrop ND-2000/200C – Thermo Fisher Scientific, USA) and the RNA integrity was evaluated with the Agilent 2100 Bioanalyzer system.

3.6.3 Reverse transcription protocol

RNA was reverse transcribed using SuperScript™ IN VILO™ (#11766500; ThermoFisher Scientific, MA, USA), a master mix for cDNA synthesis and genomic DNA elimination in RNA samples, following manufacturer's instructions (starting material: 25 µg of total RNA). The reverse transcription reaction was made with Eppendorf Mastercycler ep Gradient, (Eppendorf, Germany).

3.6.4 Real-Time PCR

After this step, the cDNA was added to a RT² SYBR Green ROX qPCR Mastermix and the final solution was charged on a custom RT^2 PCR Array (array designed by ThermoFisher Scientific, MA, USA using a set of gene of interest) and then analysed with Applied Biosystems™ 7500 Real-Time PCR Systems (ThermoFisher Scientific - Waltham, Massachusetts, USA) following the manufacturer's protocol. Due to possible critical issue connected to the use of SYBR technology, a melting curve analysis was performed at the end of each single RT^2 PCR array.

3.7 Histological analysis

For histological analysis, Masson's trichrome stained slides representative of all the five lobes were digitalized through the image analysis system NDP.scan 3.2 with NanoZoomer S-60 scanner (Hamamatsu Photonics K.K, Japan). Scans were performed using the fully automated mode and 20x objective.

3.7.1 Ashcroft score

Fibrotic lung injury was assessed histologically on the whole-slide images using the Ashcroft scoring system (*Hübner et al. 2008*) by an expert histopathology blinded to the experimental design. The analyses were performed by external laboratories: for time course BLM OA study the analysis was performed by AnaPath Services GmbH, Hammerstrasse, Switzerland; all other studies were analyzed by GLP Life Test- Istituto Ramazzini in Bologna, Italy.

In order to cover the whole surface of each lung section, a grid with rectangles of 2x1 mm was placed over the tissue area. Only rectangles where at least half of the area was covered by parenchyma, excluding large blood vessels and bronchi, were evaluated. The severity of fibrotic tissue in each field was evaluated at 10x magnification using the Ashcroft scale from grade 0 to 8 (**Table 3.1**). In each examined field, the predominant degree of fibrosis that occupied more than half of the field area, was recorded. Ashcroft scores for each animal lung were expressed as the mean of the total number of fields. Mean Ashcroft scores for each group were obtained from the mean of each animal.

Table 3.1 Description of the histological Ashcroft scoring system (taken from *Hübner et al. 2008*)

Grade of Fibrosis	Histological features
0	Alveolar septa: No fibrotic burden at the most flimsy small fibers in some alveolar walls Lung structure: Normal lung
1	Alveolar septa: Isolated gentle fibrotic changes (septum ≤3× thicker than normal) Lung structure: Alveoli partly enlarged and rarefied, but no fibrotic masses prese
2	Alveolar septa: Clearly fibrotic changes (septum >3× thicker than normal) with knot-like formation but not connected to each other Lung structure: Alveoli partly enlarged and rarefied, but no fibrotic masses
3	Alveolar septa: Contiguous fibrotic walls (septum >3× thicker than normal) predominantly in whole microscopic field Lung structure: Alveoli partly enlarged and rarefied, but no fibrotic masses
4	Alveolar septa: Variable Lung structure: Single fibrotic masses (≤10% of microscopic field)
5	Alveolar septa: Variable Lung structure: Confluent fibrotic masses (>10% and ≤50% of microscopic field). Lung structure severely damaged but still preserved
6	Alveolar septa: Variable, mostly not existent Lung structure: Large contiguous fibrotic masses (>50% of microscopic field). Lung architecture mostly not preserved
7	Alveolar septa: Non-existent Lung structure: Alveoli nearly obliterated with fibrous masses but still up to five air bubbles
8	Alveolar septa: Non-existent Lung structure: Microscopic field with complete obliteration with fibrotic masses

3.7.2 Artificial intelligence (AI)-based APP for fibrosis detection

Different grades of fibrosis severity on whole-slide images were assessed with the support of the AI deep learning Visiopharm® module. In addition to identify the lung parenchyma by excluding the basal collagen, main bronchi and blood cells, as described previously, the new APP was designed to identify the fibrotic regions and recognize different degrees of severity within these regions, classifying them as physiological, moderate and severe fibrosis *(Pontis et al. 2019)* corresponding to the different grades described in the modified Ashcroft scale (**Figure 3.5**).

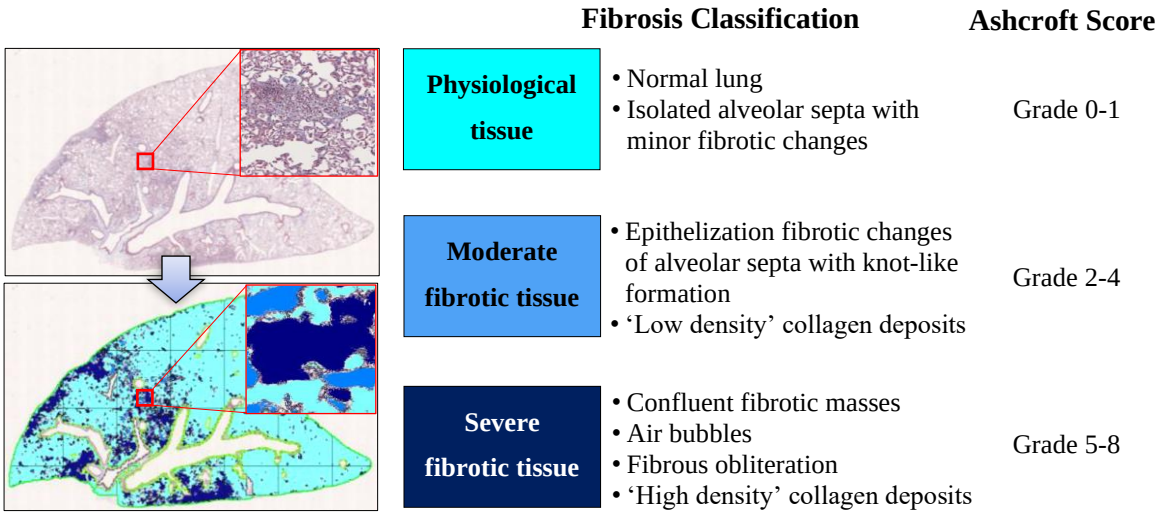

Figure 3.5 Schematic classification of lung fibrosis severity distribution by AI-based Visiopharm® APPs

3.8 Statistical analysis

All data were expressed as mean ± standard error of mean (SEM). Unpaired t-test or analysis of variance (ANOVA) followed by Sidak's or Dunnett's post hoc analysis were used to compare two or more experimental groups, respectively. The Pearson's correlation coefficient matrix (r value) was used to determine the degree of association between data. Statistical analyses were performed using GraphPad Prism 8 software (GraphPad Software Inc., San Diego, CA, USA). *$p \leq 0.05$ was considered statistically significant.

4. RESULTS

4.1 Time course study - novel readouts assessment

In order to characterize the novel readouts introduced in the murine model of BLM-induced lung fibrosis, the first experiment performed during my PhD period, was a time course study aimed to follow these readouts during the onset, the progression and the progressive resolution of fibrosis over time. In this first study, the lung fibrosis was induced in male mice by a double OA administration of BLM (n=15 for each time-point) or saline (n=4 for each time-point), at day 0 and at day 4 at a dose of 0.03 IU/mouse for each instillation. All readouts were examined at different time points (T7, T14, T21, T28, T35, T42 and T49) from the first BLM OA administration.

4.1.1 Refinement of histological analysis

The histological analysis, carried out with the Ashcroft scoring system has always been used as gold standard to grade fibrosis in preclinical model of IPF. Despite being widely used, this system is associated with some disadvantages such as being a time-consuming, operator-dependent process with limited sensitivity. To overcome these limitations, we introduced and validated an automated image analysis using an artificial intelligence (AI) approach, able to recognize histological features with more accuracy and consistency, significantly reducing the time of the analysis, and making the evaluation independent from the operator. The AI-based Visiopharm® APP was developed with the purpose to recognize and classify different degrees of fibrosis severity corresponding to the different grades described in the modified Ashcroft scale, classifying them as physiological, moderate and severe fibrosis. The Ashcroft score analysis **(Figure 4.1A)** showed that at T7, the score in the BLM group was already significantly increased, with a value of 1.15 ± 0.11, compared to 0.18 ± 0.04 of the corresponding saline group (**$p \leq 0.01$); the score gradually increased at T14 (BLM 2.59 ± 0.3 vs SAL 0.09 ± 0.04; ***$p \leq 0.001$), reaching the peak at T21 (BLM 2.79 ± 0.32 vs SAL 0.06 ± 0.045; **$p \leq 0.01$). Afterwards, the grade of fibrosis started to progressively decline (at T28 BLM 1.95 ± 0.26 vs SAL 0.06 ± 0.01; **$p \leq 0.01$; at T35 BLM 1.66± 0.26 vs SAL 0.10 ± 0.01; **$p \leq 0.01$; at T42 BLM 1.4 ± 0.26 vs SAL 0.37 ± 0.03; **$p \leq 0.01$) up to an almost complete resolution at T49 (BLM 0.74 ± 0.16 vs SAL 0.04 ± 0.04; **$p \leq 0.01$). The saline-treated group, as expected, showed normal lung

architecture (Score <1) at all points of observation with no prominent changes in the lung parenchyma.

The automated analysis of lung fibrosis performed by the AI **(Figure 4.1B)** was in line with Ashcroft score analysis, confirming a high degree of moderate (3.28 %) and severe degree of fibrosis (1.89 %) in the BLM group at T7 probably due also to an inflammatory infiltration observed in this early phase of the model; moderate and severe fibrotic tissues further increased at T14 (respectively 4.20% and 2.25%), reaching the peak at T21 (2.42% and 4.48%) and then starting to decrease at T28 (3.42% and 2.21%). At T35 the fibrotic tissue was respectively 2.02% (moderate) and 0.9% (severe) but resulted very low at T42 (1.05% moderate; 0.42% severe) and T49 (0.79% moderate; 0.23% severe).

The control group treated with saline (in the graph of the **Figure 4.1B** is shown a mean of all controls at each time points), as expected, showed 99% of physiological tissue for all points of observation, with less than 1% of fibrotic tissue.

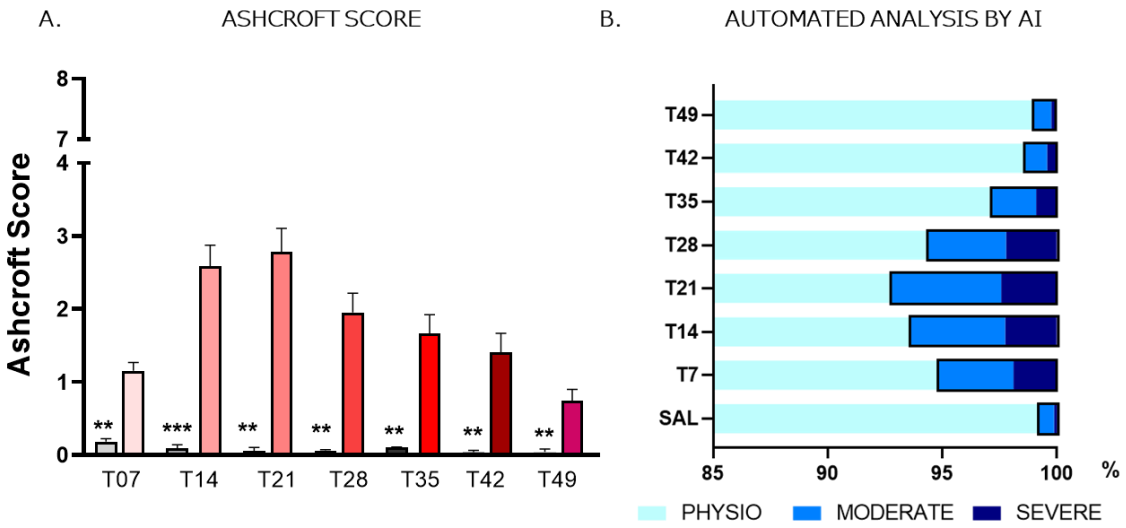

Figure 4.1 Histological analysis of pulmonary fibrosis in Masson's Trichrome stained lung sections performed in mice at different time points. **(A)** Ashcroft score analysis. Data are expressed as mean ± SEM (n=4 Saline, scale of grey bars; n=15 BLM, scale of red bars). Statistical analysis was assessed using nonparametric Mann Withney test in comparison with the relative control values (Saline group); ** $p \leq 0.01$. **(B)** Tissue classification of lung fibrosis severity distribution using AI-based APPs.

4.1.2 DFCO evaluation

The diffusing capacity of the lungs for carbon monoxide (DLCO), also known as the diffusion factor for carbon monoxide (DFCO) is a measurement that assess the lungs' ability to transfer gas from inspired air to the bloodstream and it is reported to be reduced in interstitial lung diseases including pulmonary fibrosis due to the thickening of the alveolar-

capillary membrane with a restrictive pattern on Pulmonary Function Test *(Heckman et al 2015)*. DFCO correlates with IPF disease outcomes, with more advanced impairments associated with decreased health-related quality of life and survival *(Costabel et al 2019)*, and it is commonly used as secondary endpoint in clinical trials assessing the efficacy of novel treatments for IPF.

Nonetheless, DFCO has been only seldom evaluated in mouse models, in part because the procedure is complex and/or requires dedicated equipment. In our model we assessed DFCO using a gas chromatograph to analyse changes in CO and Ne in a calibration gas mixture injected and then removed from the lungs of the mice. DFCO was then calculated as 1–(CO9/COc)/(Ne9/Nec), where the c and 9 subscripts refer to concentrations of the calibration gases injected and the gases removed after a 9 sec breath hold time, respectively. The obtained values are between 0 and 1, with 1 reflecting complete uptake of CO, and 0 reflecting no uptake of CO. The decline in DFCO of the BLM group compared to the corresponding saline (Δ value) group was already evident at T7 (BLM 0.51 vs SAL 0.66, Δ=0.15±0.03, ns) and becoming statistically significant at T14 (BLM 0.4 vs SAL 0.6, Δ=0.20±0.03, *p ≤ 0.05), T21 (BLM 0.44 vs SAL 0.69, Δ=0.25±0.03, **p ≤ 0.01) and T28 (BLM 0.48 vs SAL 0.69, Δ=0.21±0.03, *p ≤ 0.05), showing the maximum decrease at T21 in line with the histological evaluations. The drop in DFCO values observed in the BLM group after T28 started to progressively decrease, resulting in differences not statistically significant (T35, BLM 0.50 vs SAL 0.64, Δ=0.14±0.03, ns; T42, BLM 0.54 vs SAL 0.65, Δ=0.11±0.05, ns; T49, BLM 0.57 vs SAL 0.65, Δ=0.08±0.04, ns) as shown in **Figure 4.2.**

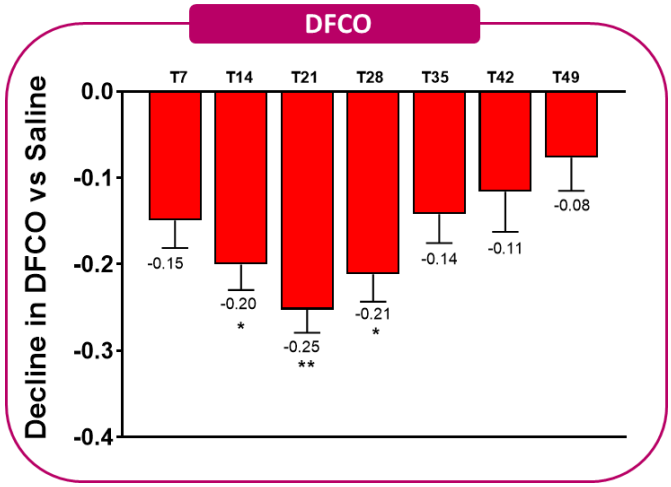

Figure 4.2 DFCO measured in mice at different time points (T7, T14, T21, T28, T35, T42 and T49) from the first BLM OA administration. Data are expressed as decline (red bars) of BLM group compared to its saline control at the same time point ± SEM (n=4 Saline; n=15 BLM). Statistical analysis was assessed using t test in comparison with the relative control values (Saline group); ** p ≤ 0.01, * p ≤ 0.05.

4.1.3 Lung Function assessment

Lung function analysis, in particular the Forced Vital Capacity (FVC), was performed using the FlexiVent System (SCIREQ) in the time-course experiment to identify changes in respiratory system mechanics upon BLM treatment over the time. The results **(Figure 4.3)** showed that at T7 the BLM group did not show any significant decline (Δ value) in FVC compared to the saline group (BLM 0.97±0.03mL vs SAL 1.01±0.03 mL, Δ=0.05±0.03, ns), but the decrease in FVC was already statistically significant at T14 (BLM 0.83±0.03 mL vs SAL 1.07±0.03 mL, Δ=0.24±0.03, **p ≤ 0.01), and further progressed at T21 (BLM 0.74±0.04 mL vs SAL 1.05±0.02 mL, Δ=0.31±0.09, ***p≤ 0.001), remaining statistically significant at T28 (BLM 0.76±0.03 mL vs SAL 1.03±0.02 mL, Δ=0.27±0.06, **p≤ 0.01) and T35 (BLM 0.85±0.03 mL vs SAL 1.05±0.03 mL, Δ=0.20±0.03, *p≤ 0.05). No significant lung function changes were observed at T42 (BLM 0.93±0.03 mL vs SAL 1.06±0.02 mL, Δ=0.13±0.04, ns) and T49 (BLM 0.98±0.03 mL vs SAL 1.1±0.03 mL, Δ=0.12±0.04, ns). The FVC decline induced by BLM over the time matched with the profile of lung fibrosis assessed by histological evaluations as well as with DFCO changes. In particular, both functional readouts reached the peak of decline at T21 when the highest level of lung fibrosis was observed, and then concurrently with a progressive resolution of fibrosis starting from T28, a gradual recovery of both DFCO and FVC decline was observed, highlighting the high correlation among all these readouts and confirming that the changes observed in respiratory mechanics after the BLM injury are secondary to the development of pulmonary fibrosis.

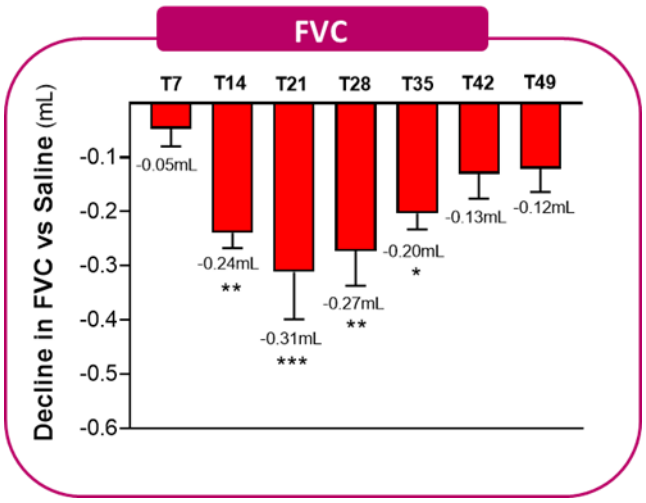

Figure 4.3 FVC measured by Flexivent System in mice at different time points (T7, T14, T21, T28, T35, T42 and T49) from the first BLM OA administration. Data are expressed as decline (red bars) of BLM group compared to its saline control at the same time point ± SEM (n=4 Saline; n=15 BLM). Statistical analysis was assessed using t test in comparison with the relative control values (Saline group); *** p ≤ 0.001, ** p ≤ 0.01, * p ≤ 0.05.

4.1.4 Biomarkers exploration

Given the disease heterogeneity, the diagnostic difficulty and the individual prognosis, the development of biomarkers for IPF that can guide diagnostic, prognostic and therapeutic approaches in managing the disease has become pivotal to tailor personalized anti-fibrotic therapies *(Quian et al 2021)*. The project PROLIFIC (PROgnostic Lung FIbrosis Consortium), born from the collaboration between the Pulmonary Fibrosis Foundation and several pharmaceutical companies, selected 12 relevant biomarkers in IPF, that have been categorized in three groups according to the different pathways involved in the pathogenesis of IPF:

- *Associated to alveolar epithelial cells (AEC) disruption;*
- *Related to ECM remodeling and fibro-proliferation;*
- *Biomarkers related to immune dysfunction.*

Among those *associated to the epithelial damage*, we measured the surfactant protein D *(SP-D)* in plasma during the time course experiment, finding a statistically significant increase of SP-D in BLM group compared to the saline group at T7 (440.2 ±48.5 ng/mL vs 8.74 ±1.98 ng/mL,***p≤ 0.001), at T14 (346.2 ±61.4 ng/mL vs 8.74±1.46 ng/mL,***p≤ 0.001) and at T21 (306.3 ±40.4 ng/mL vs 6.73 ±0.79 ng/mL,***p≤ 0.001); while remaining higher than those observed in controls, the concentrations of this circulating biomarker markedly declined at T28 (at T28 83.2 ±19.4 ng/mL vs 7.5 ±5.6 ng/mL,***p≤ 0.001) and at the following time-points (T35 38.1±7.1 ng/mL vs 6.69±0.55 ng/mL,**p≤ 0.05; at T42 32.1±1.6 ng/mL vs 8.35±0.71 ng/mL,**p≤ 0.05; at T49 17.1±1.5 ng/mL vs 6.1±0.97 ng/mL,**p≤ 0.05) **(Figure 4.4).** These data suggest that the epithelial damage occurred rapidly upon the bleomycin injury, preceding the development of fibrosis as well as its trend toward resolution over time, as shown when comparing SP-D data and the functional **(Figures 4.2-4.3)** and histological readouts **(Figure 4.1)**.

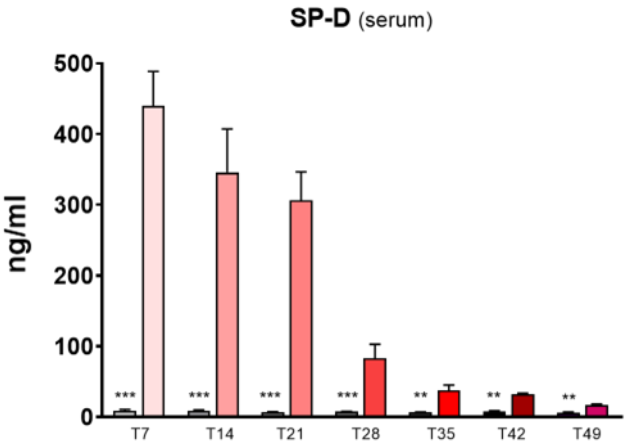

Figure 4.4 SP-D levels evaluated by ELISA assay in plasma of saline (n=4 for each time point, scale of grey bars) and bleomycin treated mice (n=15 for each time point, scale of red bars) at different time-points. Statistical analysis was assessed using t test in comparison with the relative control values (saline group); *** $p \leq 0.001$, ** $p \leq 0.01$.

Another important disruption occurring in the fibrotic process is related to *ECM remodeling and fibro-proliferation*, resulting from an excessive production of extracellular matrix. Matrix metalloproteinases (MMPs) are proteases that degrade all extracellular matrix and many non-matrix protein components, playing several roles in the fibrotic process *(Bassiouni et al 2021)*; MMP-7 in particular is considered one of the most promising prognostic biomarkers in IPF, with changes in MMP-7 associating with disease progression and severity. We therefore evaluated MMP-7 in the time-course study, showing that levels of MMP-7 **(Figure 4.5)** were elevated in BALF of BLM mice when compared to saline group at T7 (5999 ±183 pg/mL vs 1053±45 pg/mL,***p≤0.001) and decreased in a time-dependent manner at T14 (5327±294 pg/mL vs 771±55 pg/mL,***p≤0.001), at T21 (4580±398 pg/mL vs 738 ±183 pg/mL,***p≤0.001), and at T28 (2737±355 pg/mL vs 846±232 pg/mL ,*p≤0.05) reaching concentrations that were not statistically different in BLM and control mice at T35 (1421±187 pg/mLvs 894±186 pg/mL, ns) and at the following time-points (at T42 1378±190 pg/mL vs 722±150 pg/mL, ns, and at T49 1355±198 pg/mL vs 734±148 pg/mL , ns).

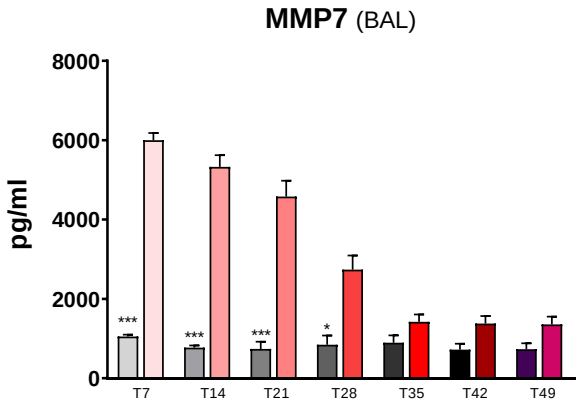

Figure 4.5 MMP-7 levels evaluated by ELISA assay in BALF of saline (n=4 for each time point, scale of grey bars) and bleomycin treated mice (n=15 for each time point, scale of red bars) at different time-points. Statistical analysis was assessed using t test in comparison with the relative control values (Saline group); *** $p \leq 0.001$, ** $p \leq 0.01$, * $p \leq 0.05$.

Collagen I and *Collagen III* are also reported to be increased in IPF patients, as are the concentrations of neoepitope *PRO-C3*, in both serum and BAL fluid.

In fact, we were able to show that levels of Collagen I **(Figure 4.6A)** resulted significantly increased in BALF obtained from the BLM mice as compared to animals treated with saline at T7 (9.55±0.73 ng/mL vs 0.42 ±0.06 ng/mL, **p≤0.01), T14 (7.45±0.68 ng/mL vs 0.28 ng/ml±0.04 ng/mL, ***p≤0.001), T21 (6.07±1.05 ng/mL vs 0.32±0.09 ng/mL, *p≤0.05), and T28 (2.27±0.59 ng/mL vs 0.36±0.19 ng/mL, *p≤0.05), while no statistically significant difference was observed beginning at T35 (1.59±0.39 ng/mL vs 0.56±0.24 ng/mL, ns; T42 1.18±0.32 ng/mL vs 0.44±0.14 ng/mL, ns; T49 0.75±0.35 ng/mL vs 0.20±0.03 ng/mL, ns).

Similar results were obtained assessing Collagen III in BALF **(Figure 4.6B)** (T7 280±10.7 ng/mL vs 2±0.01 ng/mL, BLM and saline-treated mice, respectively; **p≤0.01; T14 110.7±21.5 ng/mL vs 2±0.04 ng/mL, **p≤0.01; T21 44.8±14.2 ng/mL vs 2±0.02 ng/mL, *p≤0.05; T28 17.1±5.1 ng/mL vs 2±0.01 ng/mL, ns; T35 12.6±6.2 ng/mL vs 2±0.01 ng/mL, ns; T42 3.9±1.9 ng/mL vs 2±0.01 ng/mL, ns; and T49 2.1±0.01ng/mL vs 2±0.01ng/mL, ns).

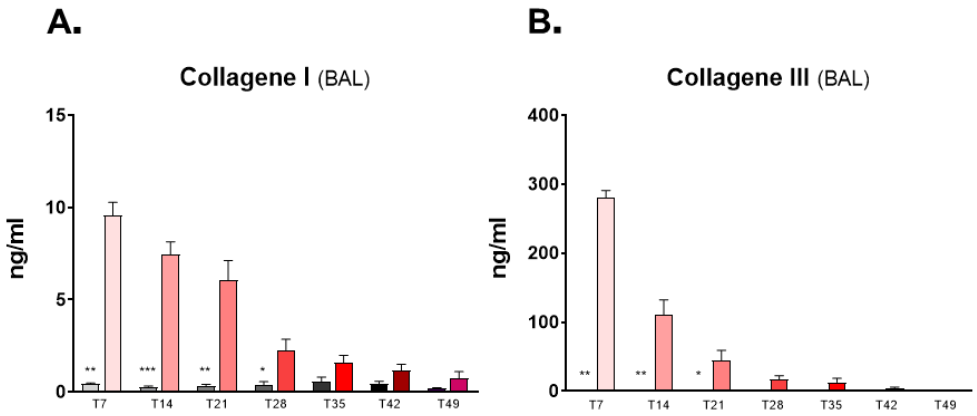

Figure 4.6 Collagen I **(A)** and Collagen III **(B)** levels evaluated by ELISA assay in BALF of saline (n=4 for each time point, scale of grey bars) and bleomycin treated mice (n=15 for each time point, scale of red bars) at different time-points. Statistical analysis was assessed using t.test in comparison with the relative control values (Saline group); *** $p \leq 0.001$, ** $p \leq 0.01$, * $p \leq 0.05$.

Focusing on the most relevant time-points where collagen was found significantly increased by bleomycin treatment, we measured PRO-C3 levels at T7, T14, T21, T28, finding this biomarker significantly increased in the BLM group compared to control animals at all the time-points evaluated (T7 17.9 ±0.6 ng/mL vs 7.4±1.7 ng/mL

***p≤0.001; T14 19.3±1.9 ng/mL vs 7.8±1.2 ng/mL **p≤0.01; T21 20.8±1.1 ng/mL vs 9.3±1.2 ng/mL ***p≤0.001; T28 15.3±1.1 ng/mL vs 10.1±1.6 ng/mL *p≤0.05) **Figure 4.7**.

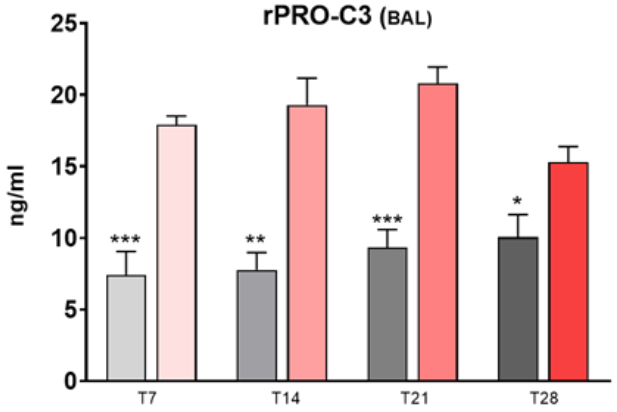

Figure 4.7 PRO-C3 levels evaluated by ELISA assay in BALF of saline (n=4 for each time point, scale of grey bars) and bleomycin treated mice (n=15 for each time point, scale of red bars) at different time-points. Statistical analysis was assessed using t-test in comparison with the relative control values (Saline group); *** p ≤ 0.001, ** p ≤ 0.01, * p ≤ 0.05.

Osteopontin (OPN), a highly phosphorylated glycoprotein produced by alveolar macrophages, is a fibrogenic cytokine, promoting migration, adhesion, and proliferation of fibroblasts during the development of fibrosis. It is involved in the progression of tissue fibrosis and its role as diagnostic biomarker to support differentiation with non-IPF ILD has been recognized. As shown in **Figure 4.8,** OPN levels in BALF of BLM-treated mice rose rapidly when compared to the control group resulting statistically elevated already at T7 (1350±98 ng/mL vs 33.7±1.4 ng/mL **p≤0.01), and progressively increasing at T14 (2841 ±168 ng/mL vs 58.0±29.8 ng/mL ***p≤0.001) up to reaching a peak at T21 (3598±399 ng/mL vs 33.9±2.8 ng/mL **p≤0.01) followed by a decrease at T28 (1993±310 ng/mL vs 28.6±1.2 ng/mL ***p≤0.001), T35 (1349±288 ng/mL vs 34.3±2.5 ng/mL **p≤0.01) and T42 (1005±166 ng/mL vs 24.4±5.5 ng/mL **p≤0.01), but remaining statistically elevated up to T49 (378±86 ng/mL vs 22.9±1.1 ng/mL **p≤0.01).

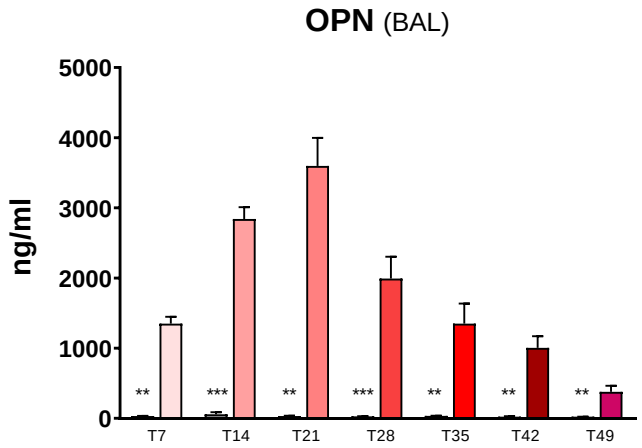

Figure 4.8 OPN levels evaluated by ELISA assay in BALF of saline (n=4 for each time point, scale of grey bars) and bleomycin treated mice (n=15 for each time point, scale of red bars) at different time-points. Statistical analysis was assessed using t-test in comparison with the relative control values (Saline group); *** p ≤ 0.001, ** p ≤ 0.01.

In the last few years, the role of the immune system in IPF pathobiology has been reconsidered; indeed, recent data suggest that a *dysfunctional immune system* may promote an unfavorable interplay with pro-fibrotic pathways thus acting as a cofactor in disease development and progression. Particularly, dysregulated B cells are implicated in the pathogenesis of IPF and *CXCL13,* which is reported to mediate B-cell trafficking, is increased in plasma of IPF patients in a manner reflecting disease activity, therefore suggesting it may represent a prognostic biomarker. Similarly, Interleukin 6 (*IL-6*) is promptly produced by immune cells in response to tissue injuries and plays a significant role in fibrosis in various organs via Janus kinase/signal transducer and activator of transcription 3 (JAK/STAT3) activation.

In our model we found significantly higher levels of CXCL13 in BALF of BLM-treated mice compared to saline at all time-points after the BLM administration (T7, 403±34 pg/mL vs 4.05±0.01 pg/mL **p≤0.01; T14, 119±13 pg/mL vs 4.05±0.01 pg/mL ***p≤0.001; T21, 153±38 pg/mL vs 4.05±0.01 pg/mL **p≤0.01; T28, 44.5±12.2 pg/mL vs 4.05±0.01 pg/mL *p≤0.05; T35, 32.4±6.9 pg/mL vs 4.05±0.02 pg/mL *p≤0.05; T42, 52.3±5.9 pg/mL vs 15.7±7.6 pg/mL **p≤0.01; T49, 36.7 ±6.9 pg/mL vs 8.82±2.96 pg/mL **p≤0.01), but with a peak at T7, as observed with SP-D, MMP-7, and collagens, suggesting a role in the development of fibrosis. IL-6 seemed to show a bi-phasic behavior, with two peaks at T7 (61.7±6.5 pg/mL vs 0.63±0.01 pg/mL **p≤0.01) and at T21 (79.9±32.7 pg/mL vs 0.63±0.01 pg/mL **p≤0.01), even if large standard errors may mask a trend similar to CXCL13 **(Figure 4.9B)**.

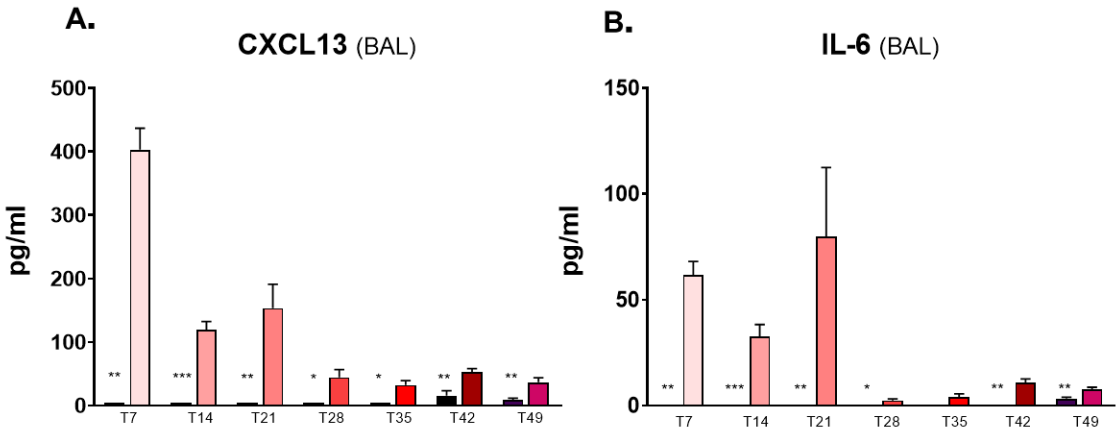

Figure 4.9 CXCL13 **(A)** and IL-6 **(B)** evaluated by ELISA assay in BALF of saline (n=4 for each time point, scale of grey bars) and bleomycin treated mice (n=15 for each time point, scale of red bars) at different time-points. Statistical analysis was assessed using t-test in comparison with the relative control values (Saline group); *** $p \leq 0.001$, ** $p \leq 0.01$, * $p \leq 0.05$.

4.2 Time course study – gene expression profiling

To provide additional support to the potential role of these biomarkers, and to find new, relevant ones, we assessed the pulmonary expression of a panel of genes involved in both fibrotic and inflammatory processes,). To this aim, a time course experiment devoted to the gene expression profiling was carried out focusing on the earlier time-points (T7, T14, T21, T28. Following the experimental protocol described in the *Paragraph 3.6.1*, mRNAs were extracted from lung homogenates of BLM (n=10 for each time-points) and saline treated mice (n=5 for each time-points) in comparison to naïve animals (n=4) as shown in **Figure 4.10**.

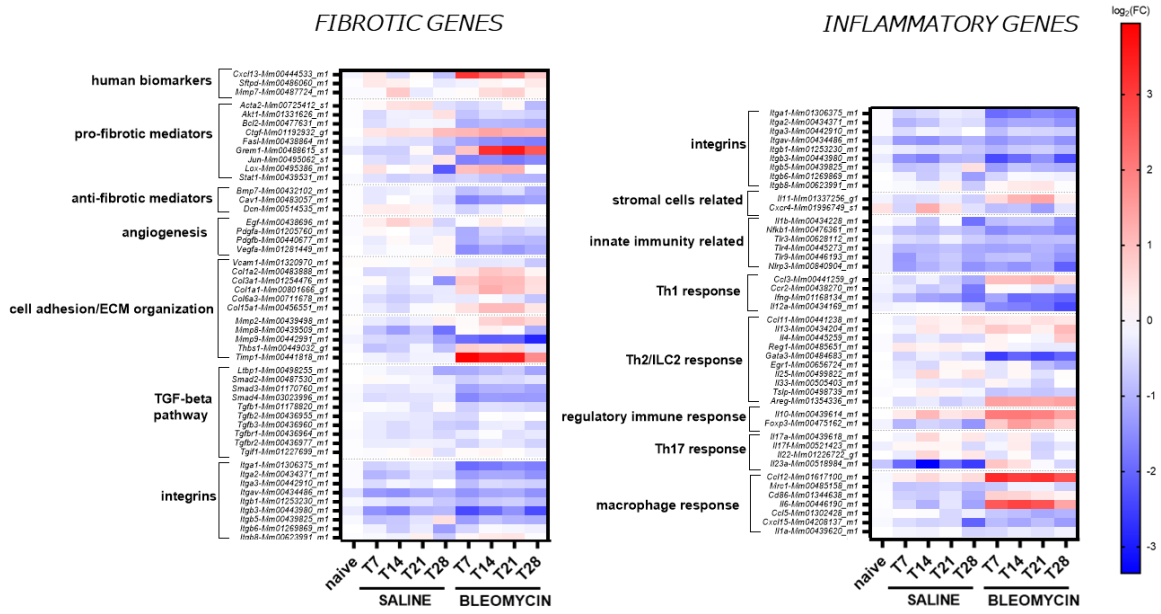

Figure 4.10 Heat-map with the difference in expression pattern of fibrotic and inflammatory response-related genes in naïve animals (n=4), saline (n=5 for each time point) and bleomycin treated mice (n=10 for each time point) at different time-points (T07, T14, T21, T28).

It is interesting to note that expression of MMP-7, despite the observed increased concentrations in BALF of BLM mice, did not reach the statistical significance at any time-points, while MMP-2 over-expression was found statistically significant (***p≤0.001) at T14, T21 and T28, with a peak at T21. Similarly, the expression of MMP-8 was significantly increased in the BLM animals at T07, T14, T21 (***p≤0.001) showing the highest mRNA expression at T14 **(Figure 4.11A)**. Collagen-I and III genes were also involved in the response to BLM, as shown by the statistically significant increased expression of genes coding for their subunits at all timepoints evaluated (Col1a1 at all time-points ***p≤0.001; Col3a1 at T7, T14, T21 ***p≤0.001 at T28 **p≤0.01) **(Figure 4.11B)**.

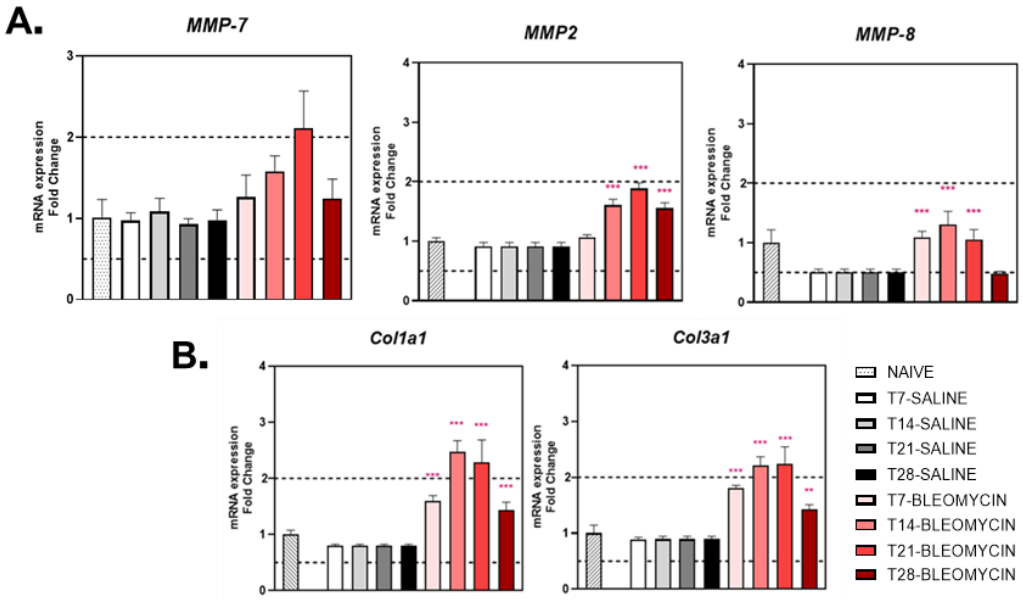

Figure 11 MMP-7, MMP-2, MMP-8, Col1a1 and Col3a1 expression fold change in Saline (n=5 for each time point, scale of grey bars) and bleomycin (n=10 for each time point, scale of red bars) treated mice at different time-points (T7, T14, T21, T28) compared to naïve animals (n=4, white bar). Statistical analysis was assessed using one-way ANOVA (Dunnett's t test) in comparison with the relative control values (Saline group); *** $p \leq 0.001$, ** $p \leq 0.01$.

In line with the observed concentrations of the chemokine in BALF, CXCL13 expression resulted increased at T7, T14 and T21 (***p<0.001) **(Figure 4.12A),** underlining the importance of macrophages in the pathogenesis of IPF and supporting CXCL13 as a biomarker of disease in BLM mice. IL-6 gene expression also reflected the time course of IL-6 concentrations in BALF of BLM-treated mice, even if only the increase observed at T14 resulted statistically significant (*p≤0.05) **(Figure 4.12B)**.

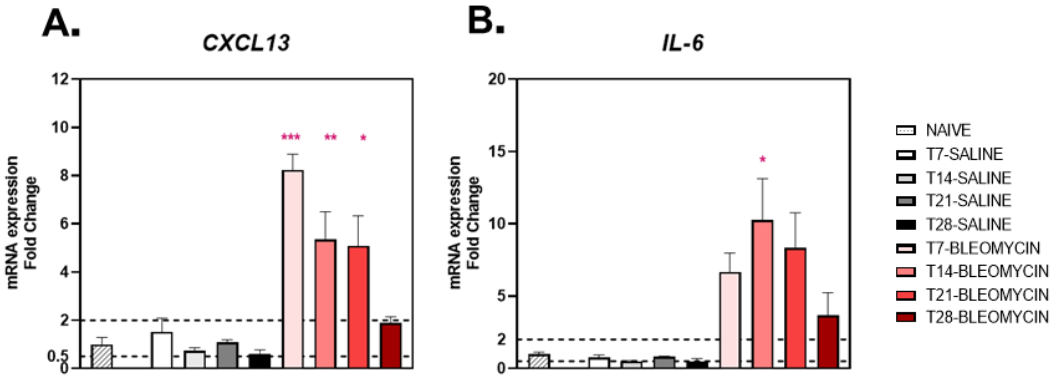

Figure 4.12 CXCL13 **(A)** and IL-6 **(B)** mRNA expression fold change in Saline (n=5 for each time point, scale of grey bars) and bleomycin treated mice (n=10 for each time point, scale of red bars) at different time-points (T7, T14, T21, T28) compared to naïve animals (n=4, white bar). Statistical analysis was assessed using one-way ANOVA (Dunnett's t test) in comparison with the relative control values (Saline group); *** $p \leq 0.001$, ** $p \leq 0.01$, * $p \leq 0.05$.

4.3 Pharmacological validation of novel readouts

After having assessed the relevance of novel readouts for the BLM model in the time course experiments and having demonstrated their strong correlation among each other, the step forward was to validate these readouts in a pharmacological study. For this purpose, we carried out a therapeutic study with Nintedanib, one of the only two approved drugs for IPF. The drug was administered orally in mice (n=15) at the dose of 50 mg/kg b.i.d., the most effective dose in mice as suggested from previous internal evidence, for 14 days starting from day 7 after the first OA of BLM, as described in the *Paragraph 3.2.4.*. All the assessments were performed at T21 since in the previous time course study this time point resulted as the one with the highest level of fibrosis and with the strongest alterations of functional assessments. As expected at T21, the Ashcroft score analysis highlighted a significant increase of the average score in the BLM mice (n=15) compared to the control mice treated with saline (n=5) (3.5 ± 0.2 vs 0.06 ± 0.01, ***p ≤ 0.001). The oral treatment with Nintedanib significantly reduced the value of Ashcroft score when compared with the BLM group (2.6 ± 0.4, 26% of inhibition vs BLM group, *p ≤ 0.05) **(Figure 4.13A)**. The efficacy of Nintedanib in reducing lung fibrosis was even more evident looking at the lung fibrosis analysis performed by AI-based Visiopharm® APPs **(Figure 4.13B)**. In particular, the automated analysis of pulmonary fibrosis revealed that BLM treatment significantly (***p≤0.001) increased the percentage of moderate and severe fibrotic tissues compared to the saline-control group (respectively 7.3% and 8.3% vs 0.76% and 0.35%, ***p ≤ 0.001) and treatment with Nintedanib caused a statistically significant (**p≤0.01) reduction by 48% of severe and moderate fibrotic areas in favor of an increase of physiological tissue compared to the BLM group (severe: 4.0% vs 8.3%; moderate: 4.7% vs 7.3%; physiological: 91.4% vs 84.4%) **(Figure 4.13B)**.

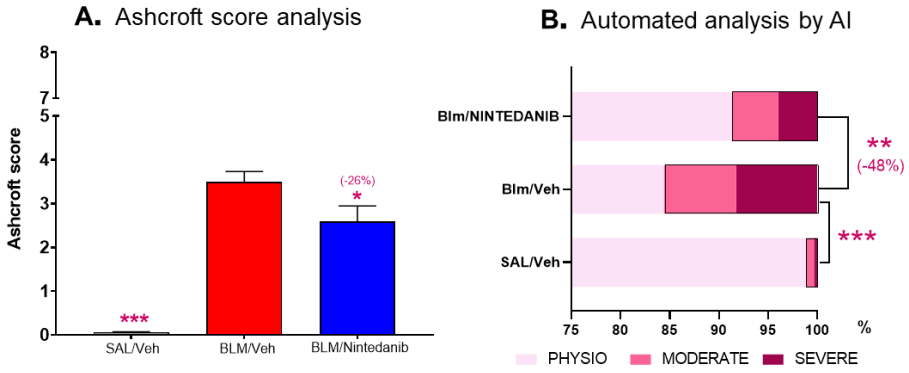

Figure 4.13 Effect of Nintedanib on **(A)** Ashcroft score analysis and **(B)** tissue classification of lung fibrosis severity distribution using AI-based Visiopharm® APPs. Data represent mean ± SEM values for Saline/Veh (n=5, grey bar), BLM/Veh (n=15, red bar) and BLM/Nintedanib (n=15, blue bar) groups of animals. Statistical analysis was assessed using one-way ANOVA followed by Dunnett's test in comparison with the BLM group; *** $p \leq 0.001$, ** $p \leq 0.01$, * $p \leq 0.05$. BLM, bleomycin; Veh, vehicle.

At T21, the DFCO evaluation showed that in BLM mice there is a significant (**p≤0.01) decrease of 0.27 in DFCO value (mean DFCO BLM: 0.41 ± 0.02 vs mean DFCO SAL: 0.68 ± 0.02) and that Nintedanib increased significantly (**p≤0.01) this value by 44% **(Figure 4.14A)**. After the DFCO assessment, the lung function tests were performed at the same endpoint (T21) by FlexiVent System. Consistently with an expected increase in lung stiffness and a restrictive pattern typical of the fibrotic disease, BLM mice showed a significant (***p≤0.001) decline of 0.29 mL when compared to the saline group (mean FVC BLM: 0.79 ± 0.03 mL vs mean FVC SAL: 1.1 ± 0.04 mL). Nintedanib treatment was able to limit BLM-induced alterations in lung function, significantly improving the FVC by 67% (0.98 ± 0.05 mL, ***p≤0.001) **(Figure 4.14 B)**.

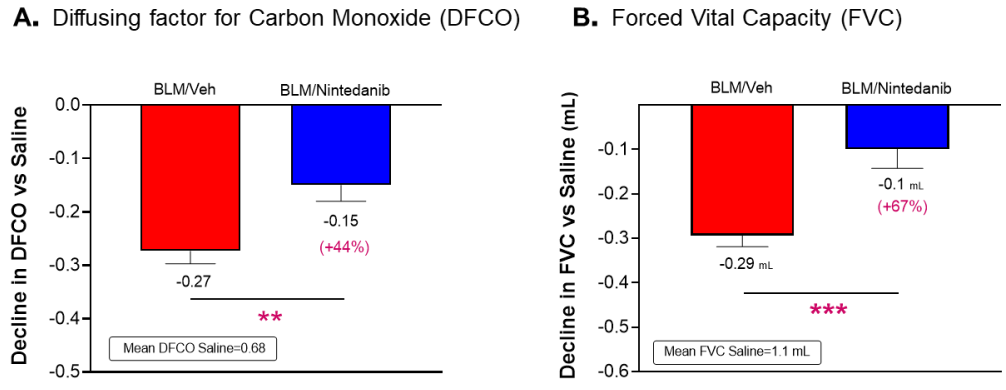

Figure 4.14 Effect of Nintedanib on the decline of DFCO **(A)** and FVC **(B)** at 21 days after BLM OA administration. Data represent mean ± SEM of values of decline for, BLM/Veh (n=15, red bar) and BLM/Nintedanib (n=15, blue bar) groups of animals compared to Saline group (n=5). Statistical analysis was assessed using one-way ANOVA followed by Dunnett's test in comparison with the BLM group; *** $p \leq 0.001$, ** $p \leq 0.01$, * $p \leq 0.05$. BLM, bleomycin; Veh, vehicle.

BALF and plasma were also collected from mice to evaluate biomarkers, and the results showed that SP-D was significantly increased in plasma of BLM mice (367.5 ± 53.9 pg/ml) compared to saline group (5.4± 0.3 pg/ml ***p≤0.001), while Nintedanib was able to markedly (67% of reduction) modulate the increase caused by BLM treatment (91.3± 21.2 pg/ml ***p≤0.001) **(Figure 4.15)**.

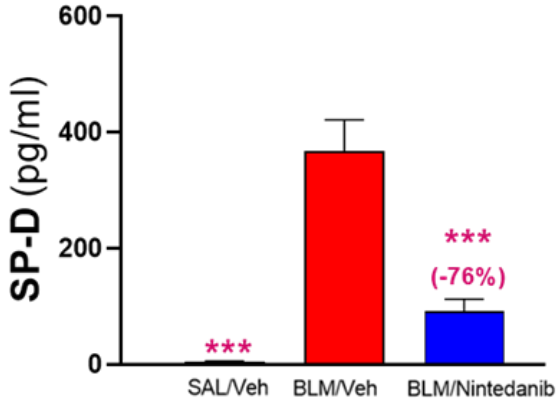

Figure 4.15 Effect of Nintedanib on SP-D in plasma at 21 days after BLM OA administration. Data represent mean ± SEM values for Saline/Veh (n=5, grey bar), BLM/Veh (n=15, red bar) and BLM/Nintedanib (n=15, blue bar) groups of animals. Statistical analysis was assessed using one-way ANOVA followed by Dunnett's test in comparison with the BLM group; *** p ≤ 0.001. BLM, bleomycin; Veh, vehicle.

MMP-7 was evaluated in BALF and resulted increased in BLM mice (1103± 92.5 pg/ml) when compared to the saline group (116.3± 24.8 pg/ml ***p≤0.001), while Nintedanib was able to reduce this increase by 57% (537.9± 114.5 pg/ml ***p≤0.001) **(Figure 4.16A)**. Moreover, as observed in clinical practice, a good correlation (R Pearson=-0.77, ***p≤0.001) between MMP-7 levels and DFCO decline was observed **(Figure 4.16B).**

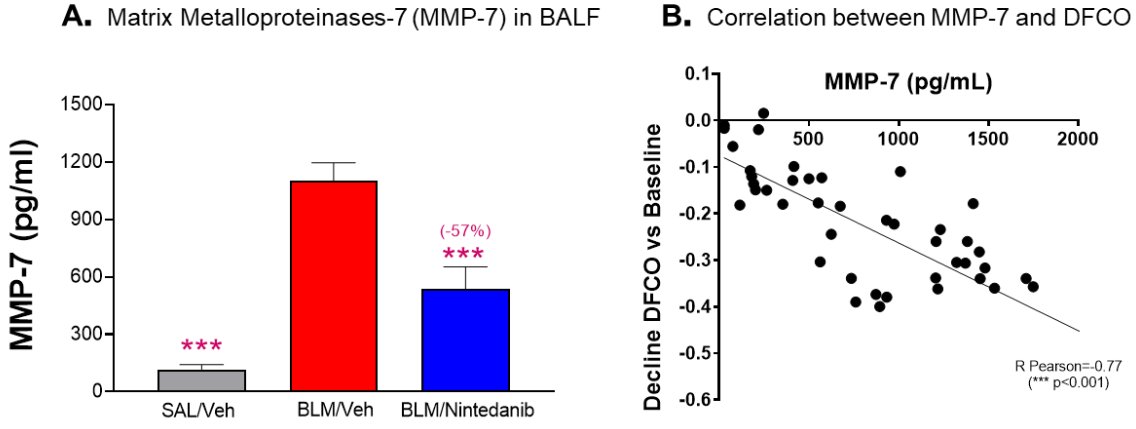

Figure 4.16 Effect of Nintedanib on MMP-7 in BALF at 21 days after BLM OA administration **(A)**. Correlation between MMP-7 and DFCO **(B)**. Data represent mean ± SEM values for Saline/Veh (n=5, grey bar), BLM/Veh (n=15, red bar) and BLM/Nintedanib (n=15, blue bar) groups of animals. Statistical analysis was assessed using one-way ANOVA followed by Dunnett's test in comparison with the BLM group; *** p ≤ 0.001, bleomycin; Veh, vehicle. Correlations were determined using Pearson's correlation coefficient matrix tests.

Collagen-1 and PRO-C3 were also evaluated in BALF samples as markers of ECM remodeling. As shown in **Figure 4.17A,** Collagen-I levels were significantly increased in BLM mice (13551±1639 pg/ml) compared to the saline group (232.2 ±25.7 pg/ml ***p≤0.001) and treatment with Nintedanib was able to significantly decrease this marker by 57% (5914 ± 766.6 pg/ml ***p≤0.001). Similarly, PRO-C3 was found increased in BLM mice (16.9±1.1 ng/ml) when compared to saline group (11.2±0.4 pg/ml ***p≤0.001) and treatment with Nintedanib blunted by 48% the increase observed in BLM mice (14.2 ±0.6 pg/ml *p≤0.05) **(Figure 4.17B)**.

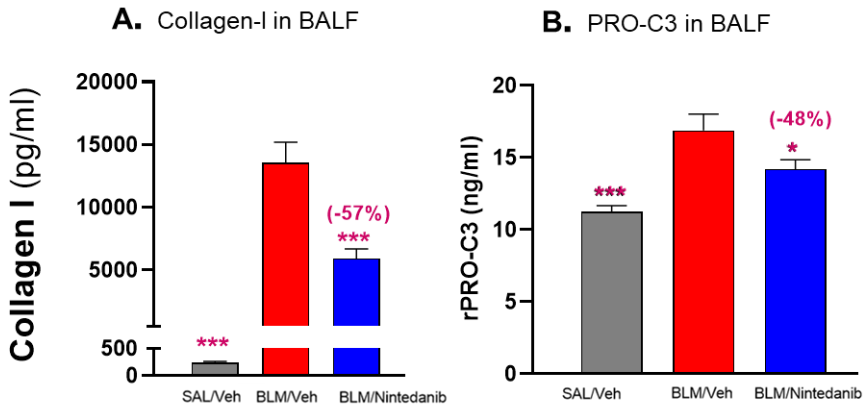

Figure 4.17 Effect of Nintedanib on Collagen-I **(A)** and PRO-C3 **(B)** in BALF at 21 days after BLM OA administration. Data represent mean ± SEM values for Saline/Veh (n=5, grey bar), BLM/Veh (n=15, red bar) and BLM/Nintedanib (n=15, blue bar) groups of animals. Statistical analysis was assessed using one-way ANOVA followed by Dunnett's test in comparison with the BLM group; *** $p \leq 0.001$, * $p \leq 0.05$. BLM, bleomycin; Veh, vehicle.

In line with the other biomarkers, OPN was found significantly increased in BALF of BLM mice compared to control animals (2183 ± 173 ng/ml vs 16.9 ± 1.3 ng/ml ***p≤0.001) and, again, the increase caused by BLM was significantly reduced by 42% by Nintedanib (1271 ± 126 ng/ml ***p≤0.001) **(Figure 4.18)**.

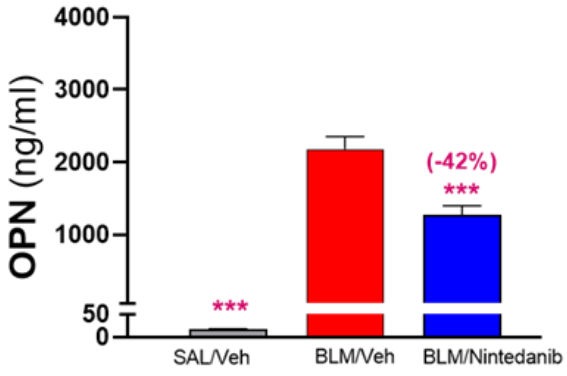

Figure 4.18 Effect of Nintedanib on OPN in BALF at 21 days after BLM OA administration. Data represent mean ± SEM values for Saline/Veh (n=5, grey bar), BLM/Veh (n=15, red bar) and BLM/Nintedanib (n=15, blue bar) groups of animals. Statistical analysis was assessed using one-way ANOVA followed by Dunnett's test in comparison with the BLM group; *** $p \leq 0.001$. BLM, bleomycin; Veh, vehicle.

Among the biomarkers of immune dysregulation, according to the time course experiment, we measured CXCL13 **(Figure 4.19A)** and IL-6 **(Figure 4.19B)** levels in BALF. Both markers were significantly increased in BLM treated mice compared to saline group (CXCL13, 188.8±28.2 pg/ml vs 6.5 ±0.9 pg/ml ***p≤0.001; IL-6, 76.2 ± 17.6 pg/ml vs 9.7 ± 1.9 pg/ml **p≤0.01) and Nintedanib significantly reduced the increase caused by BLM respectively by 42% and 67% (CXCL13, 115±16.2 pg/ml *p≤0.05; IL-6, 31.4±5.6 pg/ml *p≤0.05).

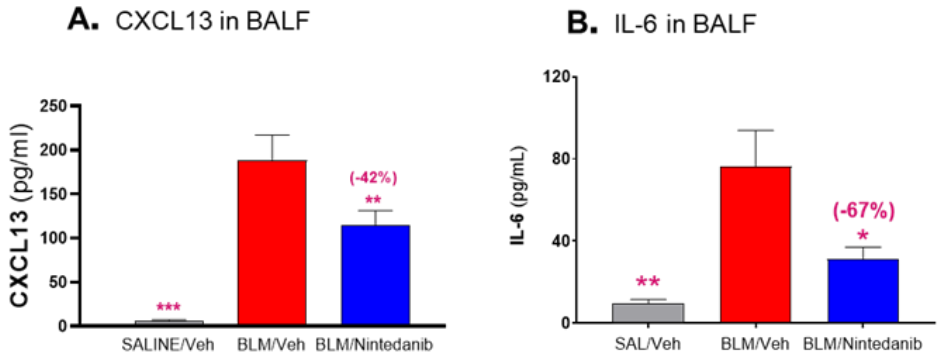

Figure 4.19 Effect of Nintedanib on CXCL13 **(A)** and IL-6 **(B)** in BALF at 21 days after BLM OA administration. Data represent mean ± SEM values for Saline/Veh (n=5, grey bar), BLM/Veh (n=15, red bar) and BLM/Nintedanib (n=15, blue bar) groups of animals. Statistical analysis was assessed using one-way ANOVA followed by Dunnett's test in comparison with the BLM group; *** p ≤ 0.001, ** p ≤ 0.01, * p ≤ 0.05. BLM, bleomycin; Veh, vehicle.

Finally, we wanted to assess if also the gene expression profile could affected by the anti-fibrotic drug. To this purpose, we carried out an additional therapeutic study with Nintedanib to assess in lung homogenates mRNA expression of a panel of genes resulted relevant from the time course experiment. The results obtained showed that among *genes associated to AEC disruption*, Serpine-1, also known as plasminogen activator inhibitor 1 (PAI-1), was significantly over-expressed (***p≤0.001) in BLM animals and down-modulated (***p≤0.001) by Nintedanib as shown in **Figure 4.20**. Serpine-1 seems to be involved in senescence of alveolar type 2 (ATII) cells, progenitors of the alveolar epithelium, that is implicated in the pathogeneses of IPF (41) and could represents an additional useful biomarker to evaluate.

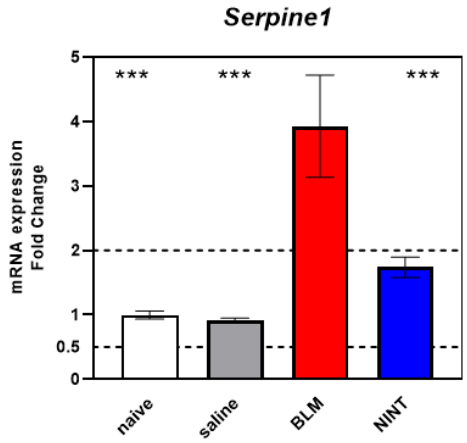

Figure 4.20 Effect of Nintedanib on mRNA expression fold change of genes related to AEC disruption. Data represent mean of fold change ± SEM values for Saline (n=4, grey bar), BLM (n=13, red bar) and Nintedanib (n=13, blue bar) groups of animals compared to naïve animals (n=4, white bar). Statistical analysis was assessed using one-way ANOVA followed by Dunnett's test in comparison with the BLM group; *** $p \leq 0.001$, * $p \leq 0.05$. BLM, bleomycin; Veh, vehicle.

Moreover, Nintedanib was also able to modulate significantly *genes involved in ECM remodeling and fibro-proliferation* which resulted overexpressed in BLM mice, such as some metalloproteinases (MMP-13 ***p≤0.01, MMP-8 **p≤0.01, MMP-14 **p≤0.01) and their inhibitor TIMP (**p≤0.01)) as shown in **Figure 4.21A**. Genes coding for subunits of Collagen I and III such as Col1a1 and Col3a1, resulted significantly overexpressed (***p≤0.001) after the BLM injury and statistically downregulated by Nintedanib (Col1a1 **p≤0.01; Col3a1 ***p≤0.01). Similar to what observed for the encoded protein, the gene for OPN (SPP1) was significantly over-expressed in BLM group (***p≤0.001) and was also downregulated by Nintedanib (***p≤0.001) **(Figure 4.21B)**.

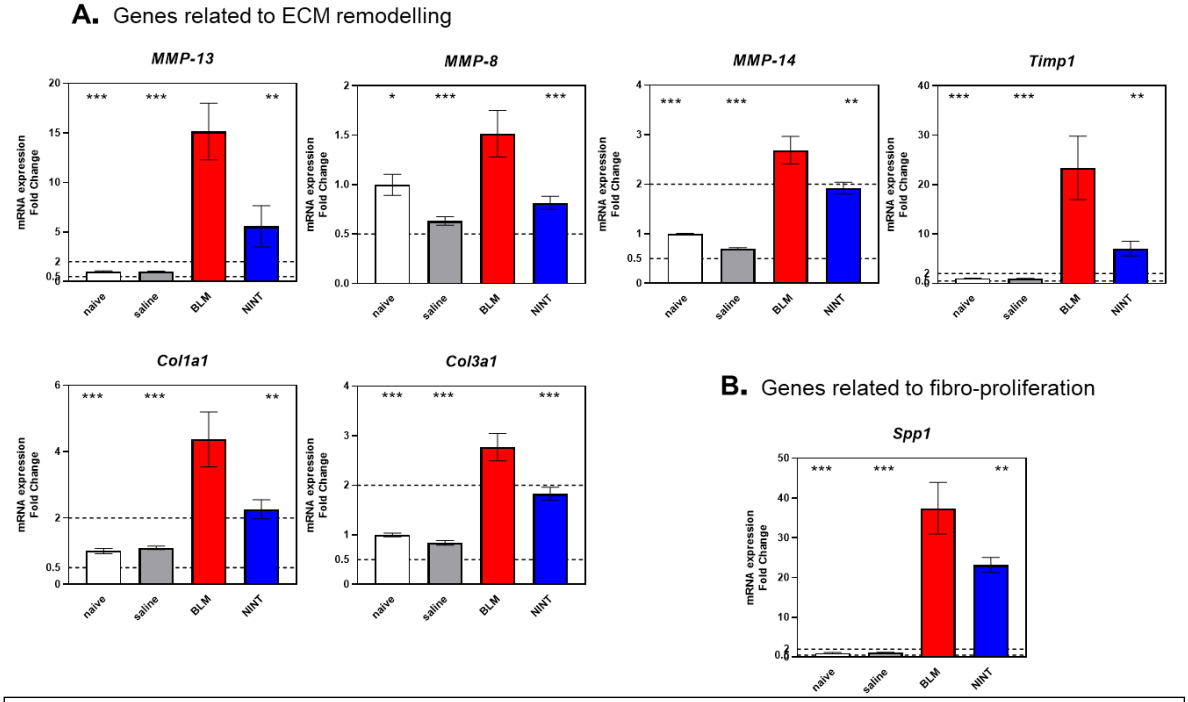

Figure 4.21 Effect of Nintedanib on mRNA expression fold change of genes related to ECM remodeling **(A)** and genes related to fibro-proliferation **(B)**. Data represent mean of fold change ± SEM values for Saline (n=4, grey bar), BLM (n=13, red bar) and Nintedanib (n=13, blue bar) groups of animals compared to naïve animals (n=4, white bar). Statistical analysis was assessed using one-way ANOVA followed by Dunnett's test in comparison with the BLM group; *** $p \leq 0.001$, * $p \leq 0.05$. BLM, bleomycin; Veh, vehicle.

Finally, the impact of Nintedanib on *genes related to a dysfunctional immune system* was also highlighted. In particular, the genes encoding for CXCL13 and IL-6 that were seen upregulated in the BLM treated mice in the time course study, were confirmed up-regulated (***p≤0.001) after the BLM challenge also in this study, and Nintedanib was able to significantly downregulate them (CXCL13 ***p≤0.001; IL-6 *p≤0.05) **(Figure 4.22)**.

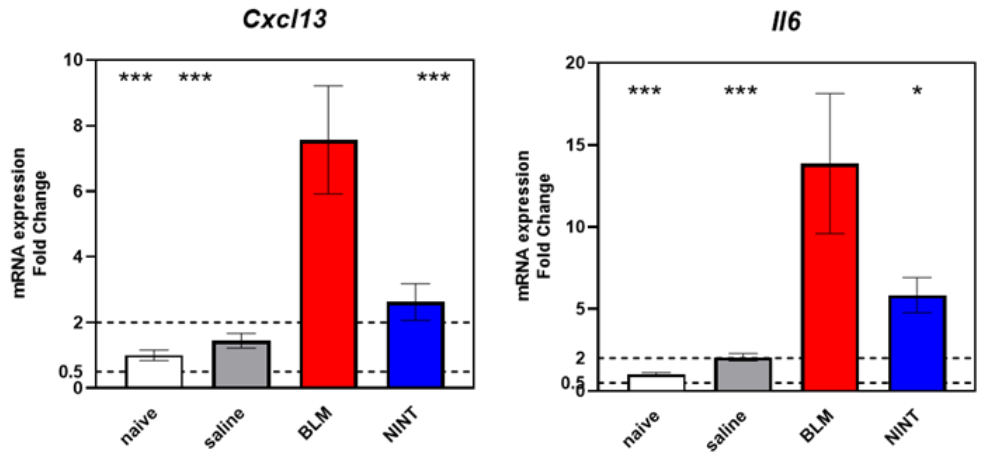

Figure 4.22 Effect of Nintedanib on mRNA expression fold change of genes related to a dysfunctional immune system. Data represent mean of fold change ± SEM values for Saline (n=4, grey bar), BLM (n=13, red bar) and Nintedanib (n=13, blue bar) groups of animals compared to naïve animals (n=4, white bar). Statistical analysis was assessed using one-way ANOVA followed by Dunnett's test in comparison with the BLM group; *** $p \leq 0.001$, * $p \leq 0.05$. BLM, bleomycin; Veh, vehicle.

5. DISCUSSION

IPF is a complex disease of unknown etiology, which makes specific drug development challenging. Considering that as of today only two drugs, Nintedanib and Pirfenidone, received formal approval from regulatory authorities and were introduced in the daily clinical practice, the medical need for this devastating disease remains very high.

Preclinical studies are crucial steps in the drug discovery process and the selection of the best drug candidate for clinical development relies on how well experimental animal models are able to predict clinical outcomes. Many potentially effective anti-fibrotic compounds showed promising results in preclinical models of pulmonary fibrosis, but only few of them successfully moved to the clinic *(Sgalla et al., 2019).*

Animal models of IPF are currently accepted as the first line approach to drug testing, but their clinical translability is debated. Firstly, they have the inherent limitation that no one exactly mimics human disease, but instead all of them develop a fibrotic condition that tends to spontaneously resolve over time, losing the progressive feature typical of IPF disease *(Moeller at al. 2008)*. Moreover, very often only prophylactic testing of the drug is performed while a therapeutic approach would better mimic the real-life situation, being more relevant as to evaluate the anti-fibrotic properties of a putative compound *(Jenkins et al. 2017, Kolb et al. 2020)*. Finally, in preclinical models the histological assessment of fibrotic tissue deposition is generally used to assess the burden of lung disease and, therefore, the efficacy of the drug. This kind of endpoint often exhibit high variability, limited sensitivity to drug efficacy, and is substantially different from the multiple endpoints currently used in clinical trials, that is functional readouts such as lung function decline or impairment in gas exchange as DFCO. It is therefore apparent that there is a need for more clinically relevant readouts which would improve the translatability from animal models to human IPF, and therefore the effectiveness of preclinical screening for new therapies.

In this scenario, assessing clinically relevant readouts in a robust animal model should have a significant impact on the ability to identify1 new therapeutic targets and novel effective compounds, ultimately leading to a significant improve in patient care.

To address this point, in this PhD work, we worked on improving the mouse Bleomycin model, one of the most widely used model of lung fibrosis and previously set up in the research laboratories of Chiesi Farmaceutici *(Stellari et. al. 2017)*, by pursuing the following goals:

- *Refinement of histological analysis*, the standard preclinical readout for the assessment of lung fibrosis, by introducing Artificial Intelligence quantification of lung fibrosis.
- *Introduction of clinically relevant parameters* (i.e., lung function tests, DFCO and clinical biomarkers).
- *Pharmacological validation of these novel readouts* testing Nintedanib, under therapeutic regimen.

The final goal of this work was to generate an improved BLM model of pulmonary fibrosis compared to that currently described in the literature, to enhance its robustness, reliability and translatability. The use of this model as a screening tool within the IPF projects of Chiesi Farmaceutici, will possibly lead to improved reliability in the identification of novel anti-fibrotic drugs, ultimately speeding up the drug discovery process.

The starting point of this PhD project was the mouse Bleomycin model previously set up in Chiesi *(Stellari et al. 2017)*, that similarly to the other models described in the literature uses the Ashcroft score, a scoring of fibrosis attributed by pathologists, as main readout for disease progression. Despite its common use in preclinical model, histological evaluation presents several limitations, including being time-consuming, prone to intrinsic error resulting from the sampling of the lung areas to analyze, and also markedly operator-dependent. To overcome as much as possible these limitations, we developed an automated image analysis APPs with Visiopharm® software to quantify the percentage of total lung parenchyma affected by fibrotic lesions and we introduced AI-based analysis to complement the automated quantification of lung fibrosis by providing information on fibrosis severity. In fact, in the last years, advances in machine learning have enabled the synergy between AI and digital pathology *(Berigei et al. 2021)* and with the support of the AI deep learning Visiopharm® module, we were able to develop a new APP that identifies and classifies three degrees of fibrosis severity corresponding to different grades as identified in the modified Ashcroft scale *(Hübner et al. 2008)*. In the time-course experiment, in which we studied Bleomycin-treated and control mice at several different times starting from 7 days from the first Bleomycin challenge up to 49 days, we found a great degree of correlation between the Ashcroft score and the automated analysis, both indicating the time point of 21 days as the peak of fibrotic lesions. The novel approach we used, capable to discriminate different types of fibrotic lesions (moderate and severe) within the analyzed tissue, resulted more reliable, more accurate and less time-consuming

when compared to the classical histological analysis based on scoring attributed by the pathologist.

The real breakthrough in the refinement and improvement of this BLM model was nevertheless achieved with the introduction of clinically relevant readouts of IPF. Indeed in IPF clinical trials, FVC and DFCO are routinely considered as the primary and the secondary endpoints, respectively, of the studies, capable of carefully assessing disease progression and the efficacy (or lack thereof) of therapeutic treatments of IPF.

While scientific papers in the literature have been suggesting that lung function parameters are important tools with undiscussed translational value in the assessment of mouse respiratory disease models *(Devos et al. 2017)*, they are rarely used at the preclinical level, because the equipment required are expensive and very specific technical competencies are needed. We therefore worked to set up and use, in the mouse Bleomycin model, DFCO assessment and lung function tests as functional parameters that may effectively mirror changes in respiratory system mechanics observed in IPF patients.

During this PhD project these novel readouts were assessed up to 49 days after the first Bleomycin treatment. In line with the results of the histological assessment, FVC and DFCO strongly declined 21 days after the first BLM administration, suggesting that both the damage of the tissue and the loss of lung functionality significantly peaked at this time point. After this time point from BLM injury, a natural resolution of fibrosis is taking place as shown by both histological and functional readouts.

Recent progress in the challenging field of IPF has also been achieved in the identification of novel protein biomarkers. In IPF, biomarkers may have the potential to enable differential diagnosis (e.g., between IPF and non-IPF fibrosing ILDs), more effective patient stratification (e.g., determine the subtype of ILD or identify patients at risk of progression), and better up-front selection of therapy. Most importantly, they may allow physicians to monitor early treatment response, which remains an important unmet medical need. In IPF, biomarkers can be categorized according to possible pathogenic pathways, broadly separating those associated with a) AECs damage and dysfunction, b) ECM remodelling and fibroproliferation, and c) immune dysregulation *(Jee et al. 2019)*. There are several promising candidates currently under evaluation, but none of them has reached widespread clinical practice use yet leaving unanswered the question of which markers to use for early diagnosis, progression and outcome of IPF *(Ley et al. 2014)*. Several research groups have been focusing their research on developing and establishing potentially relevant biomarker's signatures. The PROLIFIC collaboration, as mentioned in the Introduction section, is an example of the innovative and intensive research to advance the

application of biomarkers to IPF clinical trials and to promote translational discoveries. The goal of this research effort is to develop a well-qualified multiplex assay capable to detect the most relevant biomarkers in patients with IPF. The assay is currently including 12 specific biomarkers including markers of epithelial damage (CYFRA 21-1, SP-D, CA-19-9, KL-6), of fibrosis (MMP-7, Tenascin C, Periostin), of inflammation (CCL18, CXCL13, slCAM1), and of thrombosis (PAI-1). These biomarkers were selected based on published scientific reports describing their prognostic utility for the disease itself and their potential ability to predict how well a drug would work *(Schmidt, 2020)*. To be tested in our BLM model, we selected markers from the different subclasses listed in the panel, namely SP-D (a marker of epithelial damage), MMP-7, Collagen I -III and the neoepitope PRO-C3 (involved in the ECM remodeling process), OPN (involved in fibro-proliferative disorders) and CXCL-13 and IL-6 (involved in the immunological response). SP-D in serum of IPF patients was found associated with disease progression *(Maher et al. 2017)* and seems to be modulated by both approved drugs, Nintedanib and Pirfenidone *(Ikeda et al. 2020)*.

The excessive deposition of collagen and the ECM remodeling are events well known as pivotal for the fibrotic process. In fact, MMP-7, together with the DFCO value, was considered a predictor of mortality as well as a disease progression marker *(Inoue et al. 2020)*. It is found elevated in serum and BALF of IPF patients and appears to be modulated by the known effective treatments *(Fujishima et al 2010)*. Similarly, products of the degradation of collagen, such as the PRO-C3, were identified in patients' serum as prognostic marker and were responsive to pharmacological treatments *(Jenkins et al. 2019; Decato et al. 2022)*.

Finally, CXCL-13 is considered a circulating plasma biomarker of survival in antifibrotic-treated patients with IPF *(Alqalyoobi et al. 2020)* and together with IL-6 were found at elevated levels in patients *(Li et al. 2022)*.

The time course experiment showed that the epithelial damage and the ECM remodeling occur early after the BLM injury, as demonstrated from the levels of SP-D, MMP-7 and collagen I and III that peaked at the first time points rather than later on. Fibroblasts could contribute to the fibrogenesis slightly later, as suggested from the significant level of OPN getting the peak at 21 days from the BLM injury.

The immune system appears to play a role not only early on with the immediate inflammatory response, but also acting as an important player in fibroblast proliferation leading to sustained fibrotic process; elevated levels of CXCL-13 and IL-6 were in fact found up to 21 days after BLM, when the aberrant fibro-proliferation is significantly ongoing. Focusing on the most relevant time points (D07, D14, D21 and D28) we also

found that neoepitope of collagen (pro-C3) was significantly expressed and, considering its clinical relevance, it could be a prominent and interesting biomarker with translational value. The fact that these pro-fibrotic biomarkers are up-regulated both in IPF patients and in our BLM model further support the translational potential of the model.

The protein pattern observed in our model was also confirmed by gene expression profiling, confirming that there was a modulation of genes involved in the epithelial damage, ECM deposition, fibroblast proliferation and immune system dysregulation, providing additional support to their selection as putative translational biomarkers.

Finally, all these novel readouts were validated in a separate, therapeutic study with Nintedanib, by showing that the drug was indeed able to strongly modulate the parameters of lung function in parallel with the improvement of lung histology, as shown by the Ashcroft score analysis and the evaluation with the AI.

Despite the AI analysis has improved the histological readout increasing its accuracy and sensitivity and allowing to better appreciate the efficacy of a compound, the effect on FVC and DFCO proved to be a less time-consuming and more sensitive and accurate tool of analysis, thus representing a real turning point for the model, by providing robustness, consistency and additional translational value. Indeed, both FVC and DFCO were found not only a very reproducible measurement, but also responsive to the treatment with Nintedanib, as observed in clinical settings.

Similarly, different biomarkers such as SP-D, MMP-7, Coll-I, PRO-C3, OPN, CXCL-13 and IL-6 were found responsive to treatment with Nintedanib, supporting the relevance of this family of biomarkers in monitoring disease progression and, therefore, drug efficacy.

During this PhD project, we therefore demonstrated for the first time the potential usefulness of evaluating all these clinically relevant readouts in a preclinical model of pulmonary fibrosis, strengthening the ability to assess the efficacy of new anti-fibrotic compounds as compared to the use of histology alone, and making the mouse BLM model a more robust tool for IPF drugs screening.

5.1 Final conclusions

The incomplete understanding of the disease and the lack of safe and effective treatments make IPF a disease with considerable unmet medical need. However, drug discovery in this field is facing a lot of challenges in consideration of a very complex disease, difficult to fully understand and mimic with animal models. Considering these limitations in drug discovery for IPF, the goal of this PhD project was to generate a more reliable, predictable and robust animal model of pulmonary fibrosis through the introduction of clinically relevant endpoints, not commonly evaluated at the preclinical level, in order to generate an animal model closer to human disease and more suitable for the identification of new anti-fibrotic drugs.

We therefore worked on refining the mouse bleomycin model developed in our laboratories and moved toward bridging the gap between preclinical models and the clinic by introducing novel clinically relevant parameters, that can be fully integrated in the drug discovery process. We introduced the assessment of pulmonary function parameters, which are not commonly measured at preclinical level to assess the efficacy of drugs, as we believe they are important tools with a high translational value, in light of their critical role in clinical trials and in the management of IPF patients. Our results demonstrate that in mice it is possible to measure the same functional parameters applied in patients with IPF, such as the FVC and DFCO; the pharmacological validation with Nintedanib demonstrates that this drug is able to modulate significantly FVC and DFCO in the mouse BLM model, showing as these readouts are robust, consistent and more sensitive compared to the histological analysis and, similarly to the clinical practice, could be considered respectively the primary and secondary endpoint also in a preclinical model for drug discovery process.

The Ashcroft score analysis, widely used at preclinical level as histological outcome, is a time-consuming process, generates operator-dependent results and, most critically, is showing a relative low sensibility to effectively detect drugs efficacy. We also worked on refining this analytical approach by introducing the automated analysis of images, especially the AI-assisted analysis, consistently improving the histological outcome, by gaining in accuracy, sensitivity and speed of the method. Automated analysis resulted in an increased ability to appreciate the potential efficacy of compounds tested, when compared to the simple Ashcroft scoring system, by providing the possibility to assess the separate reduction in the severe and moderate components of fibrosis. While Ashcroft score analysis still remains an important element in IPF preclinical models, considering its significant and positive degree of correlation with the automated analysis (Pearson r 0.87, $p < 0.0001$; data not shown), we believe that coupling these different histological evaluations can provide a

more comprehensive and reliable view of fibrosis, therefore improving the ability to detect changes resulting from the effects of the drugs tested. Finally, the introduction of different readouts that are showing significant correlations among each other **(Figure 5.1)** showed an increased robustness of the model and the effective use of functional readouts moved this preclinical model closer to the level of complexity that mirrors the one observed in human IPF.

Overall, this PhD work has enhanced the translational and predictivity value of the mouse BLM model, potentially increasing the ability of selecting promising compounds to advance to clinical trials and leading to significant benefits to drug discovery process in the IPF research by improving the quality and the reliability of the search for novel anti-fibrotic drugs.

The results obtained provide evidence of a novel approach to the assessment of new drugs in IPF casting the light on the importance to introduce the use of clinical endpoints in preclinical trials to improve the selection process of new anti-fibrotic drugs to move into clinical trials.

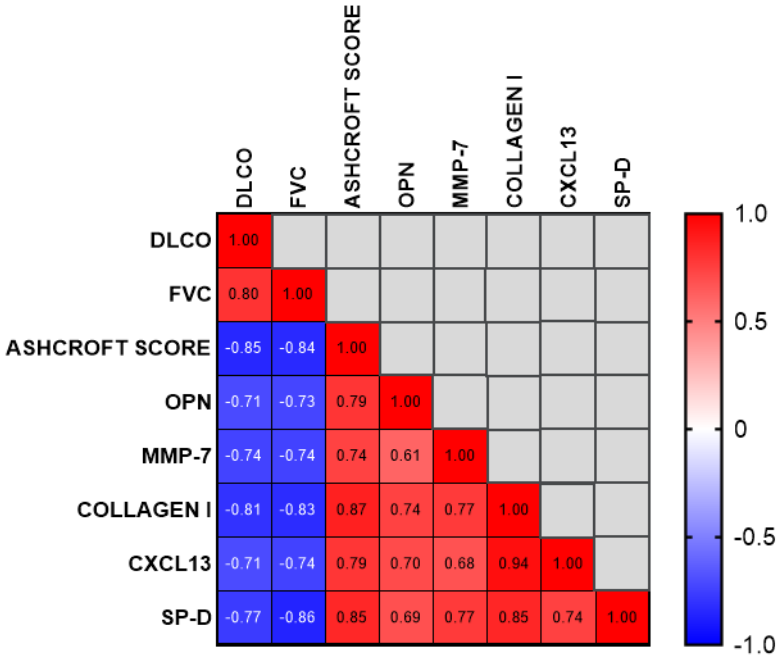

Figure 5.1 Correlations between Ashcroft score analysis, FVC, DFCO, OPN, MMP-7, Collagen -I, CXCL-13 and SP-D at day 21 after BLM OA administration in mice treated with Nintedanib. Correlations were determined using Pearson's correlation coefficient matrix tests.

6. REFERENCES

Ayabe S, Kida T, Hori M, Ozaki H, Murata T. *"Prostaglandin D2 inhibits collagen secretion from lung fibroblasts by activating the DP receptor"*. J Pharmacol Sci. **2013;**121(4):312–7.

Alhamad E. H., Lynch J. P., Martinez F. J. *"Pulmonary function tests in interstitial lung disease: what role do they have?"*. Clin Chest Med. **2001**; 22(4):715-50.

Alqalyoobi S., Adegunsoye A., Linderholm A., Hrusch C., et al. *"Circulating Plasma Biomarkers of Progressive Interstitial Lung Disease"* Am J Respir Crit Care Med. **2020**;201(2):250-253.

Alsafadi H. N., Staab-Weijnitz C. A., Lehmann M., Lindner M., Peschel B., Königshoff M., Wagner D. E. *"An ex vivo model to induce early fibrosis-like changes in human precision-cut lung slices"*. Am J Physiol Lung Cell Mol Physiol. **2017**; 312(6):L896-L902.

Aoki J., Inoue A., Okudaira S. "Two pathways for lysophosphatidic acid production". Biochim Biophys Acta. **2008**; 1781(9):513-8.

Appel J. Z., Lee S. M., Hartwig M. G., Li B., Hsieh C. C., et al. *"Characterization of the innate immune response to chronic aspiration in a novel rodent model"*. Respir Res. **2007**;8(1):87.

Bai L., Zhang L., Pan T., Wang W., Wang D., Turner C. et al. *"Idiopathic pulmonary fibrosis and diabetes mellitus: a meta-analysis and systematic review"* Respir Res. **2021**; 22: 175.

Balikian J. P., Jochelson M. S., Bauer K. A., Skarkin A. T., Garnick M. B., Canellos G. P., Smith E. H. *"Pulmonary complications of chemotherapy regimens containing bleomycin"*. AJR Am J Roentgenol. **1982**; 139(3):455-61.

Barros A., Oldham J., Noth I. *"Genetics of Idiopathic Pulmonary Fibrosis" The American Journal of the Medical Sciences 2019 Volume 357, Issue 5, Pages 379-383.*

Bassiouni et al. *"Multifunctional intracellular matrix metalloproteinases: implications in disease"* The FEBS Journal 288; **2021**: 7162–7182;

Baumgartner K. B., Samet J. M., Coultas D. B., Stidley C. A., Hunt W. C., Colby T. V., Waldron J. A. *"Occupational and environmental risk factors for idiopathic pulmonary fibrosis: a multicenter case-control study"*. Am J Epidemiol. **2000**; 152(4):307-15.

Behr J., Bendstrup E., Crestani B., Günther A., Olschewski H., et al. *"Safety and tolerability of acetylcysteine and pirfenidone combination therapy in idiopathic pulmonary fibrosis: a randomised, double-blind, placebo-controlled, phase 2 trial"*. Lancet Respir Med. **2016**; 4(6):445-53.

Berigei S., Roop B., Nandy S., Knipe R. S., et al. *"Artificial Intelligence Algorithm for Automated Fibrosis Quantification in Preclinical Bleomycin Model of Pulmonary Fibrosis"*. Am J Respir Crit Care Med. **2021**; 203:A4231.

Betensley A., Sharif R., and Karamichos D. *"A Systematic Review of the Role of Dysfunctional Wound Healing in the Pathogenesis and Treatment of Idiopathic Pulmonary Fibrosis"*. J. Clin. Med. **2016**; 6 (1).

Biernacka, A., Dobaczewski, M., and Frangogiannis, N. G. *"TGF-β Signaling in Fibrosis". Growth Factors"* **2011**; 29 (5), 196–202.

Bonniaud P., Kolb M., Galt T., Robertson J., Robbins G., et al. *"Smad3 null mice develop airspace enlargement and are resistant to TGF-beta-mediated pulmonary fibrosis"*. J Immunol. **2004**; 173(3):2099-108.

Borok Z., Horie M., Flodby P., Wang H., Liu Y. et al. *"Grp78 Loss in Epithelial Progenitors Reveals an Age-linked Role for Endoplasmic Reticulum Stress in Pulmonary Fibrosis"*. Am J Respir Crit Care Med. **2020** Jan 15;201(2):198-211.

Brown K.K., Inoue Y., Flaherty K.R., Martinez F.J. et al. *"Predictors of mortality in subjects with progressive fibrosing interstitial lung diseases"*. Respirology. **2022** Apr;27(4):294-300.

Brownell R., Moua T., Henry T. S., Elicker B. M., White D., Vittinghoff E., et al. *"The use of pretest probability increases the value of high-resolution CT in diagnosing usual interstitial pneumonia"*. Thorax. **2017**; 72(5):424-429.

Calaway A. C., Foster R. S., Adra N., Masterson T. A., Albany C., et al. *"Risk of Bleomycin-Related Pulmonary Toxicities and Operative Morbidity After Postchemotherapy Retroperitoneal Lymph Node Dissection in Patients With Good-Risk Germ Cell Tumors"*. J Clin Oncol. **2018**; 36(29):2950-2954.

Carrington R., Jordan S., Pitchford S. C., Page C. P. *"Use of animal models in IPF research"*. Pulm Pharmacol Ther. **2018**; 51:73-78.

Cavazza A., Rossi G., Carbonelli C., Spaggiari L., Pacie M., Roggeri A. *"The role of histology in idiopathic pulmonary fibrosis: An update"*. Respir Med. **2010**; 104 Suppl 1:S11-22.

Cerri S., Monari M., Guerrieri A., Donatelli P., Bassi I. et al. *"Real-life comparison of pirfenidone and nintedanib in patients with idiopathic pulmonary fibrosis: A 24-month assessment".* Respir Med. **2019** Nov;159:105803.

Chen C. Z., Raghunath M. *"Focus on collagen: in vitro systems to study fibrogenesis and antifibrosis state of the art"*. Fibrogenesis Tissue Repair. **2009**; 2:7.

Chen Y. W., Huang S. X., de Carvalho A. L. R. T., Ho S. H., Islam M. N., Volpi S., Notarangelo L. D., et al. *"A three-dimensional model of human lung development and disease from pluripotent stem cells"*. Nat Cell Biol. **2017**; 19(5):542-549.

Cheresh P., Morales-Nebreda L., Kim S. J., Yeldandi A., Williams D. B., et al. *"Asbestos-induced pulmonary fibrosis is augmented in 8-oxoguanine DNA glycosylase knockout mice"*. Am J Respir Cell Mol Biol. **2015**; 52(1):25-36.

Clapp L.H.., Abu-Hanna J.H.J., Patel J.A. *"Diverse pharmacology of prostacyclin mimetics: implications for pulmonary hypertension. Molecular mechanism of congenital heart disease and pulmonary hypertension"*. Springer; **2020**. p. 31–61.

Claussen C. A., Long E. C. *"Nucleic Acid recognition by metal complexes of bleomycin"*. Chem Rev. **1999**; 99(9):2797-816.

Collard H. R., Moore B. B., Flaherty K. R., Brown K. K., et al. *"Acute Exacerbations of Idiopathic Pulmonary Fibrosis"*. Am J Respir Crit Care Med. **2007**; 176(7):636-43.

Collard H. R., Yow E., Richeldi L., Anstrom K. J., Glazer C., IPFnet investigators. *"Suspected acute exacerbation of idiopathic pulmonary fibrosis as an outcome measure in clinical trials"*. Respir Res. **2013**;14(1):73.

Corboz M.R., Zhang J., Lasala D. et al. *"Therapeutic administration of inhaled INS1009, a treprostinil prodrug formulation, inhibits bleomycin-induced pulmonary fibrosis in rats"*. Pulm Pharmacol Ther.**2018**;49:95–103.

Costabel U., Inoue Y., Richeldi L., Collard H. R., Tschoepe I., Stowasser S., Azuma A. *"Efficacy of Nintedanib in Idiopathic Pulmonary Fibrosis across Prespecified Subgroups in INPULSIS"*. Am J Respir Crit Care Med. **2016**; 193(2):178-85.

Costabel U., Albera C., Glassberg M..K.. et al *"Effect of pirfenidone in patients with more advanced idiopathic pulmonary fibrosis"* Respir Res **2019**; 20, 55.

Coward W. R., Saini G. and Jenkins G. *"The Pathogenesis of Idiopathic Pulmonary Fibrosis"*. Ther. Adv. Respir. Dis. **2010**; 4 (6), 367–388.

Decato B.E., Leeming D.J., Sand J.M.B. et al. *"LPA1 antagonist BMS-986020 changes collagen dynamics and exerts antifibrotic effects in vitro and in patients with idiopathic pulmonary fibrosis"*. Respir Res 23, 61 (**2022**).

Degryse A. L., Tanjore H., Xu X. C., Polosukhin V. V., Jones B. R., et al. *"Repetitive intratracheal bleomycin models several features of idiopathic pulmonary fibrosis"*. Am J Physiol Lung Cell Mol Physiol. **2010**; 299(4):L442-52.

Devos F. C., Maaske A., Robichaud A., Pollaris L., Seys S., Lopez C. A. *"Forced expiration measurements in mouse models of obstructive and restrictive lung diseases"*. Respir Res. **2017**; 18(1):123.

Dillingh M. R., van den Blink B., Moerland M., van Dongen M. G. J., Levi M., et al. *"Recombinant human serum amyloid P in healthy volunteers and patients with pulmonary fibrosis".* Pulm Pharmacol Ther. **2013**; 26(6):672-6.

Duran-Ortiz S., List E. O., Basu R. and Kopchick J. J. *"Extending Lifespan by Modulating the Growth Hormone/insulin-like Growth Factor-1 axis: Coming of Age".* Pituitary **2021**;24 (3), 438–456.

Engler A. J., Sen S., Sweeney H. L., Discher D. E. *"Matrix elasticity directs stem cell lineage specification"*. Cell. **2006**; 126(4):677-89.

Evans C. M., Fingerlin T. E., Schwarz M. I., Lynch D., Kurche J., Warg L., Yang I. V., Schwartz D. A. *"Idiopathic Pulmonary Fibrosis: A Genetic Disease That Involves Mucociliary Dysfunction of the Peripheral Airways"*. Physiol Rev. **2016**; 96(4):1567-91.

Falke L. L., He N., Chuva de Sousa Lopes S. M., Broekhuizen R., Lyons K., Nguyen T. Q. et al. *"Correction to: FoxD1-Driven CCN2 Deletion Causes Axial Skeletal Deformities, Pulmonary Hypoplasia, and Neonatal Asphyctic Death"*. J. Cell Commun Signal **2020**; 14 (1), 47–52.

Fang Y., Eglen R. M. *"Three-Dimensional Cell Cultures in Drug Discovery and Development"*. LAS Discov. **2017**; 22(5):456-472.

Flaherty K. R., Fell C. D., Huggins J. T., Nunes H., Sussman R., et al. *"Safety of nintedanib added to pirfenidone treatment for idiopathic pulmonary fibrosis"*. Eur Respir J. **2018**; 52(2):1800230.

Frantz C., Stewart K.M., Weaver V.M. *"The extracellular matrix at a glanc*e". J Cell Sci **2010;** 123: 4195–4200.

Fujishima S., Shiomi T., Yamashita S., Yogo Y. et al.. *"Production and activation of matrix metalloproteinase 7 (matrilysin 1) in the lungs of patients with idiopathic pulmonary fibrosis"*. Arch Pathol Lab Med. **2010**;134(8):1136-42.

Fukihara J., Kondoh Y., Brown K.K., Kimura T., Kataoka K., Matsuda T. et al. *"Probable usual interstitial pneumonia pattern on chest CT: is it sufficient for a diagnosis of idiopathic pulmonary fibrosis?"* Eur Respir J **2020**;55:1802465.

Gelfand E. W. *"Mice are a good model of human airway disease"*. Am J Respir Crit Care Med. **2002**; 166(1):5-6; discussion 7-8.

Getsy J. A., Harper D., Levy M., Burggraaf J., Moerland M., et al. *"The Effects Of Recombinant Human Pentraxin-2, (prm-151), On Circulating Fibrocytes In Idiopathic Pulmonary Fibrosis (IPF)"*. Colorado Convention Center. INTERSTITIAL LUNG DISEASE: NOVEL MANAGEMENT AND OUTCOME STRATEGIES. **2011**. Poster Discussion Session /

Glass D, Grossfeld D, Renna H. A., Agarwala P. et al *"Idiopathic pulmonary fibrosis: Molecular mechanisms and potential treatment approaches"* Respir Investig. **2020**;58(5):320-335.

Gorina E., Richeldi L., Raghu G., Fernandez Perez E., Costabel U., et al. *"PRAISE, a randomized, placebo-controlled, double-blind Phase 2 clinical trial of pamrevlumab (FG-3019) in IPF patients"*. Eur Respir J. **2017**; 50: OA3400.

Gruden J. F., Panse P. M., Leslie K. O., Tazelaar H. D., Colby T. V. *"UIP diagnosed at surgical lung biopsy, 2000-2009: HRCT patterns and proposed classification system"*. AJR Am J Roentgenol. **2013**; 200(5):W458-67.

Guiot J., Henket M., Corhay J. L., Moermans C. and Louis R. *"Sputum Biomarkers in IPF: Evidence for Raised Gene Expression and Protein Level of IGFBP-2, IL-8 and MMP-7".* PLoS One **2017**; 12 (2), e0171344.

Guo F., Sun Y. B., Su L., Li S., Liu Z. F., Li J., Hu X. T., Li J. *"Losartan attenuates paraquat-induced pulmonary fibrosis in rats"*. Hum Exp Toxicol. **2015**; 34(5):497-505.

Gustafson T., Dahlman-Höglund A., Nilsson K., Ström K., Tornling G., Torén K. *"Occupational exposure and severe pulmonary fibrosis"*. Respir Med. **2007**; 101(10):2207-12.

Hancock L.A., Hennessy C.E., Solomon G.M. et al *"Muc5b overexpression causes mucociliary dysfunction and enhances lung fibrosis in mice"* Nature Communications **2018** Vol 9, Article number: 5363

Heckman et al. *"Pulmonary Function Tests for Diagnosing Lung Disease"* JAMA **2015**.

Hettiarachchi S. U., Li Y. H., Roy J., Zhang F., Puchulu-Campanella E., Lindeman S. D., et al. *" Targeted Inhibition of PI3 kinase/mTOR Specifically in Fibrotic Lung Fibroblasts Suppresses Pulmonary Fibrosis in Experimental Models"*. Sci. Transl Med. **2020**; 12 (567).

Heukels P., Moor C. et al. *"Inflammation and immunity in IPF pathogenesis and treatment"* Respir Med. **2019**:147:79-91.

Hewlett J. C., Kropski J. A. and Blackwell T. S.*"Idiopathic Pulmonary Fibrosis: Epithelial-Mesenchymal Interactions and Emerging Therapeutic Targets".* Matrix Biol. **2018**; 71-72, 112–127.

Hilberg F., Roth G. J., Krssak M., Kautschitsch S., Sommergruber W., Tontsch-Grunt U., et al. *"BIBF 1120: triple angiokinase inhibitor with sustained receptor blockade and good antitumor efficacy"*. Cancer Res. **2008**; 68(12):4774-82.

Homma S., Bando M., Azuma A., Sakamoto S., Sugino K., Ishii Y., et al. *"Japanese guideline for the treatment of idiopathic pulmonary fibrosis"*. Respir Investig. **2018**; 56(4):268-291.

Hoppo T., Jarido V., Pennathur A., Morrell M. et al. *"Antireflux surgery preserves lung function in patients with gastroesophageal reflux disease and end-stage lung disease before and after lung transplantation"*. Arch. Surg. **2011**, 146, 1041–1047.

Hostettler K. E., Zhong J., Papakonstantinou E., Karakiulakis G., Tamm M., et al. *"Anti-fibrotic effects of nintedanib in lung fibroblasts derived from patients with idiopathic pulmonary fibrosis"*. Respir Res. **2014**; 15(1):157.

HuangY., Xie Y.,Abel P.W.,Wei P., Plowman J.,Toews M.L. et al.*"TGF-β1-induced miR-424 Promotes Pulmonary Myofibroblast Differentiation by Targeting Slit2 Protein Expression"*. Biochem. Pharmacol. **2020**; 180, 114172.

Hübner R.H., Gitter W., El Mokhtari NE, Mathiak M., Both M., Bolte H., Freitag-Wolf S., Bewig B. *"Standardized quantification of pulmonary fibrosis in histological samples"*. Biotechniques. **2008**; 44(4):507-511, 514-517.

Ikeda K., Shiratori M., Chiba H., Nishikiori H., Yokoo K., Saito A., et al. *"Serum surfactant protein D predicts the outcome of patients with idiopathic pulmonary fibrosis treated with pirfenidone"*. Respir Med. **2017**; 131:184-191.

Ikeda K., Chiba H., Nishikiori H. et al. *"Serum surfactant protein D as a predictive biomarker for the efficacy of pirfenidone in patients with idiopathic pulmonary fibrosis: a post-hoc analysis of the phase 3 trial in Japan"*. Respir Res **2020**; 21, 316.

Inchingolo R., Varone F., Sgalla G., Richeldi L. *"Existing and emerging biomarkers for disease progression in idiopathic pulmonary fibrosis"*. Expert Rev Respir Med. **2019**; 13(1):39-51.

Inoue Y., Kaner R. J., Guiot J., Maher T. M., Tomassetti S., et al. *"Diagnostic and Prognostic Biomarkers for Chronic Fibrosing Interstitial Lung Diseases With a Progressive Phenotype"*. Chest. **2020**; 158(2):646-659.

Inui N., Sakai S. and Kitagawa, M. *"Molecular Pathogenesis of Pulmonary Fibrosis, with Focus on Pathways Related to TGF-β and the Ubiquitin-Proteasome Pathway"*. Int. J. Mol. Sci. **2021**; 22 (11).

Ishikawa N., Hattori N., Yokoyama A., Kohno N. *"Utility of KL-6/MUC1 in the clinical management of interstitial lung diseases"*. Respir Investig. **2012**; 50(1):3-13.

Izbicki G., Segel M. J., Christensen T. G., Conner M.W., Breuer R. *"Time course of bleomycin-induced lung fibrosis"*. Int J Exp Pathol. **2002**; 83(3):111-9.

Jee A. S., Sahhar J., Youssef P., Bleasel J., Adelstein S., Nguyen M., Corte T. J. *"Review: Serum biomarkers in idiopathic pulmonary fibrosis and systemic sclerosis associated interstitial lung disease - frontiers and horizons".* Pharmacol Ther. **2019**; 202:40-52.

Jenkins R. G., Su X., Su G., Scotton C. J., Camerer E., Laurent G. J., et al. *"Ligation of Protease-Activated Receptor 1 Enhances Alpha(v)beta6 Integrin dependent TGF-Beta Activation and Promotes Acute Lung Injury"*. J. Clin. Invest. **2006**;116 (6), 1606–1614.

Jenkins R. G., Moore B.B., Chambers R.C., Eickelberg O., Königshoff M., Kolb M., Laurent GJ., Nanthakumar C.B., Olman M.A., Pardo A., Selman M., et al. *"An Official American Thoracic Society Workshop Report: Use of Animal Models for the Preclinical Assessment of Potential Therapies for Pulmonary Fibrosis"*. Am J Respir Cell Mol Biol. **2017**; 56(5):667-679.

Jenkins et al. *"Effect of Nintedanib on blood biomarkers in patients with IPF in the INMARK trial"* European Respiratory Journal **2019**; 54: PA2254;

Jenkins R. G., Noth I., Selman M., Cottin V., Nishioka Y., et al. *"Effects of nintedanib on markers of epithelial damage in subjects with IPF: data from the INMARK trial"*. Eu Respir J. **2020**; 56:5187.

John A. E.,Graves R.H., Pun K. T., Vitulli G., Forty E. J.,Mercer P. F., et al. *"Translational Pharmacology of an Inhaled Small Molecule αvβ6 Integrin Inhibitor for Idiopathic Pulmonary Fibrosis"*. Nat. Commun. **2020**; 11 (1), 4659.

Karsdal M., Nielsen S., Leeming D., Langholm L. et al. *"The good and the bad collagens of fibrosis–their role in signaling and organ function"*. Adv Drug Deliv Rev. **2017**;121:43–56..

Kaur A., Mathai S. M., Schwartz D. A. *"Genetics in Idiopathic Pulmonary Fibrosis Pathogenesis, Prognosis, and Treatment"*. Front Med (Lausanne). **2017**; 4:154.

Kim D. S., Park J. H., Park B. K., Lee J. S., Nicholson A. G., Colby T. *"Acute exacerbation of idiopathic pulmonary fibrosis: frequency and clinical features"*. Eur Respir J. **2006**;27(1):143-50.

Kim D. S. *"Acute Exacerbation of Idiopathic Pulmonary Fibrosis"*. Clin Chest Med. **2012**; 33(1):59-68.

Kim J. S., Podolanczuk A. J., Borker P., Kawut S. M., Raghu G., Kaufman J. D., et al. *"Obstructive Sleep Apnea and Subclinical Interstitial Lung Disease in the Multi-Ethnic Study of Atherosclerosis (MESA)"*. Ann Am Thorac Soc. **2017**; 14(12):1786-1795.

Kim S. N., Lee J., YangH. S., Cho J. W., Kwon S., et al. "*Dose-response Effects of Bleomycin on Inflammation and Pulmonary Fibrosis in Mice*". Toxicol Res. **2010**; 26(3):217-22.

King Jr T. E., Bradford W. Z., Castro-Bernardini S., Fagan E. A., Glaspole I., et al. *"A phase 3 trial of pirfenidone in patients with idiopathic pulmonary fibrosis"*. N Engl J Med. **2014**; 370(22):2083-92.

Kishi M., Aono Y., Sato S., Koyama K., Azuma M., Abe S., et al. *"Blockade of Platelet-Derived Growth Factor Receptor-β, Not Receptor-α Ameliorates Bleomycin-Induced Pulmonary Fibrosis in Mice"*. PLoS One 2018; 13 (12), e0209786.

Knudsen L., Ruppert C., Ochs M. *"Tissue remodelling in pulmonary fibrosis"*. Cell Tissue Res. **2017**;367(3):607-626.

Kolb M., Margetts P. J., Anthony D. C., Pitossi F., Gauldie J. *"Transient expression of IL-1beta induces acute lung injury and chronic repair leading to pulmonary fibrosis"*. J Clin Invest. **2001**; 107(12):1529-36.

Kolb M., Raghu G., Wells A. U., Behr J., Richeldi L., et al. *"Nintedanib plus Sildenafil in Patients with Idiopathic Pulmonary Fibrosis"*. N Engl J Med. **2018**; 379(18):1722-1731.

Kolb P., Upagupta C., Vierhout M., Ayaub E., Bellaye P. S., et al. *"The importance of interventional timing in the bleomycin model of pulmonary fibrosis"*. Eur Respir J. **2020**; 55(6):1901105.

Koli K., Sutinen E., Rönty M., Rantakari P., Fortino V., et al. *"Gremlin-1 Overexpression in Mouse Lung Reduces Silica-Induced Lymphocyte Recruitment - A Link to Idiopathic Pulmonary Fibrosis through Negative Correlation with CXCL10 Chemokine"*. PLoS One. **2016**; 11(7):e0159010.

Kono M., Nakamura Y., Suda T., Kato M., Kaida Y., Hashimoto D., et al. *"Plasma CCN2 (connective tissue growth factor; CTGF) is a potential biomarker in idiopathic pulmonary fibrosis (IPF)"*. Clin Chim Acta. **2011**; 412(23-24):2211-5.

Kropski J.A., Blackwell T. S., Loyd J.E. *"The genetic basis of idiopathic pulmonary fibrosis"* Eur Respir J. 2015 Jun;45(6):1717-27.

Kuwano K., Maeyama T., Inoshima I., Ninomiya K., et al. *"Increased circulating levels of soluble Fas ligand are correlated with disease activity in patients with fibrosing lung diseases"*. Respirology. **2002**;7(1):15-21.

Kwon B.S., Choe J., Do K.H., Hwang H.S., Chae E.J., Song J.W. *"Computed tomography patterns predict clinical course of idiopathic pulmonary fibrosis"*. Respir Res **2020**;21:295.

Lambers C., Roth M., Jaksch P. et al. *"Treprostinil inhibits proliferation and extracellular matrix deposition by fibroblasts through cAMP activation".* Sci Rep. **2018**;8(1):1087.

Lancaster L., Bonella F., Inoue Y., Cottin C., Siddall J., Small M., Langley J. *"Idiopathic pulmonary fibrosis: Physician and patient perspectives on the pathway to care from symptom recognition to diagnosis and disease burden"*. Respirology. **2021** Oct 5.

Lederer D. J., Jelic S., Basner R. C., Ishizaka A., Bhattacharya J. *"Circulating KL-6, a biomarker of lung injury, in obstructive sleep apnoea"*. Eur Respir J. **2009**; 33(4):793-6.

Lee H. L., Ryu J. H., Wittmer M. H., Hartman T. E., Lymp J. F., Tazelaar H. D., Limper A. H. *"Familial idiopathic pulmonary fibrosis: clinical features and outcome"*. Chest. **2005**; 127(6):2034-41.

Lee J.S., Ryu J.H., Elicker B.M. et al. *"Gastroesophageal reflux therapy is associated with longer survival in patients with idiopathic pulmonary fibrosis".* Am. J. Respir. Crit. Care Med. **2011**, 184, 1390–1394.

Ley B., Brown K. K., Collard H. R. *"Molecular biomarkers in idiopathic pulmonary fibrosis"*. Am J Physiol Lung Cell Mol Physiol. **2014**; 307(9):L681-91.

Ley B., Collard H. R., King Jr T. E. *"Clinical course and prediction of survival in idiopathic pulmonary fibrosis"*. Am J Respir Crit Care Med. **2011**; 183(4):431-40.

Le Saux C. J. and Chapman H. A. *"Idiopathic Pulmonary Fibrosis: Cell Death and Inflammation Revisited"*. Am. J. Respir. Cell Mol Biol **2018**; 59 (2), 137–138.

Li L., Ma B. B. Y., Chan A. T. C., Chan F. K. L., Murray P. and Tao Q. *"Epstein-Barr Virus-Induced Epigenetic Pathogenesis of Viral-Associated Lymphoepithelioma-like Carcinomas and Natural Killer/T-Cell Lymphomas"*. Pathogens **2018**; 7 (3).

Li Y., Zhao J., Yin Y., Li K., Zhang C., Zheng Y. *"The Role of IL-6 in Fibrotic Diseases: Molecular and Cellular Mechanisms".* Int J Biol Sci. **2022**;18(14):5405-5414.

Li J., Li K. Tian J. et al. *"Effective-compounds of Jinshui Huanxian formula ameliorates fibroblast activation in pulmonary fibrosis by inhibiting the activation of mTOR signaling"* Phytomedicine **2023** Volume 109, 154604.

Limjunyawong N., Fallica J., Ramakrishnan A., Datta K., Gabrielson M., Horton M., Mitzner W. *"Phenotyping mouse pulmonary function in vivo with the lung diffusing capacity"*. J Vis Exp. **2015** Jan 6;(95):e52216.

Lin C. H., Shih C. H., Lin Y. C., Yang Y. L. and Chen B. C. *"MEKK1, JNK, and SMAD3 Mediate CXCL12-Stimulated Connective Tissue Growth Factor Expression in Human Lung Fibroblasts"*. J. Biomed. Sci. **2018**; 25 (1), 19.

Lipinski J. H., , Moore B.B., O'Dwyer D.N. "*The evolving role of the lung microbiome in pulmonary fibrosi"* Am J Physiol Lung Cell Mol Physiol. 2020;319(4):L675-L682.

Liu M. H., Lin A. H., Ko H. K., Perng D. W., Lee T. S., Kou Y. R. *"Prevention of Bleomycin-Induced Pulmonary Inflammation and Fibrosis in Mice by Paeonol"*. Front Physiol. **2017**; 8:193.

Liu T., De Los Santos F. C., Phan S. H. *"The Bleomycin Model of Pulmonary Fibrosis"*. Methods Mol Biol. **2017**; 1627:27-42.

Lorenzo-Salazar J. M. et al. *"Novel idiopathic pulmonary fibrosis susceptibility variants revealed by deep sequencing*" ERJ Open Res. **2019** Jun;5(2):00071-2019.

Lynch D.A, Sverzellati N., Travis W.D., Brown K.K., Colby T.V., Galvin J.R. et al. *"Diagnostic criteria for idiopathic pulmonary fibrosis: a Fleischner Society white paper"*. Lancet Respir Med **2018**;6:138–153.

Maher T. M., Oballa E., Simpson J. K., Porte J., Habgood A., Fahy W. A., et al. *"An epithelial biomarker signature for idiopathic pulmonary fibrosis: an analysis from the multicentre PROFILE cohort study"*. Lancet Respir Med. **2017**; 5(12):946-955.

Maher T. M., van der Aar E. M., Van de Steen O., Allamassey L., Desrivot J., et al. *"Safety, tolerability, pharmacokinetics, and pharmacodynamics of GLPG1690, a novel autotaxin inhibitor, to treat idiopathic pulmonary fibrosis (FLORA): a phase 2a randomised placebo-controlled trial"*. Lancet Respir Med. **2018**; 6(8):627-635.

Maher T. M., Kreuter M., Lederer D. J., Brown K. K., Wuyts W., et al. *"Rationale, design and objectives of two phase III, randomised, placebo-controlled studies of GLPG1690, a novel autotaxin inhibitor, in idiopathic pulmonary fibrosis (ISABELA 1 and 2)"*. BMJ Open Respir Res. **2019**; 6(1):e000422.

MaherT., Bendstrup E., Dron L., Langley J., Smith G., Khalid J. M., Patel H., Kreuter M. *"Global incidence and prevalence of idiopathic pulmonary fibrosis"* Respir Res. **2021**;22(1):197. 2

Maher T.M., Ford P., Brown K.K., Costabel U., Cottin V. et al. *"ISABELA 1 and 2 Investigators. Ziritaxestat, a Novel Autotaxin Inhibitor, and Lung Function in Idiopathic Pulmonary Fibrosis: The ISABELA 1 and 2 Randomized Clinical Trials."* JAMA. **2023** May 9;329(18):1567-1578.

Matsuhira T, Nishiyama O, Tabata Y, et al. *"A novel phosphodiesterase 4 inhibitor, AA6216, reduces macrophage activity and fibrosis in the lung".* Eur J Pharmacol **2020**; 885: 173508.

Martinez F. J., Collard H. R., Pardo A., Raghu G., Richeldi L., et al. *"Idiopathic pulmonary fibrosis"*. Nat Rev Dis Primers. **2017**; 3:17074.

Massagué J. *"TGFβ Signalling in Context"*. Nat. Rev. Mol. Cell Biol **2012**; 13 (10), 616–630.

Mei Q., Liu Z., Zuo H., Yang Z. and Qu J. *"Idiopathic Pulmonary Fibrosis: An Update on Pathogenesis"*. Front. Pharmacol. **2022**; 12:797292.

Meyer K.C. *"Diagnosis and management of interstitial lung disease"* Transl Respir Med. **2014** 13:2:4.

Méthot D.B., Leblanc E., Lacasse Y. *"Meta-analysis of Gastroesophageal Reflux Disease and Idiopathic Pulmonary Fibrosis"* Chest. **2019**;155(1):33-43.

Miyake Y., Sasaki S., Yokoyama T., Chida K., Azuma A., Suda T., Kudoh S., et al. *"Occupational and environmental factors and idiopathic pulmonary fibrosis in Japan"*. Ann Occup Hyg. **2005**; 49(3):259-65.

Moeller A., Ask K., Warburton D., Gauldie J., Kolb M. *"The bleomycin animal model: a useful tool to investigate treatment options for idiopathic pulmonary fibrosis?"*. Int J Biochem Cell. Biol. **2008**; 40(3):362-382.

Molina-Molina M., Aburto M., Acosta O., Ancochea J., Rodríguez-Portal J.A., Sauleda J., Lines C., Xaubet A. *"Importance of early diagnosis and treatment in idiopathic pulmonary fibrosis"*. Expert Rev Respir Med. **2018** Jul;12(7):537-539.

Molyneaux P. L., Cox M. J., Willis-Owen S. A. G., Mallia P., Russell K. E., Russell A. M., et al. *"The role of bacteria in the pathogenesis and progression of idiopathic pulmonary fibrosis".* Am J Respir Crit Care Med. **2014**; 190(8):906-13.

Molyneaux P. L., Maher T. M. *"The role of infection in the pathogenesis of idiopathic pulmonary fibrosis"*. Eur Respir Rev. **2013**; 22(129):376-81.

Montesi S. B., Mathai S. K., Brenner L. N., Gorshkova I. A., et al. *"Docosatetraenoyl LPA is elevated in exhaled breath condensate in idiopathic pulmonary fibrosis"*. BMC Pulm Med**. 2014**; 14:5

Moore B. B., Lawson W. E., Oury T. D., Sisson T. H., Raghavendran K., Hogaboam C. M. *"Animal Models of Fibrotic Lung Disease"*. Am J Respir Cell Mol Biol. **2013**; 49, (2): 167-179.

Moore C., Blumhagen R. Z., Yang I. et al. *"Resequencing Study Confirms That Host Defense and Cell Senescence Gene Variants Contribute to the Risk of Idiopathic Pulmonary Fibrosis"* Am J Respir Crit Care Med. **2019**;200(2):199-208.

Morais A., Beltrão M., Sokhatska O., Costa D., Melo N., et al. *"Serum metalloproteinases 1 and 7 in the diagnosis of idiopathic pulmonary fibrosis and other interstitial pneumonias"*. Respir Med. **2015**; 109(8):1063-8.

Morse C., Tabib T., Sembrat J., Buschur K. L., Bittar H. T., Valenzi, E., et al. *"Proliferating SPP1/MERTK-Expressing Macrophages in Idiopathic Pulmonary Fibrosis"*. Eur. Respir. J. **2019**; 54 (2).

lìMurray L. A., Rosada R., Moreira A. P., Joshi A., Kramer M. S., et al. *"Serum amyloid P therapeutically attenuates murine bleomycin-induced pulmonary fibrosis via its effects on macrophages"*. PLoS One. **2010**; 5(3):e9683.

Murray L. A., Zhang H., Oak S. R., Coelho A. L., Herath A., FlahertyM K. R., et al. *"Targeting interleukin-13 with tralokinumab attenuates lung fibrosis and epithelial damage in a humanized SCID idiopathic pulmonary fibrosis model"*. Am J Respir Cell Mol Biol. **2014**; 50(5):985-94.

Nabhan A. N, Brownfield D.G., Harbury P.B., Krasnow M.A., Desai T.J. *"Single-cell Wnt signaling niches maintain stemness of alveolar type 2 cells"* Science. **2018**;359(6380):1118-1123.

Naugle J.E., Olson E.R., Zhang X., Mase S.E. et al. *"Type VI collagen induces cardiac myofibroblast differentiation: implications for postinfarction remodeling"*. Am J Phys Heart Circ Phys. **2006**;290:H323–30.

Naikawadi R. P., Disayabutr S., Mallavia B., Donne M. L., Green G., et al. *"Telomere dysfunction in alveolar epithelial cells causes lung remodeling and fibrosis"*. JCI Insight. **2016**; 1(14):e86704.

Nho R. S., Hergert P., Kahm J., Jessurun J. and Henke C. *"Pathological Alteration of FoxO3a Activity Promotes Idiopathic Pulmonary Fibrosis Fibroblast Proliferation on Type I Collagen Matrix"*. Am. J. Pathol. **2011**; 179 (5), 2420–2430.

Noble P. W., Albera C., Bradford W. Z., Costabel U., Glassberg M. K., Kardatzke D., et al. *"Pirfenidone in patients with idiopathic pulmonary fibrosis (CAPACITY): two randomised trials"*. Lancet. **2011**; 377(9779):1760-9.

Noble P. W., Albera C., Bradford W. Z., Costabel U., du Bois R. M., Fagan E. A., et al. *"Pirfenidone for idiopathic pulmonary fibrosis: analysis of pooled data from three multinational phase 3 trials"*. Eur Respir J. **2016**; 47(1):243-53.

Noth I., Zhang Y., Ma S. F., C., Barber M., Huang Y., et al. *"Genetic variants associated with idiopathic pulmonary fibrosis susceptibility and mortality: a genome-wide association study"*. Lancet Respir Med. **2013**; 1(4):309-317.

O'Dwyer D. N., Ashley S. L., Gurczynski S. J., Xia M. et al. *"Lung Microbiota Contribute to Pulmonary Inflammation and Disease Progression in Pulmonary Fibrosis"* Am J Respir Crit Care Med. **2019**;199(9):1127-1138.

Ogura T., Taniguchi H., Azuma A., Inoue Y., Kondoh Y., et al. *"Safety and pharmacokinetics of nintedanib and pirfenidone in idiopathic pulmonary fibrosis"*. Eur Respir J. **2015**; 45(5):1382-92.

Oikonomou N., Mouratis M. A., Tzouvelekis A., Kaffe E., Valavanis C., et al. *"Pulmonary autotaxin expression contributes to the pathogenesis of pulmonary fibrosis"*. Am J Respir Cell Mol Biol. **2012**; 47(5):566-74.

Okuda R., Hagiwara E., Baba T., Kitamura H., Kato T., Ogura T. *"Safety and efficacy of pirfenidone in idiopathic pulmonary fibrosis in clinical practice"*. Respir Med. **2013**;107(9):1431-7.

Ongenaert M., Dupont S., Blanqué R., Brys R., van der Aar E. M., Heckmann B. *"Strong reversal of the lung fibrosis disease signature by autotaxin inhibitor GLPG1690 in a mouse model for IPF"*. Eu Resp J. **2016**; 48: OA4540.

Organ L.A., Duggan A.R., Oballa E., Taggart S.C. et al. *"Biomarkers of collagen synthesis predict progression in the PROFILE idiopathic pulmonary fibrosis cohort"*. Respir Res. **2019** Jul 12;20(1):148.

Ornatowski W., Lu Q., Yegambaram M. et al. *"Complex interplay between autophagy and oxidative stress in the development of pulmonary disease"* Redox Biol. **2020**:36:101679.

Palmer S. M., Snyder L., Todd J. L., Soule B., Christian R., et al. *"Randomized, Double-Blind, Placebo-Controlled, Phase 2 Trial of BMS-986020, a Lysophosphatidic Acid Receptor Antagonist for the Treatment of Idiopathic Pulmonary Fibrosis"*. Chest. **2018**; 154(5):1061-1069.

Pardo A., Selman M. *"The Interplay of the Genetic Architecture, Aging, and Environmental Factors in the Pathogenesis of Idiopathic Pulmonary Fibrosis"*. American Journal of Respiratory Cell and Molecular Biology **2020**; Volume 64, Issue 2.

Parimon T., Yao C., Stripp B. R, Noble P. W., Chen P. *"Alveolar Epithelial Type II Cells as Drivers of Lung Fibrosis in Idiopathic Pulmonary Fibrosis"* Int J Mol Sci. **2020**;21(7):2269.

Paun A., Kunwar A., Haston C. K. *"Acute adaptive immune response correlates with late radiation-induced pulmonary fibrosis in mice"*. Radiat Oncol. **2015**; 10:45.

Phan S. H., Kunkel S. L. *"Lung cytokine production in bleomycin-induced pulmonary fibrosis"*. Exp Lung Res. **1992**; 18(1): 29–43.

Phan T. H. G., Paliogiannis P., Nasrallah G. K., Giordo R., Eid A. H., Fois A. G. et al. *"Emerging Cellular and Molecular Determinants of Idiopathic Pulmonary Fibrosis"*. Cell Mol Life Sci **2021**; 78 (5), 2031–2057.

Phillips JE. *"Inhaled phosphodiesterase 4 (PDE4) inhibitors for inflammatory respiratory diseases"*. Front Pharmacol **2020**;11: 259.

Pilling D., Roife D., Wang M., Ronkainen S. D., Crawford J. R., Travis E. L., Gomer R. H. *"Reduction of bleomycin-induced pulmonary fibrosis by serum amyloid P"*. J Immunol. **2007**; 179(6):4035-44.

Plataki M., Cho S. J., Harris R. M., Huang H. R. et al. *"Mitochondrial Dysfunction in Aged Macrophages and Lung during Primary Streptococcus Pneumoniae Infection Is Improved with Pirfenidone"*. Sci. Rep. **2019**; 9 (1), 971.

Pontis S., Bignami F., Miglietta D., et al. *"Automated Histological Image Analysis for the Assessment of Bleomycin-Induced Pulmonary Fibrosis in Rodents"*. Eu Resp J. **2019**; 54: PA2420.

Qian W., Cai X., Qian Q., Zhang X.. *"Identification and Validation of Potential Biomarkers and Pathways for Idiopathic Pulmonary Fibrosis by Comprehensive Bioinformatics Analysis"*. Biomed Res Int. **2021** Jul 4;2021:5545312.

Raghu G., Freudenberger T. D., Yang S., Curtis J. R., Spada S., Hayes J., Sillery J. K., Pope C. E., Pellegrini C. A. *"High prevalence of abnormal acid gastro-oesophageal reflux in idiopathic pulmonary fibrosis"*. Eur Respir J. **2006**; 27(1):136-42.

Raghu G., Collard H. R., Egan J. J., Martinez F. J., Behr J., Brown K. K., et al. *"An official ATS/ERS/JRS/ALAT statement: idiopathic pulmonary fibrosis: evidence-based guidelines for diagnosis and management"*. Am J Respir Crit Care Med. **2011**; 183: 788-824.

Raghu G. et al. *"An Official ATS/ERS/JRS/ALAT Clinical Practice Guideline: Treatment of Idiopathic Pulmonary Fibrosis"* Am J Respir Crit Care Med **2015** Vol 192, Iss 2, pp e3–e19.

Raghu G., Chen S. Y., Yeh W. S., Maroni B., Li Q., Lee Y. C., Collard H. R. *"Idiopathic pulmonary fibrosis in US Medicare beneficiaries aged 65 years and older: incidence, prevalence, and survival, 2001-11"*. Lancet Respir Med. **2014**; 2(7):566-72.

Raghu G., Selman M. *"Nintedanib and pirfenidone. New antifibrotic treatments indicated for idiopathic pulmonary fibrosis offer hopes and raises questions"*. Am J Respir Crit Care Med. **2015**; 191(3):252-4.

Raghu G., Wells A. U., Nicholson A. G., Richeldi L., Flaherty K. R., et al. *"Effect of Nintedanib in Subgroups of Idiopathic Pulmonary Fibrosis by Diagnostic Criteria"*. Am J Respir Crit Care Med. **2017**; 195(1):78-85.

Raghu G., Remy-Jardin M., Myers J. L., Richeldi L., Ryerson C. J., Lederer D. J., Behr J., Cottin V., et al. *"Diagnosis of Idiopathic Pulmonary Fibrosis. An Official ATS/ERS/JRS/ALAT Clinical Practice Guideline"*. Am J Respir Crit Care Med. **2018**; 198(5):e44-e68.

Raghu G., Pellegrini C. A., Yow E., Flaherty K. R., Meyer K., Noth I., et al. *"Laparoscopic anti-reflux surgery for the treatment of idiopathic pulmonary fibrosis (WRAP-IPF): a multicentre, randomised, controlled phase 2 trial"*. Lancet Respir Med. **2018**; 6(9):707-714.

Raghu G., van den Blink B., Hamblin M. J., Brown A. W., Golden J. A., et al. *"Effect of Recombinant Human Pentraxin 2 vs Placebo on Change in Forced Vital Capacity in Patients With Idiopathic Pulmonary Fibrosis: A Randomized Clinical Trial"*. JAMA. **2018**; 319(22):2299-2307.

Raghu G., Remy-Jardine M., Richeldi L., Thomson C., Inoue I. et al. *"Idiopathic Pulmonary Fibrosis (an Update) and Progressive Pulmonary Fibrosis in Adults: An Official ATS/ERS/JRS/ALAT Clinical Practice Guideline"* Am J Respir Crit Care Med. **2022**; 205(9):e18-e47.

Rangarajan S., Bone N. B., Zmijewska A. A., Jiang S., Park D. W., Bernard K., et al. *"Metformin reverses established lung fibrosis in a bleomycin model"*. Nat Med. **2018**; 24(8):1121-1127.

Rao L. Z.,Wang Y., Zhang L., Wu G., Zhang L., Wang F. X. et al. *"IL-24 Deficiency Protects Mice against Bleomycin-Induced Pulmonary Fibrosis by Repressing IL-4-induced M2 Program in Macrophages"*. Cell Death Differ **2021**; 28 (4),1270–1283.

Redente E. F., Jacobsen K. M., Solomon J. J., Lara A. R., et al. *"Age and sex dimorphisms contribute to the severity of bleomycin-induced lung injury and fibrosis"*. Am J Physiol Lung Cell Mol Physiol. **2011;** 301(4):L510-8.

Reyfman P.A., Walter J.M., Joshi N., Anekalla K.R., McQuattie-Pimentel A.C., Chiu S. et al. *"Single-Cell Transcriptomic Analysis of Human Lung Provides Insights into the Pathobiology of Pulmonary Fibrosis"*. Am J Respir Crit Care Med. **2019** Jun 15;199(12):1517-1536.

Richeldi L., Costabel U., Selman M., Kim D. S., Hansell D. M., Nicholson A. G., et al. *"Efficacy of a tyrosine kinase inhibitor in idiopathic pulmonary fibrosis"*. N Engl J Med. **2011**; 365(12):1079-87.

Richeldi L., du Bois R. M., Raghu G., Azuma A., Brown K. K., Costabel U., Cottin V., et al. *"Efficacy and safety of nintedanib in idiopathic pulmonary fibrosis"*. N Engl J Med. **2014**; 370(22):2071-82

Richeldi L., Cottin V., du Bois R. M., Selman M., Kimura T., et al. *"Nintedanib in patients with idiopathic pulmonary fibrosis: Combined evidence from the TOMORROW and INPULSIS(®) trials"*. Respir Med. **2016**; 113:74-9

Richeldi L., Collard H. R., Jones M. J. *"Idiopathic pulmonary fibrosis"* Lancet. **2017** May 13;389(10082):1941-1952.

Richeldi L., Varone F., Bergna M., de Andrade J., Falk J., Hallowell R., et al. *"Pharmacological management of progressive-fibrosing interstitial lung diseases: a review of the current evidence"*. Eur Respir Re **2018**; 27(150):180074.

Richeldi L., Fletcher S., Adamali H., Chaudhuri N., et al. *"No relevant pharmacokinetic drug-drug interaction between nintedanib and pirfenidone"*. Eur Respir J. **2019**; 53(1):1801060

Richeldi L., Fernández Pérez E. R., Costabel U., Albera C., Lederer D. J., et al. *"Pamrevlumab, an anti-connective tissue growth factor therapy, for idiopathic pulmonary fibrosis (PRAISE): a phase 2, randomised, double-blind, placebo-controlled trial"*. Lancet Respir Med. **2020**; 8(1):25-33.

Roberts M.J., May L.T., Keen A.C. Liu B., Lam T. et al. *"Inhibition of the Proliferation of Human Lung Fibroblasts by Prostacyclin Receptor Agonists is Linked to a Sustained cAMP Signal in the Nucleus".* Front Pharmacol. **2021** Apr 29;12:669227.

Rochwerg B., Neupane B., Zhang Y., Garcia C. C., Raghu G., et al. *"Treatment of idiopathic pulmonary fibrosis: a network meta-analysis"*. BMC Med. **2016**; 14:18.

Rosas I. O., Richards T. J., Konishi K., Zhang Y., Gibson K., Lokshin A. E., et al. *"MMP1 and MMP7 as potential peripheral blood biomarkers in idiopathic pulmonary fibrosis"*. PLoS Med. **2008**; 5(4):e93.

Rosen G., Sivaraman L., Cheng P., Murphy B., Chadwick K., et al. *"LPA1 antagonists BMS-986020 and BMS-986234 for idiopathic pulmonary fibrosis: Preclinical evaluation of hepatobiliary homeostasis"*. Eu Resp J. **2017**; 50: PA1038.

Ruaro B., Pozzan R., Confalonieri P., Tavano S. et al. "*Gastroesophageal Reflux Disease in Idiopathic Pulmonary Fibrosis: Viewer or Actor? To Treat or Not to Treat?"* Pharmaceuticals (Basel). **2022**;15(8):1033.

Ruwanpura S.M., Thomas B.J., Bardin P.G. *"Pirfenidone: Molecular Mechanisms and Potential Clinical Applications in Lung Disease"*. Am J Respir Cell Mol Biol. **2020** Apr;62(4):413-422.

Ruscitti F., Ravanetti F., Bertani V., Ragionieri L., Mecozzi L., et al. *"Quantification of Lung Fibrosis in IPF-Like Mouse Model and Pharmacological Response to Treatment by Micro-Computed Tomography"*. Front Pharmacol. **2020**; 11:1117.

Sa¨fholm J., Manson M.L., Bood J. et al. *"Prostaglandin E2 inhibits mast cell-dependent bronchoconstriction in human small airways through the E prostanoid subtype 2 receptor"*. J Allergy Clin Immunol. **2015**;136(5):1232-9.

Saini G., Jenkins G., Mckeever T., Simpson J., Hubbard R., Johnson S., Braybrooke R., et al. *"The Profile Study: A Prospective Study Of Fibrosis In Lung Endpoints To Discover And Qualify Biomarkers For Use In Clinical Trials".* Am J Respir Crit Care Med. **2012**; 185:A5169.

Sandbo N. "*Mechanisms of Fibrosis in IPF*". Idiopathic Pulmonary Fibrosis. Chapter 8. **2013**; pp 161-205.

Sakamoto S., Kataoka K., Kondoh Y., et al. *"Diffuse Lung Diseases Research Group of the Ministry of Health, Labour and Welfare, Japan. Pirfenidone plus inhaled N-acetylcysteine for idiopathic pulmonary fibrosis: a randomised trial."* Eur Respir J. **2021** Jan 5;57(1):2000348.

Sakkas L.I., Mavropoulos A., Bogdanos D.P. *"Phosphodiesterase 4 Inhibitors in Immune-mediated Diseases: Mode of Action, Clinical Applications, Current and Future Perspectives"*. Curr Med Chem. **2017**;24(28):3054-3067.

Sato N., Takasaka N., Yoshida M., Tsubouchi K., Minagawa S., Araya J., Saito N., et al. *"Metformin attenuates lung fibrosis development via NOX4 suppression"*. Respir Res. **2016**; 17(1):107.

Schäfer S. C., Funke-Chambour M., and Berezowska S. *"Idiopathic Pulmonary Fibrosis-Epidemiology, Causes, and Clinical Course"*. Pathologe **2020**; 41 (1), 46–51.

Scotton C. J., Chambers R. C. *"Bleomycin revisited: towards a more representative model of IPF?"*. Am J Physiol Lung Cell Mol Physiol. **2010**; 299(4):L439-41.

Scotton C. J., Hayes B., Alexander R., Datta A., Forty E. J., Mercer P. F., Blanchard A., Chambers R. C. *"Ex vivo micro-computed tomography analysis of bleomycin-induced lung fibrosis for preclinical drug evaluation"*. Eur Respir J. **2013**; 42(6): 1633-1645

Selman M., Carrillo G., Estrada A., Mejia M., Becerril C., Cisneros J., Gaxiola M., et al. *"Accelerated variant of idiopathic pulmonary fibrosis: clinical behavior and gene expression pattern"*. PLoS One. **2007**; 2(5):e482.

Selman M., Pardo A. *"Revealing the pathogenic and aging-related mechanisms of the enigmatic idiopathic pulmonary fibrosis. an integral model"*. Am J Respir Crit Care Med. **2014**; 189(10):1161-72.

Senoo S., Taniguchi A., Itano J., Oda N., Morichika D., Fujii U. et al. *"Essential Role of IL-23 in the Development of Acute Exacerbation of Pulmonary Fibrosis"*. Am. J. Physiology-Lung Cell Mol. Physiol. **2021**; 321, L925–L940.

Sgalla G., Larici A.R., Sverzellati N. et al. *"Quantitative analysis of lung sounds for monitoring idiopathic pulmonary fibrosis: a prospective pilot study*". Eur Respir J **2019**; 53: 1802093

Shao X., Li M., Luo C., Wang Y., Lu Y. Y., Feng S., et al. *"Effects of rapamycin against paraquat-induced pulmonary fibrosis in mice"*. J Zhejiang Univ Sci B. **2015**; 16(1):52-61.

Shulgina L., Cahn A. P., Chilvers E. R., Parfrey H., Clark A. B., Wilson E. C. F., et al. *"Treating idiopathic pulmonary fibrosis with the addition of co-trimoxazole: a randomised controlled trial"*. Thorax. **2013**; 68(2):155-62.

Somogyi V., Chaudhuri N., Torrisi S.E., Kahn N., Müller V., Kreuter M. *"The therapy of idiopathic pulmonary fibrosis: what is next?"* Eur Respir Rev. **2019**;28(153):190021.

Smithmyer M. E., Sawicki L. A., Kloxin A. M. *"Hydrogel scaffolds as in vitro models to study fibroblast activation in wound healing and disease"*. Biomater Sci. **2014**; 2(5):634-650.

Song M., Peng H., Guo W., Luo M., Duan W., Chen P., Zhou Y. *"Cigarette Smoke Extract Promotes Human Lung Myofibroblast Differentiation by the Induction of Endoplasmic Reticulum Stress"* European Respiratory Journal **2019**; 54: Suppl. 63, PA1285.

Song D., Tang L., Wang L., Huang J., Zeng T., Fang H. et al. *"Roles of TGFβ1 in the Expression of Phosphoinositide 3-kinase Isoform Genes and Sensitivity and Response of Lung Telocytes to PI3K Inhibitors"*. Cell Biol Toxicol 2020; 36 (1), 51–64.

Sonnenberg, A. *"Effects of environment and lifestyle on gastroesophageal reflux disease"*. Dig. Dis. **2011**, 29, 229–234.

Spagnolo P., Tzouvelekis A., Bonella F. *"The Management of Patients With Idiopathic Pulmonary Fibrosis"* Front Med 2018;5:148.

Spagnolo P., Luppi F., Maher T., Wuyts W., Grutters J. *"Primary endpoints in phase 3 clinical trials in idiopathic pulmonary fibrosis: one step at a time"* Am J Respir Crit Care Med 2013;187(11):1271-2.

Stellari F.F., Ruscitti F., Ravanetti F., Cacchioli A., Villetti G., Civelli M. *"Pharmacological validation of a new IPF bleomycin-induced mouse model"*. Eu Respir J. **2017**; 50:PA1053.

Stuart B. D., Lee J. S., Kozlitina J., Noth I., Devine M. S., Glazer C. S., Torres F., et al. *"Effect of telomere length on survival in patients with idiopathic pulmonary fibrosis: an observational cohort study with independent validation"*. Lancet Respir Med. **2014**; 2(7):557-65.

Sun W., Jing X., Yang X., Huang H., Luo Q., Xia S. et al. *"Regulation of the IGF1 Signaling Pathway Is Involved in Idiopathic Pulmonary Fibrosis Induced by Alveolar Epithelial Cell Senescence and Core Fucosylation"*. Aging (Albany NY) **2021**; 13 (14), 18852–18869.

Sundarakrishnan A., Chen Y., Black L. D., Aldridge B. B., Kaplan D. L. *"Engineered Cell and Tissue Models of Pulmonary Fibrosis"*. Adv Drug Deliv Rev. **2018**; 129, 78-94.

Surolia R., Li F.J., Wang Z., Li H., Liu G. et al. "3D pulmospheres serve as a personalized and predictive multicellular model for assessment of antifibrotic drugs". JCI Insight. **2017**; 2(2).

Tager A. M., Lacamera P., Shea B. S., Campanella G. S., Selman M., Zhao Z., Polosukhin V., et al. *"The lysophosphatidic acid receptor LPA1 links pulmonary fibrosis to lung injury by mediating fibroblast recruitment and vascular leak"*. Nat Med **2008**; 14: 45-54.

Tager A. M. *"Autotaxin emerges as a therapeutic target for idiopathic pulmonary fibrosis: limiting fibrosis by limiting lysophosphatidic acid synthesis"*. Am J Respir Cell Mol Biol. **2012**; 47(5):563-5.

Tanjore H., Blackwell T. S., Lawson W. E. *"Emerging evidence for endoplasmic reticulum stress in the pathogenesis of idiopathic pulmonary fibrosis"*. Am J Physiol Lung Cell Mol Physiol. **2012**; 302(8): L721-9.

Tashiro J., Rubio G. A., Limper A. H., Williams K., Elliot S. J., Ninou I., Aidinis V., Tzouvelekis A., Glassberg M. K. *"Exploring Animal Models That Resemble Idiopathic Pulmonary Fibrosis"*. Front Med. **2017**; 4:118.

Tcherakian C., Cottin V., Brillet P. Y., Freynet O., Naggara N., et al. *"Progression of idiopathic pulmonary fibrosis: lessons from asymmetrical disease"*. Thorax. **2011**; 66(3):226-31.

Tsukui T., Sun K. H., Wetter J. B., Wilson-Kanamori J. R., Hazelwood L. A., Henderson N. C., et al. *"Collagen-producing Lung Cell Atlas Identifies Multiple Subsets with Distinct Localization and Relevance to Fibrosis"*. Nat.Commun. **2020**;11 (1), 1920.

Uhl F. E., Vierkotten S., Wagner D. E., Burgstaller G., Costa R., et al. *"Preclinical validation and imaging of Wnt-induced repair in human 3D lung tissue cultures"*. Eur Respir J. **2015**; 46(4):1150-66.

Umezawa H., Maeda K., Takeuchi T., Okami Y. *"New antibiotics, bleomycin A and B"*. J Antibiot (Tokyo). **1966**; 19(5): 200-209.

Vanoirbeek J. A. J., Rinaldi M., De Vooght V., Haenen S., Bobic S., et al. *"Noninvasive and invasive pulmonary function in mouse models of obstructive and restrictive respiratory diseases"*. Am J Respir Cell Mol Biol. **2010**; 42(1):96-104.

van den Blink B., Dillingh M. R., Ginns L. C., Morrison L. D., Moerland M., et al. *"Recombinant human pentraxin-2 therapy in patients with idiopathic pulmonary fibrosis: safety, pharmacokinetics and exploratory efficacy"*. Eur Respir J. **2016**; 47(3):889-97.

van der Aar E. M., Heckmann B., Blanque, R., et al. *"Pharmacological profile and efficacy of GLPG1690, a novel autotaxin inhibitor for the treatment of idiopathic pulmonary fibrosis"*. Am J Respir Crit Care Med. **2016**; 193: A4523.

Vancheri C., Kreuter M., Richeldi L., Ryerson C. J., Valeyre D., et al. *"Nintedanib with Add-on Pirfenidone in Idiopathic Pulmonary Fibrosis. Results of the INJOURNEY Trial"*. Am J Respir Crit Care Med. **2018**; 197(3):356-363.

Veidal S.S., Karsdal M.A., Vassiliadis E., Nawrocki A. et al. *"MMP mediated degradation of type VI collagen is highly associated with liver fibrosis–identification and validation of a novel biochemical marker assay"*. PLoS One. **2011**;6:e24753.

Wang Q., Usinger W., Nichols B., Gray J., Xu L., Seeley T. W., Brenner M., Guo G., Zhang W., Oliver N., Lin A., Yeowell D. *"Cooperative interaction of CTGF and TGF-β in animal models of fibrotic disease"*. Fibrogenesis Tissue Repair. **2011**; 4(1): 4.

Wang X., Cui H. and Wu, S. *"CTGF: A Potential Therapeutic Target for Bronchopulmonary Dysplasia"*. Eur. J. Pharmacol. **2019**; 860, 172588.

Wang D., Ma Y., Tong X., Zhang Y., Fan H. *"Diabetes Mellitus Contributes to Idiopathic Pulmonary Fibrosis: A Review From Clinical Appearance to Possible Pathogenesis"*. Front Public Health. **2020**; 8:196.

Wang Z., Qu S., Zhu J., Chen F. and Ma L. *"Comprehensive Analysis of lncRNA-Associated Competing Endogenous RNA Network and Immune Infiltration in Idiopathic Pulmonary Fibrosis"*. J. Thorac. Dis. **2020**; 12 (5), 1856–1865.

Wipff P.J., Rifkin D.B., Meister J.J., Hinz B. "Myofibroblast contraction activates latent TGF-beta1 from the extracellular matrix2. J Cell Biol. **2007** Dec 17;179(6):1311-23.

Wollin L., Maillet I., Quesniaux V., Holweg A., Ryffel B. *"Antifibrotic and anti-inflammatory activity of the tyrosine kinase inhibitor nintedanib in experimental models of lung fibrosis"*. J Pharmacol Exp Ther. **2014**; 349(2):209-20.

Wollin L., Wex E., Pautsch A., Schnapp G., Hostettler K. E., Stowasser S., Kolb M. *"Mode of action of nintedanib in the treatment of idiopathic pulmonary fibrosis".* Eur Respir J. **2015**; 45(5):1434-45.

Wu Q., Xu Y., Zhang K.J., Jiang S.M., Zhou Y., Zhao Y. "A Clinical Model for the Prediction of Acute Exacerbation Risk in Patients with Idiopathic Pulmonary Fibrosis". Biomed Res Int. **2020**;2020:8848919.

Xia H., Diebold D., Nho R., Perlman D., Kleidon J., Kahm J., et al. *"Pathological Integrin Signaling Enhances Proliferation of Primary Lung Fibroblasts from Patients with Idiopathic Pulmonary Fibrosis"*. J. Exp. Med. **2008**; 205 (7), 1659–1672.

Yanagihara T., Chong S. G., Vierhout M., Hirota J. A., Ask K., Kolb M. *"Current Models of Pulmonary Fibrosis for Future Drug Discovery Efforts"*. Expert Opin Drug Discov. **2020**; 15 (8), 931-941.

Yoshihara T., Nanri Y., Nunomura S., Yamaguchi Y., Feghali-Bostwick C., Ajito K. et al. *"Periostin Plays a Critical Role in the Cell Cycle in Lung Fibroblasts".* Respir. Res. **2020**; 21 (1), 38.

Zhang Q., Wang Y. et al. *"The Possible Pathogenesis of Idiopathic Pulmonary Fibrosis considering MUC5B"* Biomed Res Int. **2019**: 9712464.

Zaman T., Lee J. *"Risk factors for the development of idiopathic pulmonary fibrosis: A review"*. Curr Pulmonol Rep. **2018**; 7 (4), 118-125.

Zhang Y., Lu W., Zhang X., Lu J. et al. *"Cryptotanshinone protects against pulmonary fibrosis through inhibiting Smad and STAT3 signaling pathways".* Pharmacol Res. **2019** Sep;147:104307.

Zhou Z., Qu J., He L., Zhu Y., Yang S. Z., Zhang F. et al. (2020). *"Stiff Matrix Instigates Type I Collagen Biogenesis by Mammalian Cleavage Factor I Complex-Mediated Alternative Polyadenylation"*. **2020**; JCI insight 5 (3).

Zolak J. S. and de Andrade J. A. *"Idiopathic Pulmonary Fibrosis"*. Immunol. Allergy Clin. North. Am. **2012**; 32 (4), 473–485.